Infrastructure planning for electrified transportation

Author:
Zhang, Jingqi

Publication Date:
2022

DOI:
https://doi.org/10.26190/unsworks/24132

Infrastructure planning for electrified transportation

Jingqi Zhang
M.E., B.E.(Honours), B.Sc.

A thesis in fulfilment of the requirements for the degree of

Doctor of Philosophy

School of Electrical Engineering and Telecommunications

Faculty of Engineering

The University of New South Wales

October 2021

Thesis submission for the degree of Doctor of Philosophy

Thesis Title and Abstract | **Declarations** | Inclusion of Publications Statement | Corrected Thesis and Responses

ORIGINALITY STATEMENT

☑ I hereby declare that this submission is my own work and to the best of my knowledge it contains no materials previously published or written by another person, or substantial proportions of material which have been accepted for the award of any other degree or diploma at UNSW or any other educational institution, except where due acknowledgement is made in the thesis. Any contribution made to the research by others, with whom I have worked at UNSW or elsewhere, is explicitly acknowledged in the thesis. I also declare that the intellectual content of this thesis is the product of my own work, except to the extent that assistance from others in the project's design and conception or in style, presentation and linguistic expression is acknowledged.

COPYRIGHT STATEMENT

☑ I hereby grant the University of New South Wales or its agents a non-exclusive licence to archive and to make available (including to members of the public) my thesis or dissertation in whole or part in the University libraries in all forms of media, now or here after known. I acknowledge that I retain all intellectual property rights which subsist in my thesis or dissertation, such as copyright and patent rights, subject to applicable law. I also retain the right to use all or part of my thesis or dissertation in future works (such as articles or books).

For any substantial portions of copyright material used in this thesis, written permission for use has been obtained, or the copyright material is removed from the final public version of the thesis.

AUTHENTICITY STATEMENT

☑ I certify that the Library deposit digital copy is a direct equivalent of the final officially approved version of my thesis.

Thesis submission for the degree of Doctor of Philosophy

Thesis Title and Abstract **Declarations** **Inclusion of Publications Statement** **Corrected Thesis and Responses**

UNSW is supportive of candidates publishing their research results during their candidature as detailed in the UNSW Thesis Examination Procedure.

Publications can be used in the candidate's thesis in lieu of a Chapter provided:

- The candidate contributed **greater than 50%** of the content in the publication and are the "primary author", i.e. they were responsible primarily for the planning, execution and preparation of the work for publication.
- The candidate has obtained approval to include the publication in their thesis in lieu of a Chapter from their Supervisor and Postgraduate Coordinator.
- The publication is not subject to any obligations or contractual agreements with a third party that would constrain its inclusion in the thesis.

☑ The candidate has declared that **their thesis has publications - either published or submitted for publication - incorporated into it in lieu of a Chapter/s. Details of these publications are provided below.**.

Publication Details #1

Full Title:	Planning of hydrogen refueling stations in urban setting while considering profitability
Authors:	Jingqi Zhang, Chaojie Li, Guo Chen, Zhaoyang Dong
Journal or Book Name:	IEEE-IAS Advanced Technology and Application for Hydrogen-Integrated Transportation and Power Systems

Volume/Page Numbers:	
Date Accepted/Published:	
Status:	published
The Candidate's Contribution to the Work:	Jingqi Zhang designed the model, implemented the model, conducted simulation experiments, analyzed results, drafted the initial manuscript, revised the manuscript, approved the final manuscript. Jingqi Zhang was responsible for revisions required by the journal reviewers and editors.
Location of the work in the thesis and/or how the work is incorporated in the thesis:	Chapter 5

Publication Details #2

Full Title:	Planning of Electric VehicleCharging Stations andDistribution System with High Renewable Penetrations
Authors:	Jingqi Zhang, Shu Wang, Cuo Zhang, Fengji Luo, Zhao Yang Dong, Yingliang Li
Journal or Book Name:	IET Electrical Systems in Transportation
Volume/Page Numbers:	Volume 11, Issue 3, Page 256-268
Date Accepted/Published:	25 March 2021
Status:	published
The Candidate's Contribution to the Work:	Jingqi Zhang designed the model, implemented the model, conducted simulation experiments, analyzed results, drafted the initial manuscript, revised the manuscript, approved the final manuscript, submitted the manuscript for publication. Jingqi Zhang was responsible for revisions required by the journal reviewers and editors.
Location of the work in the thesis and/or how the work is incorporated in the thesis:	Chapter 4

Publication Details #3

Full Title:	Review on Hydrogen Technology in The E-mobility Transformation: Challenges and Opportunities
Authors:	Jingqi Zhang, Chaojie Li, Guo Chen, ZhaoYang Dong, Qing-long Han
Journal or Book Name:	IEEE Transactions on Smart Grid
Volume/Page Numbers:	
Date Accepted/Published:	
Status:	submitted
The Candidate's Contribution to the Work:	Jingqi Zhang reviewed the literature, extracted data, drafted the initial manuscript, revised the manuscript, approved the final manuscript. Jingqi Zhang will be responsible for making all changes requested by journal reviewers and editors.
Location of the work in the thesis and/or how the work is incorporated in the thesis:	Chapter 2

Candidate's Declaration

I confirm that where I have used a publication in lieu of a chapter, the listed publication(s) above meet(s) the requirements to be included in the thesis. I also declare that I have complied with the Thesis Examination Procedure.

THE UNIVERSITY OF NEW SOUTH WALES
Thesis/Dissertation Sheet

Surname or Family name: **Zhang**

First name: **Jingqi** Other name/s:

Abbreviation for degree as given in the University calendar: **PhD**

School: **School of Electrical Engineering and Telecommunications** Faculty: **Faculty of Engineering**

Title: Infrastructure planning for electrified transportation

Abstract

Due to the climate crisis, the importance of reducing greenhouse gas (GHG) has been recognized by governments, private companies and the general public alike. Yet carbon capturing-based approaches are difficult to integrate with transportation, which is one of the largest GHG producing sectors, Therefore, electrification is the only viable approach to reduce emissions from transportation, by greatly increasing the market share of electric vehicles (EVs). However, the mass adoption of either (or both) of battery EVs (BEVs) and fuel cell EVs (FCEVs) require a large amount of supporting infrastructures, particularly the construction of EV charging stations (EVCSs) for BEVs and hydrogen refueling stations (HRSs) for FCEVs. The goal of this study is to provide effective approaches for the sizing and sitting of EVCSs and HRSs to facilitate the deployment of BEVs and FCEVs.

The background and an overview of the thesis are provided in Chapter 1, where the gaps in the current research are pointed out and the objectives of the thesis are formulated. Chapter 2 reviewed the current state of technologies regarding the hydrogen life cycle as well as the popular planning models for EVCSs and HRSs. In Chapter 3, to achieve a competitive strategy from the perspective of private companies, a market-based framework is proposed for the problem of EVCS planning by leveraging Graph Convolutional Network (GCN) and game theory. In Chapter 4, a multi-objective planning model is developed for EVCSs and the expansion of distribution network with significant renewable components while considering uncertainties in EV charging behaviour. Additionally, in Chapter 5, a planning model of HRS maximises the long-term profit while considering different practical constraints. The HRS planning model also addresses short-term demand uncertainty via redistribution. The models that are developed in this study are validated using either synthetic or real-world case studies, and the simulation results showed the effectiveness of the proposed models. Finally Chapter 6 summarises the major achievements of the thesis and provide directions for further research.

Declaration relating to disposition of project thesis/dissertation

Signature **Jingqi Zhang** Witness Date **29 October, 2021**

FOR OFFICE USE ONLY Date of completion of requirements for Award

Abstract

Due to the climate crisis, the importance of reducing greenhouse gas (GHG) has been recognized by governments, private companies and the general public alike. Yet carbon capturing-based approaches are difficult to integrate with transportation, which is one of the largest GHG producing sectors, Therefore, electrification is the only viable approach to reduce emissions from transportation, by greatly increasing the market share of electric vehicles (EVs). However, the mass adoption of either (or both) of battery EVs (BEVs) and fuel cell EVs (FCEVs) require a large amount of supporting infrastructures, particularly the construction of EV charging stations (EVCSs) for BEVs and hydrogen refuelling stations (HRSs) for FCEVs. The goal of this study is to provide effective approaches for the sizing and sitting of EVCSs and HRSs to facilitate the deployment of BEVs and FCEVs.

The background and an overview of the thesis are provided in Chapter 1, where the gaps in the current research are pointed out and the objectives of the thesis are formulated. Chapter 2 reviewed the current state of technologies regarding the hydrogen life cycle as well as the popular planning models for EVCSs and HRSs. In Chapter 3, to achieve a competitive strategy from the perspective of private companies, a market-based framework is proposed for the problem of EVCS planning by leveraging Graph Convolutional Network (GCN) and game theory. In Chapter 4, a multi-objective planning model is developed for EVCSs and the expansion of distribution network with significant renewable components while considering uncertainties in EV charging behaviour. Additionally, in Chapter 5, a planning model of HRS maximises the long-term profit while considering different practical constraints. The HRS planning model also addresses short-term demand uncertainty via redistribution. The models that are developed in this study are validated using either synthetic or real-world case studies, and the simulation results showed the effectiveness of the proposed models. Finally Chapter 6 summarises the major achievements of the thesis and provides directions for further research.

Acknowledgement

Throughout the writing of this thesis as well as my entire PhD study I have received a great deal of support and assistance from people around me.

Firstly, I would like to thank my supervisor Prof. Zhao Yang Dong for taking me as a PhD student, leading me into the field of electric vehicle infrastructure planning. In the past several years, he guided me through a treacherous research journey with patience and meticulousness.

Then I would like to thank my colleague and mentor, Dr. Chaojie Li, who has been supportive and encouraging. Especially, his help enabled the transformation of ideas into research outputs. I would also like to thank all my coauthors for their input and constructive comments during my research.

I would like to thank my dear wife, who is also my best friend and the reason that I even considered to pursue a PhD degree. Her continued love is what drives me forward. Finally I would like to give my thanks to my family who supported me during my PhD.

Publications and Presentations

List of Publications

Published

- C. Li, Z. Dong, G. Chen, B. Zhou, J. Zhang, and X. Yu, "Data-driven planning of electric vehicle charging infrastructure: A case study of Sydney, Australia," IEEE Transactions on Smart Grid, 2021.
- J. Zhang, S. Wang, C. Zhang, F. Luo, Z. Y. Dong, and Y. Li, "Planning of electric vehicle charging stations and distribution system with highly renewable penetrations," IET Electrical Systems in Transportation, 2021.
- J. Zhang, C. Li, G. Chen, and Z. Dong, "Planning of hydrogen refueling stations in urban setting while considering hydrogen redistribution," IEEE Transactions on Industry Applications, 2022.

Under review

- J. Zhang, C. Li, G. Chen, Z. Y. Dong, and Q-L. Han, "Review on Hydrogen Technology in The E-mobility Transformation: Challenges and Opportunities," manuscript submitted to IEEE Transactions on Smart Grid for publication.

Contents

List of Figures

List of Tables

Abbreviations

1-PDTSP	One-commodity Pickup-and-Delivery Traveling Salesman Problem
AEC	Alkaline Electrolysis Cell
AEMFC	Anion-Exchange Membrane Fuel Cell
AFC	Alkaline Fuel Cell
AFV	Alternative Fuel Vehicle
ALS	Alternating-Least-Squares algorithm
BES	Battery Energy Storage
BEV	Battery Electric Vehicle
BFC	Biofuel cell
BR	Backward Reduction
CCS	Carbon Capture and Storage
CFRLM	Capacitated Flow Refuelling Location Model
CHP	Combined Heat and Power
CPI	Consumer Price Index
DAFC	Direct Alcohol Fuel Cell
DEFC	Direct Ethanol Fuel Cell
DEGFC	Direct Ethylene Glycol Fuel Cell
DMFC	Direct Menthol Fuel Cell
DN	Distribution Network
EFC	Enzymatic Fuel Cell
EV	Electric Vehicle

EVCS	Electric Vehicle Charging Station
FCEV	Fuel Cell Electric Vehicle
FCLM	Flow Capturing Location Model
FFS	Fast Forward Selection
FRLM	Flow Refueling Location Model
GCN	Graph Convolutional Network
GHG	Greenhouse Gas
GPS	Global Positioning System
GRU	Gated Recurrent Unit
GSP	Gross State Product
HEV	Hybrid Electric Vehicle
HRS	Hydrogen Refueling Station
HTS	Household Travel Survey
ICE	Internal Combustion Engine
IEA	International Energy Agency
LOHC	Liquid Organic Hydrogen Carrier
MCFC	Molten Carbonate Fuel Cell
MCLP	Maximal Covering Location Problem
MCMC	Markov Chain Monte-Carlo
MCS	Monte-Carlo Simulation
MEA	Membrane Electrode Assembly
MFC	Microbial Fuel Cell
MILP	Mixed-Integer Linear Program
MOEA/D	Multiobjective Evolutionary Algorithm Based on Decomposition
MONAA	Multi-Objective Natural Aggregation Algorithm
NAA	Natural Aggregation Algorithm
NREL	National Renewable Energy Laboratory
NSGA-II	Nondominated Sorting Genetic Algorithm

PAFC	Phosphoric Acid Fuel Cell
PDP	Pick-up and Delivery Problem
PEM	Proton Exchange Membrane
PEMEC	Proton Exchange Membrane Electrolysis Cell
PEMFC	Proton Exchange Membrane Fuel Cell
POX	Partial Oxidation
PV	Photovoltaic
RPPI	Residential Property Price Index
SCP	Set Covering Problem
SDP	Semidefinite Programming
SG	Scenario Generation
SMR	Steam Methane Reform
SOCP	Second-Order Cone Programming
SOEC	Solid Oxide Electrolysis Cell
SOFC	Solid Oxide Fuel Cell
SR	Steam Reforming
TCO	Total Cost of Ownership
TN	Transportation Network
TOU	Time Of Use
UAV	Unmanned Aerial Vehicles
UPS	Uninterruptible Power Systems
WGS	Water Gas Shift
WPI	Wage Price Index

Chapter 1

Introduction

1.1 Research background

Due to the growing concerns of the climate crisis in recent decades, countries have begun implementing procedures and policies to reduce Greenhouse Gas (GHG) emissions and the world's dependence on fossil fuels. For instance, to reduce emissions from the energy sector—the largest GHG producer [1]—various renewable energy sources (such as wind, solar, hydro and geothermal) and clean energy sources (such as nuclear) have received unprecedented or renewed interest. As a result of this surge of interest, renewable generation, mainly wind and solar, accounts for 90% of the new power generation capacity in 2021 and 2022 worldwide [17]. Additionally, Carbon Capture and Storage (CCS) technologies are being tested for the industry sector—the third-largest GHG producer—as well as existing fossil fuel power plants [18].

In line with the measures being implemented by other sectors to curb GHG emissions, it stands to reason that efforts should be made to reduce emissions in the second-largest GHG producing sector: transportation. This sector consumes half of the world's oil supply and accounts for more than 25% of CO_2 emissions [1]. As the transportation sector is made up of millions of cars and thousands of ships, locomotives and aeroplanes, it is a nontrivial task to integrate CCS-based emission reduction mechanisms. Currently, electrification is the only path that can effectively reduce GHG emissions from transportation. This means replacing internal combustion engine (ICE) vehicles with electric vehicles (EVs), including both battery electric vehicles (BEVs) and fuel cell electric vehicles (FCEVs). Yet, progress in reducing GHG emissions from transportation has been lacking. Despite EVs in road transport ramping up significantly as of 2020, BEVs only account for around 1% of all road vehicles and 4% of new road vehicles sales [19], while FCEVs have a market share of about 0.1% [20]. As for forms of transportation, fully electric ships and planes are still being trialled or developed [21, 22], and the only form of transportation that is highly electrified is rail [23].

One of the reasons hindering the deployment of BEVs and FCEVs for road transport is the lack of electric vehicle charging stations (EVCSs) and hydrogen refueling stations (HRSs). Some researchers refer to this as a 'chicken-and-egg' problem [24],that is, BEVs and FCEVs would not be widely accepted unless there is a large network of EVCSs and HRSs. However, EVCSs and HRSs will not be built unless there is already a fleet of BEVs and FCEVs. Luckily, governments worldwide have recognised this issue and seek to resolve it through favourable policies and investments. For example, both China and the European Union have announced plans to promote BEVs and FCEVs to replace ICE vehicles, along with massive investments in related infrastructure [2, 25]. Increased commitment and investment in EVs infrastructure has another benefit, boosting the public's acceptance and indirectly reducing the cost of EVs. At the time of writing in 2021, all EVs are more expensive than ICE vehicles in terms of Total Cost of Ownership (TCO) [2]. Contributing factors of TCO include initial capital cost as well as operational costs. Since more infrastructure means it will be cheaper to recharge or refill a BEV or FCEV, it will boost the number of BEVs and FCEVs. As more consumers choose a EV over an ICE vehicle, the price of EVs will reduce as a result of both economies of scale and competition. In fact, it is projected that both BEVs and FCEVs will be cheaper to own than ICE vehicles in terms of TCO by 2023 at the latest [2].

To maximise the effect of the investment, it is vital to size the EVCSs and HRSs optimally.

Moreover, appropriately locating EVCSs and HRSs will increase the acceptance of BEVs and FCEVs and further speed up the pace of electrifying the transportation sector as a whole. Therefore, this thesis aims to develop efficient EVCS and HRS planning models to facilitate BEV and FCEV deployment, and in turn, speed up the electrification of road transportation.

1.2 Motivation for this thesis

Over the last decade a large number of research works and publications have focused on locating and sizing EVCSs and HRSs. Various approaches have been applied to find optimal solutions, such as genetic algorithm optimisation (e.g., [26–31]), integer programming (e.g., [32–38]), and particle swarm optimisation (e.g., [39–41]). There has even been a planning model developed for combined EVCS and HRS aiming to service both BEVs and FCEVs (e.g., [42]).

1.2.1 Identified research gaps

Even though the planning of EVCS and HRS has been extensively studied, several identified research gaps are as follows:

1. Despite many studies aiming to leverage hydrogen to reduce GHG emissions from transportation, there is no a systematic review of the entire hydrogen life cycle. The hydrogen life cycle includes production, storage and transportation, HRS planning and fuel cell technologies. Other review focus on sections of the hydrogen life cycle. However, it is difficult for readers to be fully informed from just sections of the life cycle. A good understanding of the entire hydrogen life cycle will help researchers optimize each stage of the life cycle in a comprehensive manner rather than isolated stages. For example, more realistic HRS planning methods can be designed by considering limits from other stages, such as hydrogen production and transportation

as well as FCEVs.

2. The majority of studies on EVCS and HRS planning focus on obtaining a global optima in the absence of competition. In a free-market economy where private companies compete with each other, a global optima often cannot be achieved. Moreover, in case studies for EVCS and HRS planning, most of the current research uses synthetic data, because real-world data often suffers from practical issues, for example missing data. Using synthetic data for case studies means that some real world implications might be overlooked. Further, infrastructure planning (i.e., EVCS and HRS planning) generally requires a prediction of future demand. Yet, a generalised traffic flow prediction model cannot encompass the case-specific characteristics. A flexible practically-relevant traffic flow prediction approach is needed.

3. In the literature, a trade-off often has to be made between computational time and the optimality of the planning results. It is advantageous to design an approach that can simultaneously increase approximation accuracy and reduce computation time. For instance, probabilistic modelling of the charging or refueling demand is widely used in EVCS and HRS planning. Monte-Carlo Simulations (MCSs) and scenario reduction techniques are commonly used to generate BEV charging demands. The approximation accuracy increases with the initial number of scenarios and so does computation time. It is desirable to directly generate a small number of representative scenarios, thereby skipping the time-consuming scenario reduction step. Another example is, due to the computational complexity of multi-objective optimisation algorithms, near-optimal results are often chosen to speed up the calculation. Currently, the worst-case complexity of extensively used algorithms is in quadratic time. An algorithm with a worst-case complexity of linear or near-linear time, that can obtain similar or better optimization results, would be preferred.

4. In terms of optimisation objectives, the current HRS planning models are based on some form of social benefit, such as minimising detours, wait times or investments. However, private businesses are generally motivated by profits. Therefor, it is necessary for the modelling to account for the profitability of HRSs. Additionally, the

current planning models only focus on long-term operation, but short-term fluctuations in refuelling demand may lead to hydrogen imbalances among the HRSs. To overcome this imbalance, a hydrogen redistribution mechanism is needed.

1.2.2 Thesis objectives

To address the aforementioned research gaps, the following research objectives are formulated:

- review and summarise the current status of technologies and research related to the hydrogen life cycle to facilitate decision-making for policy makers and future studies for researchers (Chapter 2)
- develop a data-driven market-based planning framework for EVCSs that is practical and flexible (Chapter 3)
- develop a multi-objective optimisation model that can simultaneously plan the sizing and sitting of EVCSs as well as the local Distribution Network (DN) expansion, while adopting a novel scenario generation method to speed up computation and improve accuracy, and using a new multi-objective optimisation tool with less computational complexity (Chapter 4)
- develop a planning model that optimises the location and capacity of HRSs and their components (electrolysers, solar panels and storage tanks) while maximising the captured traffic flow and profit, and propose a hydrogen redistribution mechanism (Chapter 5).

1.3 Thesis structure

This thesis is structured as follows:

Chapter 1 gives a general background, outlines identified gaps in the current research, and provides the research objectives.

Chapter 2 (submitted as [43]) consists of a systematic review of all the steps in the hydrogen life cycle, including hydrogen production techniques, hydrogen storage and transportation methods, HRS planning models and fuel cell technologies.

Chapter 3 (published as [44]) presents a data-driven framework for EVCS planning. To address the issue of missing data, a spatial-temporal data imputation method derived from matrix factorisation is deployed. Additionally, a multi-relation graph convolutional network (GCN) is adopted to predict the EV charging demands, and a Cournot competition game model is used to obtain the budget allocation for different companies operating in the same area. The Cournot competition equilibrium is obtained with a new parallel computational algorithm. The optimal EVCSs sizing at each zone is solved as a mixed-integer linear programming (MILP) problem. The effectiveness of the proposed framework is demonstrated with a case study of Sydney, Australia.

In Chapter 4 (published as [45]), a multi objective planning model that optimises the sizing and location of EVCSs as well as local distribution network expansions is presented. The objectives of the planning model are to minimise the investment cost while maximising the captured traffic flow. The uncertainties of renewable generation and EV charging behaviour are also considered. In particular, a recent scenario generation (SG) method is used to speed up the process of generating total EV charging load from the probabilistic model. Finally, the Multi-Objective Natural Aggregation Algorithm (MONAA) is used to obtain the final planning results. Simulation results shows that SG-based MONAA outperforms other commonly used methods.

In Chapter 5 (published as [46]), a modified Capacitated Flow Refuelling Location Model (CFRLM) is used for the planning of HRSs where the objective is to maximise the overall profit. Various real-world constrains such as Traffic Network (TN) constraints, DN constraints, hydrogen balance constraints and range constraints for FCEVs are considered. The short-term uncertainty of hydrogen refuelling demand is resolved by a redistribution method based on solving the One-commodity Pickup-and-Delivery Traveling Salesman Problem (1-PDTSP). A case study of Western Sydney with real-world data is used to validate the planning model, while the effectiveness of the redistribution method is tested in a numerical simulation.

Finally, Chapter 6 summarises the main contributions of this thesis and provides some directions for future research.

Chapter 2

Review on Hydrogen Technology in The E-mobility Transformation: Challenges and Opportunities

2.1 Relationship to the Thesis

As mentioned in Chapter 1, the majority of current review works regarding using hydrogen as a energy carrier for transportation only cover parts of the hydrogen life cycle. To offer the readers a more comprehensive knowledge base, various literature related to the entire hydrogen life cycle is reviewed in this chapter.

This Chapter has been submitted for publication as J. Zhang, C. Li, G. Chen, Z. Y. Dong, and Q-L. Han, "Review on Hydrogen Technology in The E-mobility Transformation: Challenges and Opportunities"

2.2 Abstract

The growing concerns regarding the climate emergency has led to an increase in efforts to reduce greenhouse gas emissions. As for reducing the emission from the transportation sector, the current consensus is that electrification would be the best approach. Hydrogen and fuel cell electric vehicles are viewed as key elements in this transformation. At the moment, hydrogen is only widely used in chemical industry and is mostly generated from fossil fuels. The wide adoption of hydrogen in the transportation sector requires eco-friendly and efficient methods in the entire life-cycle, i.e. the production, storage and transportation, distribution, and utilization of hydrogen. To this end, this review covers both reform and electrolysis production techniques; gases, liquid as well as hydrogen carrier storage and transportation methods; point based and flow based location models for hydrogen refueling station planning; and major types of fuel cells. The strengths and weaknesses of each of these techniques/methods/technologies are pointed out. This chapter severs as an overview of the current status technological of using hydrogen in transportation.

2.3 Introduction

As the climate crisis worsens, methods to reduce greenhouse gas (GHG) emissions drew more and more attention from police makers and general public alike. As shown in Fig. 2.1 the transportation sector is the the second largest CO_2 producing sector in the world. This is because currently more than 90% of energy used in transportation is supplied by fossil fuels [1]. However, unlike in energy production or industry sectors where the CO_2 emission is concentrated, the distributed nature of the transportation means that carbon capture and storage (CCS) approaches cannot be easily integrated. Therefore, the only feasible solution to reduce GHG from transportation is by electrification coupled with the decarbonisation of electricity generation. In other words, the current internal combustion engine (ICE) vehicles needs to be replaced by alternative fuel vehicles (AFVs) such as, fuel cell electric vehicles (FCEVs), battery electric vehicles (BEV), hybrid electric vehicles

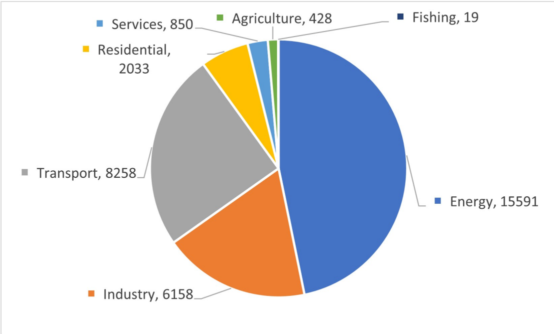

Figure 2.1: World's CO_2 emission by sector in million tonnes (data from [1]).

(HEVs) and biofuel vehicles. Additionally, the alternate fuels need to be generated from renewable or clean energy sources such as solar, wind, hydro or nuclear power plants.

Hydrogen, being the substances with the highest known gravimetric energy density (~ 120 kJ/g) [47], is viewed by many to be a good alternative fuel to replace fossil fuels and help lower the GHG emission in transportation [46]. The attempt to using hydrogen as an energy source in vehicles dates back to the early 1800s, with the initial idea being to use hydrogen in ICE vehicles [3]. The principle of using fuel cell to generate electricity is first demonstrated in 1839 [2]. However the notion of using fuel cells to power EVs with hydrogen did not gain much traction until the late-20th century, and only in the 21st century, due to the increasing awareness of the climate crisis, did FCEVs saw wider commercial deployment. The major milestone of fuel cell and FCEV development is presented in Fig.2.2.

Compared to other AFVs and alternate fuels, FCEVs and hydrogen offer some distinct advantages. For example, as shown in Fig. 2.3, FCEVs offer the greatest reduction in CO_2 emissions especially when the hydrogen is produced from renewable sources (around 90% reduction compared to ICE vehicles). Moreover, hydrogen does not generate any GHG at the point of usage, where as biofuel, such as corn ethanol, will still generate some CO_2 when the energy is released. Furthermore, unlike BEVs, which still have limited range, the travel ranges of FCEVs are greater therefore are more convenient for the driver. The extended driving range of FCEVs also means that less refueling stations needs to be built.

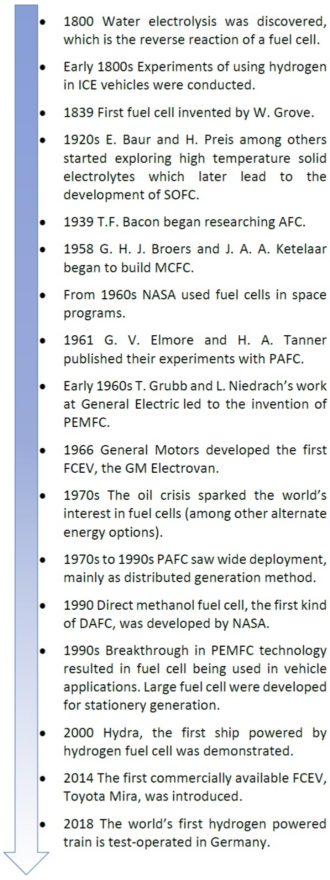

Figure 2.2: Timeline of fuel cell development and applications. (modified from [2, 3])

It is worth noting that despite being the most abundant element in the universe, pure hydrogen does not exist naturally on Earth. Thus, hydrogen is an energy carrier/secondary energy source just like electricity and must be produced from a primary source. The energy sources for producing hydrogen and hydrogen's potential uses are illustrated in Fig.2.4. Currently, hydrogen is already an established commodity with more than 70 million ton demand annually [48]. The majority of demand for pure hydrogen today is in oil refining ($\sim$ 51%) followed by chemical (mainly ammonia) synthesis ($\sim$ 43%) [49]. Additionally hydrogen (in the form of syngas) is also being used in metal refining as a way to reduce GHG emission [48]. Apart from being an alternate fuel in the transportation sector, hydrogen also has other uses as an energy carrier. For instance, hydrogen can be used to produce electricity as well as heat in a fuel cell or gas turbine in the MW range [5]. In this way hydrogen can function as an energy storage medium. Hydrogen energy storage is an

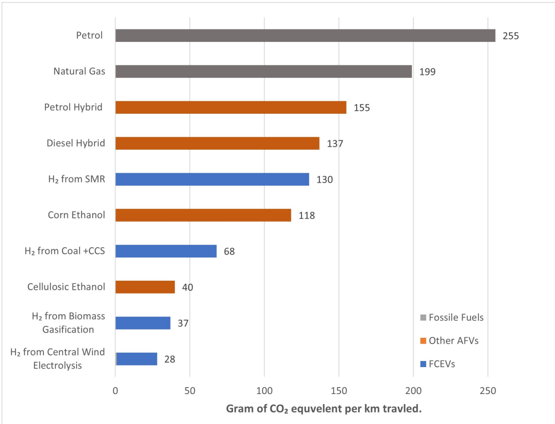

Figure 2.3: Well-to-wheel analysis of potential reduction in GHG emissions. (modified from [4])

effective method to regulate the variable output of renewable production from sources like wind and solar. Moreover, hydrogen is a valid fuel for distributed generation [5]. Hydrogen can also be injected to the current natural gas network to lower the GHG emission of other sectors. When reacted with CO_2, hydrogen can also be used to produce synthetic fuels. Synthetic fuels produced from green hydrogen can have net zero carbon emissions. Using hydrogen as an energy carrier fall in the frame work of Power to Power [50]. In this case it means converting one form of power, usually electricity, to hydrogen, and then converting hydrogen back to a form of power, electricity, at a different time and/or place.

Right now, more than 95% of the worlds hydrogen is produced from fossil fuel reforms with high CO_2 emissions [48]. Although various projections envision that the production of hydrogen will ramp up significantly and the majority of it will be green hydrogen by 2050 [51, 52]. To achieve this vision, reform based hydrogen production methods needs to be coupled with CCS technology, and the percentage of hydrogen from electrolysis needs to increase [20].

The produced hydrogen needs appropriate storage methods. Hydrogen can be stored as a compressed gas, a cryogenic liquid or in various carriers [11]. Each of these storage methods have different characteristics, transportation methods, and level of energy input.

The Hydrogen Refueling Stations (HRSs) are the final point of distribution for hydrogen.

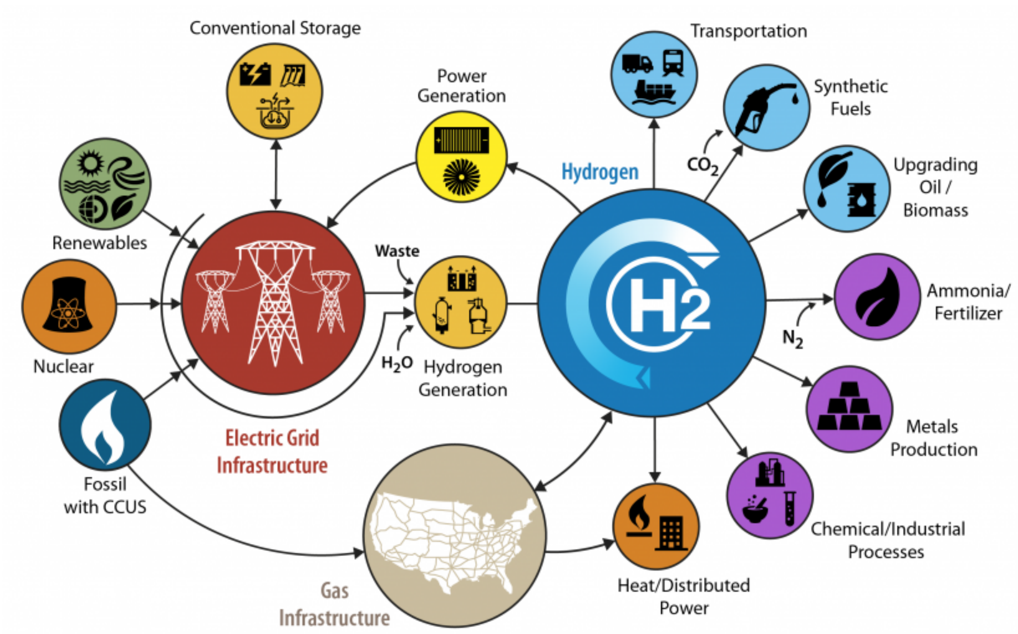

Figure 2.4: Energy sources for hydrogen production and hydrogen usages (obtained from [5])

Their availability and serviceability is vital to the wide adoption and acceptance of FCEVs [53]. The importance of a planning of hydrogen infrastructure, particularly the location of HRSs, has been recognized since 1990s [54, 55]. Although BEVs and FCEVs are both considered as candidates to replace ICE vehicles in order to combat climate change [42], the constrains related to the corresponding infrastructures are different. Currently BEVs still have limited range and long charging time thus electric vehicle charging stations (EVCSs) needs to be built closer together and with many chargers [44], whereas the refueling stations for FCEVs are more like petrol/diesel stations due to FCEVs' longer range and faster refueling time [46]. Moreover, EVCSs put additional loads on the local electrical networks [56], whereas HRSs have different hydrogen delivery/ production methods that may or may not require electricity.

Hydrogen is ultimately converted to electricity by fuel cells to power FCEVs. There are many different types of duel cells, including Alkaline Fuel Cell (AFC), Phosphoric Acid Fuel Cell (PAFC), Proton Exchange Membrane Fuel Cells (PEMFC), Solid Oxide Fuel Cell (SOFC), and Molten Carbonate Fuel Cell (MCFC). All of these aforementioned fuel

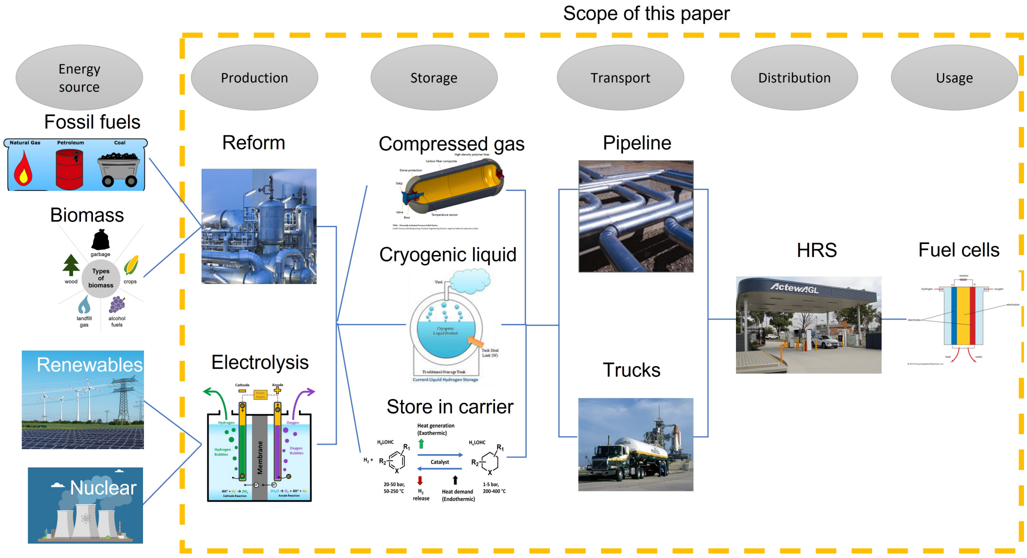

Figure 2.5: A Sustainable Pathway for Energy Transition.

cells use hydrogen as fuel. There also exist fuel cells that uses different kinds of fuels, such as Direct Alcohol Fuel Cell (DAFC) that uses various alcohols as fuel and Biofuel cell (BFC) that utilizes organic compounds.

The life cycle of hydrogen in the context of transportation is shown in Fig. 2.5. There have been many papers covering a single section of the life cycle of hydrogen. For example, a review of fuel cell technologies focuses on using fuel cell as distributed generation system is given in [12]. In [57], an overview of hydrogen production methods is provided, mainly covering reforming and pyrolysis, while also discussing other methods such as electrolysis/photoelectrolysis and thermochemical water splitting. A systemic review of fuel cell technologies and applications was done by Sharaf and Orhan [13], with an emphasis on hydrogen fuel cells. A brief discussion of the advantage of using hydrogen as energy carrier can be found in [58], which also covered the storage method of hydrogen in detail. In [59] the formulations and constrains of HRS location models are discussed, different models are categorised based on the number of objectives. However to the best of the authors' knowledge, there is no paper that reviews all the sections of the hydrogen life cycle, namely hydrogen production, hydrogen storage and transportation, HRS planning and fuel cell technologies.

The rest of the chapter is organised as follows. Section 2.4 outlines the motivations for this chapter. Section 2.5 covers the production methods of hydrogen. Section 2.6 reviews the storage and transportation methods for hydrogen. Section 2.7 discusses the planning strategies for HRSs. Different fuel cell technologies are covered in Section 2.8. Finally Section 2.9 concludes this chapter.

2.4 Motivations

Despite their ability to greatly reduce GHG emissions, FCEVs and hydrogen in general are still not widely deployed in transportation [51]. Case in point, FCEVs only account for 0.5% of all AFV sales in 2019 [20]. The main reason that the public and private sectors are reluctant to adopt FCEVs is the high expenditure. Today the Total Cost of Ownership (TCO) of an FCEV is still higher than BEV and almost double that of an ICE vehicle. As a result, the high upfront cost of buying an FCEV as well as the expensive price of hydrogen are the major obstacle that lays ahead [2] . Another main challenge that currently hinders the deployment of FCEV is the lack of hydrogen infrastructure. This lack of hydrogen infrastructure manifests in many forms, the most notable to the end user is the lack of HRSs. Since FCEVs can only operate in areas with HRSs. Hence, The construction of HRSs must precede the deployment of FCEVS. Yet, currently there are only about 500 HRSs around the world [20]. To put the lack of HRSs into perspective, Germany has more than 14000 fuel stations for ICE vehicles.

In recent years, having recognised FCEVs' potential in reducing GHG emissions countries and regions such as China [25], the European Union [2], United States [5], Japan [20] and South Korea [38] have all announced national policies along with significant investments focused on promoting the adoption of FCEVs and hydrogen. For instance the EU countries announced 45-50 billion euro investments in hydrogen by 2030 and the total investment will be more than 180 billion euros by 2050 [2]. South Korea also announced national strategies to boost FCEV and hydrogen acceptance, among which is the commitment to build 1200 HRSs by 2040 [20]. In addition, the costs of both FCEVs and hydrogen are projected to decrease dramatically in the near term due to technological improvements combined with the economy of scale. In fact, it is estimated that FCEVs will undercut both BEVs and ICE vehicles in terms of TCO by 2030 [2].

A reduction of TCO coupled with favourable governmental policies and investments will likely lead to a mass adoption of FCEVs. Consequently, it is imperative that to properly and optimally direct further research and locate HRSs in order to maximize the reduction of GHG emissions from FCEVs and hydrogen. This chapter aims to review the current state of technologies and methods, to help better direct future research and development efforts as well as allow policy makers and private companies to make informed decisions.

2.5 Hydrogen production techniques

As stated in Section 2.3, hydrogen, which does not exist in element form on earth, must be produced from a primary source. This primary source can be fossil fuels, biomass or even water. In this section we review the currently used hydrogen production methods as well as the leading experimental methods in the literature.

2.5.1 Reformed hydrogen

The vast majority of hydrogen is currently produced by reforming some form of hydrocarbons or carbohydrates. Depending on the carbon source, the hydrogen reforming can be further separated into two categories, namely fossil fuel based reforms and renewable source based reforms (biomass gasification).

The four main processes used in reforming are Steam Reforming (SR), Partial Oxidation (POX), pyrolysis, and Water Gas Shift (WGS). The general chemical reactions when using hydrocarbon as feedstock are given below.

Steam Reforming

$$\mathrm{C}_m\mathrm{H}_n + \mathrm{mH_2O} \longrightarrow \mathrm{mCO} + (\mathrm{m} + \frac{1}{2}\mathrm{n})\mathrm{H}_2, \tag{2.1}$$

Partial Oxidation

$$C_mH_n + \frac{1}{2}\,mO_2 \longrightarrow mCO + \frac{1}{2}\,nH_2, \tag{2.2}$$

Pyrolysis

$$C_mH_n \longrightarrow mC + \frac{1}{2}\,nH_2, \tag{2.3}$$

Water Gas Shift

$$CO + H_2O \longrightarrow CO_2 + H_2, \tag{2.4}$$

Combustion

$$CO + \frac{1}{2}\,O_2 \longrightarrow CO_2, \tag{2.5}$$

$$H_2 + \frac{1}{2}\,O_2 \longrightarrow H_2O, \tag{2.6}$$

$$C + \frac{1}{2}\,O_2 \longrightarrow CO_2, \tag{2.7}$$

The chemical process of biomass gasification is more complex and the exact procedure varies depending on the feedstock [60]. Biomass gasification is considered to be POX-based but Eq (2.1)-(2.7) all happen simultaneously in different regions of the reactor [61].

The initial product of SR/POX/pyrolysis/gasification is known as syngas, a mixture of H_2 and CO that contains CO_2 among other impurities. Purified syngas has several applications itself, most notably as an energy source and a reduction agent in metal refining [48]. To obtain pure hydrogen the syngas is passed though several WGS reactors to convert as much CO to H_2 as possible [62]. The energy efficiency of hydrocarbon reforms vary between 50-85 [63] with Steam Methane Reform (SMR) being the most energy efficient and the most widely used. Biomass gasification methods generally have lower energy efficiencies as the water content in the feedstock is also vaporized in the process [61]. Moreover, the current gasification process will result in up to 20 wt% tar present in the final product, which lowers the efficiency and requires additional cleanup processes as well [64]. For a detailed review of hydrogen from various carbon sources see [65].

Table 2.1: Typical specifications of electrolyzers (modified from [7] with updated information from [8–10])

Specification	AECs	PEMECs	SOECs
Technology maturity	Commercialization	Commercialization	Demonstrations
Cell temperature (°C)	$60-80$	$50-80$	$700-1000$
Cell pressure (Mpar)	$1-3$	$2-5$	$0.1-1.5$
Current density (A/cm^2)	$0.25-0.45$	$1.0-2.0$(up to 20)	0.3-1.0
Cell voltage (V)	$1.8-2.4$	$1.8-2.2$	$0.95-1.3$
Cell efficiency (%)	$59-70$	$67-82$	up to 100
Specific system energy consumption[1](kWh/Nm^3)	$4.2-4.8$	$4.4-5.0$	$2.5-3.5$
Minimum partial load (%)	$10-40$	$0-10$	-
Cell area (m^2)	$3-3.6$	< 0.13	< 0.06
Hydrogen production per stack (Nm^3/h)	1400	400	< 10
Stack lifetime (kh)	$55-120$	$60-100$	$8-20$
System lifetime (years)	$20-30$	$10-20$	-
Hydrogen purity (%)	99.8	99.999	-
Cold start-up time (min)	60	$5-10$	hours
Investment costs (€/kW^1)	$800-1500$	$1400-2100$	$2000-5000$

[1] Excluding rectifier and utilities ($0.4-0.8$kWh/Nm^3).

Regardless of the reform processes and feedstock a significant amount of CO_2 is released when producing hydrogen. Take SMR as an example, which is used to produce half of the world's current H_2 supply [66], 7-10 kg of CO_2 is released per kg of H_2 produced [66, 67]. To address this issue CCS methods have been proposed at the expense of reduced efficiency and increased cost. [66]. Nevertheless, in the near to mid term different reforms are going to be main methods of hydrogen production. Interestingly one type of fuel cells, MCFCs, can actually assist in the concentration and removal of CO_2 in the flue gas. More details are given in Section 2.8.6

2.5.2 Hydrogen from Electrolysis

Electrolysis

$$\frac{1}{2}\,H_2O + \text{electricity} \longrightarrow H_2 + \frac{1}{2}\,O_2, \tag{2.8}$$

The overall reaction for electrolysis is given in Eq 2.8. Currently, less than 1% of the worlds annual hydrogen production is from electrolysis [20]. As stated in Section 2.5.1 generating reformed hydrogen also produces a considerable amount of CO_2. Thus, for hydrogen to become a more effective tool in combating climate change and reducing CO_2 emissions, a significant potion of hydrogen needs to be generated by electrolysis. Moreover, the electrolyzers needs to be powered by renewable sources, such as solar and wind, or cleaner energy sources, e.g. nuclear. In this section the electrolysis technologies that have been commercialized or are nearing commercialization are reviewed, namely Alkaline Electrolysis Cells (AECs), Proton Exchange Membrane Electrolysis Cells (PEMECs) and Solid Oxide Electrolysis Cells (SOECs). Being essentially the reverse of fuel cells AECs, PEMECs and SOECs have similar operating conditions and structures as their fuel cell counter parts. The important parameters for the different electrolysis cells are summarized in Table 2.1.

2.5.2.1 Alkaline Electrolysis Cells (AECs)

AECs are the earliest and most mature form of electrolysis and have seen many commercial uses [7]. The nickle-based anode and cathode of AEC are submerged in the liquid electrolyte separated by a diaphragm. The electrolytes in AECs are 30% NaOH and/or KOH solutions in water. Being the most widely used electrolysis method, AECs are usually supplied by stable grid power and are not suitable to be coupled to renewable energy sources [8], like wind and solar. Because AECs have have poor performance in low loading conditions and have a long response time to load changes while the output of renewable sources fluctuate constantly [68]. Moreover, as seen in Table 2.1 AECs have additional draw backs such as low current density and low purity [69].

2.5.2.2 Proton Exchange Membrane Electrolysis Cells (PEMECs)

Unlike AEC which uses liquid electrolyte, PEMEC uses a solid polymer electrolyte, which is called a Proton Exchange Membrane (PEM) because it only allows proton to pass though but not electrons. The electrolytes along with the solid membrane forms the Membrane Electrode Assembly (MEA). The main advantage of PEMECs is the quick response and to load variations making it the ideal candidate to be coupled to renewable generation methods [8,68]. As seen in Table 2.1 PEMECs also have additional advantages including compact and modular design, high current density, high H_2 purity and high output pressure, making PEMECs suitable for industrial hydrogen generation [8]. The main roadblock to wide utilization of PEMECs is their prohibitively high cost. in terms of both capital investment and operational cost [9]. However despite the draw backs, more and more PEMEC plants are being built around the world [20], due to their ability to work with renewable power sources.

2.5.2.3 Solid Oxide Electrolysis Cells (SOECs)

SOECs, due to their up to 1000°C operating temperature, are considered as high temperature electrolysis cells. As the high operating temperature lowers the anode and cathode overpotentials, SOECs have a higher efficiency compared to other electrolysis methods [70]. Another feature of SOECs is their ability to electrolyze CO_2 to form CO [71,72]. Thus, when steam and CO_2 are supplied to SOECs simultaneously syngas can be produced. Nuclear power, being a cleaner energy source than fossil fuels [73], has been considered by many researchers to be the best energy source for SOECs as the nuclear reactor can supply both the thermal and electrical energy [74, 75]. Currently SOECs are only in demonstration phase due to limited life span and harsh operating conditions.

An up to date review of the history and current status of water electrolysis can be found in [10].

2.5.3 Other hydrogen production methods

Apart from the previous mentioned production techniques, various alternative hydrogen production methods have been proposed and tested, such as plasma reforming [76], aqueous phase reforming [77], ammonia reforming [78], thermochemical water splitting [79], photolysis [80], dark fermentation [81], photo fermentation [82] and microbial electrolysis cells [83]. Currently all of these alternative production methods are still in the research phase and are far from commercialization. Interested readers can refer to the respective reference for more information.

2.6 Hydrogen storage and transportation

The storage of hydrogen falls into two categories, storing hydrogen in its pure form or storing hydrogen in a carrier. Since the methods of transporting hydrogen are closely related to the storage methods, they will be discussed in this section as well.

2.6.1 Pure hydrogen

Pure hydrogen exists as a gas at room temperature and atmospheric pressure with very low volumetric energy density (9.9 MJ/m^3) [84]. Therefor, to increase the energy density and reduce the size of the storage container, pure hydrogen is usually stored as a compressed gas or a liquid.

2.6.1.1 Compressed hydrogen

There exists four type of pressure vessels to store compressed hydrogen, namely (with descending weight but increasing cost) Types I, II, III and IV [11, 85]. Type I pressure vessel is fully metallic, made with aluminum or steel and can be pressured to 50 Mpa. Type II is a metallic vessel with a composite overwrap and is around 40% lighter than Type I while the cost is 1.5 times of Type I. Interestingly, there is no practical limit on the pressure a Type II vessel can hold. Both Type III and IV are regarded as fully composite pressure vessels. The distinction lies in the propose of the liner. In a Type III vessel, the (usually metal) liner also contributes to the mechanical strength of the vessel. Whereas in a Type IV vessels the polymer or metal liner is purely for sealing propose. Usually Type III vessels are rated for 45 Mpa while Type IV vessels can withstand up to 100 Mpa. The application and a compromise of performance and cost effectiveness usually decides which type of vessel is chosen for storing hydrogen. Currently, industrial applications stores hydrogen at $20-30$ MPa Type I cylinders [85]. For stationary hydrogen storage both Types I and II tanks can be used, While the on-board storage tanks of FCEVs are usually Type III or IV [86, 87].

The transportation of gases hydrogen can be done with pressurized pipelines (up to 20 Mpa [88]) or with tube trailers (up to 70 Mpa [89]). Although a pipeline system can deliver hydrogen to HRSs more cheaply and quickly [90, 91], such a system does not (widely) exist yet. As of 2016 there are only around 4500 km of hydrogen pipelines around the world [92], these pipelines are almost exclusively located near oil refineries or chemical plants [91]. For reference the current total length of natural gas pipelines exceeds 1 million km [93]. Thus, enormous amount of investment needs to be allocated to building hydrogen pipelines (the natural gas pipeline is unfit to transport pure hydrogen [94]). In the mean while tube trailers are a transportation method with acceptable of cost [53].

2.6.1.2 Liquid hydrogen

The volumetric density of liquid is more than doable that of compressed hydrogen [95]. However, the boiling point of liquid hydrogen is around 20 K or -253°C, thus gases hydrogen have to be cooled to that temperature for it to liquefy. The liquefaction of hydrogen requires large amount of energy and time. It is calculated that liquefaction process costs between $30-40\%$ of the energy of stored hydrogen, in comparison compressed hydrogen only loses 10% of its energy content [85, 96]. Additionally, liquid hydrogen tanks also loses $0.1-1\%$ of its content due to boil off each day, the exact rate is inversely related to the volume to area ratio [97]. Liquid hydrogen is only suitable for large quantity transport over long distances. Liquefied hydrogen can be transferred by cryogenic tanker (ship, train or truck). In theory liquid hydrogen can also be transported by a pipeline system. However the entire pipeline will need to be cryogenically cooled, which will increasing the energy loss. More over the pipe line system will also experience a larger boil off effect due to increased surface area.

There exists a third method of storing and transferring pure hydrogen called cyro-compressed hydrogen. This method keeps hydrogen at high pressure and low temperature as a supercritical fluid. Hydrogen in this supercritical fluid state has an even higher density than liquid hydrogen. But currently, the overall energy efficiency of cyro-compressed hydrogen is worse than liquid hydrogen. For more details about this technology please refer to [98].

2.6.2 Hydrogen in a carrier

There are two main types of hydrogen carriers: chemical carriers that absorb and release hydrogen though chemical reactions, and physical carriers that are porous and hold hydrogen in the void spaces within the carrier materials. The storage capacity for these carriers are summarized in Table 2.2. One of the most studied chemical carrier is metal hydrides, which is considered as one of the more promising candidates for on-board storage to replace the current compressed gas storage method [99]. Another type of chemical carriers that received more attention lately is the Liquid Organic Hydrogen Carriers (LOHCs). However the low storage capacity, as seen in Table 2.2, limits the application of LOHCs. Although hydrogen carriers have much better storage capacities (in terms of wt%) than compressed or liquid hydrogen [85], various technical challenges, like charge-discharge kinetics, material weight and cost still needs to be addressed before any of them are commercialized. More information can be found in the references given in 2.2. Recent review of different hydrogen carriers can also be found in [99].

In terms of transportation methods, some of the chemical hydrogen carriers are in the liquid form, e.g. LOHCs and formic acid, and can be transferred via specialized pipeline systems or trucks. In the mean time, all of the physical carriers and several chemical carriers, like metal hydrides, are in solid form. In this case the carrier material needs to be processed and integrated into the storage containers [11], which can then be carried by trucks.

Table 2.2: Maximum storage capacities (percentage of weight wt%) reported for a number of different physical and chemical hydrogen carriers. (modified from [11])

	Carrier	wt%	References
Chemical	Ammonia Borane	19.4	[100,101]
	Metal Hydrides	12.6	[102,103]
	Alanates	9.3	[104,105]
	Formic Acid	4.4	[106,107]
	Carbohydrate	14.8	[108]
	LOHCs	7.2	[109,110]
Physical	Carbon Materials	8	[111,112]
	Zeolites	9.2	[113,114]
	Glass Capillary Arrays	10	[115,116]
	Glass Microspheres	14	[117]

2.7 Hydrogen Refueling Station (HRS) location models

In this section the various approaches for planning FCEV refueling stations are discussed. Despite their different sets of constrains, both HRS planning and EVCS planning are special cases of the facility location problem [118,119], The facility location problem has many other real world applications, for example, supply chain management [120]. In the literature, there are many different ways to categorize the works regarding the facility location problem, such as, number of objectives [59] single/multi objective,randomness in the modelling [118] deterministic/Stochastic models, solving approaches [120] general solver/dedicated algorithm, structure of the planning area [121] discrete/continuous spaces or networks and types of demand modeling [122] point demand/flow based demand. As there is a clear preference to use flow based demand in traffic related models, in this review we classify the papers based on how demand is modelled in them.

2.7.1 Point demand models

In point demand models, the demand for service is localized at individual points or small polygonal sectors within the planning area [122]. There are three main sub categories covering problem, P-median problem and P-center problem. The following notations are used in this section for the formulation of these problems:

i	Index of customer/demand locations
j	Index of candidate facility locations
x_j	Binary variable equal to 1 if a facility is built at j, 0 otherwise,
y_i	Binary variable equal to 1 if node i is covered by a facility, 0 otherwise,
c_j	Cost of building a facility at location j,
a_{ij}	Binary variable with value 1 if the demand at location i can be serviced by facility at location j, 0 otherwise,
d_i	Demand at location i,
D_{ij}	Distance between demand location i and facility location j, which can be 0,
P	Limit for number of facilities,
z	Maximum distance between customer locations and their nearest facilities.

2.7.1.1 Covering problem

In covering problems, a facility can only service customers within a limited distance, that is to say there exists a limit S such that $a_{ij} = 1$ if and only if $D_{ij} \leq S$. Note in covering problems, a demand location can be covered/serviced by several facilities.

A straight forward objective of the model would be to cover all of the customer while minimizing the total cost of building facilities, such problems is referred to as total covering problems, first being formulated in 1971 [123]. Total covering problem is a real world application of the Set Covering Problem (SCP) [124]. The general formulation of the total covering problem is as follows:

$$\min \sum_j c_j x_j, \tag{2.9}$$

subject to

$$\sum_j a_{ij} x_j \geq 1; \forall i, \tag{2.10}$$

$$x_j \in \{0, 1\}; \forall j. \tag{2.11}$$

The objective function (2.9) aims to minimize the total cost of facilities. Eq. (2.10) ensures that every customer is covered by at least one facility. This type of formulation is applicable to the planning of emergency services, infrastructure and war-time facilities [121], where all of the demands must be covered.

In the original paper [123], it is assumed that it costs the same to locate a facility at any of the candidate locations, i.e. $c_j = 1, \forall j$, thus the objective function becomes:

$$\min \sum_j x_j. \tag{2.12}$$

which minimizes the number of the facilities instead of cost. The authors utilized integer programming method to solve this problem in the context of locating emergency services.

In [125] the total covering problem is applied to the planning of HRSs while considering each driver's scheduling and routing needs. In this study, to simplify the formulation and speed up the computing time, the maximum number of refuels per vehicle per day is set to 1. The case study of Irvine and Newport Beach showed that the proposed method can reduce the minimum number of facilities compared to models that does not consider routing.

The covering model is expanded by Tu et al. [122] to include temporal constrains, such as arrival time, wait time and charging duration, in the planning of charging stations for electric taxis. The objective of the modified problem is to maximize charging service level as well as the service level of electric taxis. A genetic algorithm is adopted to obtain the final solutions and a case study is conducted using GPS data in Shenzhen, China.

If the total number of facilities or cost is limited and the objective is to cover as many demand as possible then it is called a Maximal Covering Location Problem (MCLP), first being described in 1974 [126]. The general formulation is as follows:

$$\max \sum_i d_i y_i, \tag{2.13}$$

subject to

$$\sum_j a_{ij} x_j \geq y_i, \forall i \tag{2.14}$$

$$\sum_j x_j \leq P, \tag{2.15}$$

$$y_i, x_j \in \{0, 1\}, \forall i, \forall j, \tag{2.16}$$

Objective function (2.13) maximizes the demand covered. Constraint (2.14) ensures that demand can only be covered if a facility is within range. Constrain (2.15) limits the total number of facilities built. Constrain (2.16) is the integrity constrain. As noted by [126] such an approach is well suited for the planning of public services.

For example, in [127] the maximal covering approach is used to optimize the police patrol areas in Dallas, Texas in the US. This study also proposed a backup covering model, then geographic information system is combined with linear programming to find and convey the optimal solutions. Simulations carried out in this paper shows that the proposed method can achieve better incident coverage than existing arrangements.

To address the need of planning HRSs in the country of South Korea, in [38], a multistage planning method is developed. Firstly, the point based refueling demand is estimated using statistics from government agencies. Secondly, the total number of HRSs is determined based on a service level model. Then, the capacitated MCLP is solved to determine the locations of of HRSs. Finally, the P-median problem is solved to further improve the location results.

In the past four decades, researchers have developed many different variants of both SCP and MCLP, interested readers can refer to [128] for a detailed review of covering problems in the area of facility location.

2.7.1.2 P-median problem

Being described in 1964 by Hakimi [129], both the P-median and the P-center problem are actually relaxations of the covering problem [118], where theoretically any facility locations can service any one of the demand locations in the planning area. The P-median problem can be modeled as:

$$\min \sum_i \sum_j D_{ij} d_i a_{ij}, \tag{2.17}$$

subject to

$$\sum_j a_{ij} = 1, \forall i \tag{2.18}$$

$$\sum_j x_j \leq P, \tag{2.19}$$

$$a_{ij} \leq x_j, \forall i, \forall j, \tag{2.20}$$

$$a_{ij}, x_j \in \{0, 1\}, \forall i, \forall j. \tag{2.21}$$

As it can be seen in Eq. (2.17), the aim of this model is to minimize the total cost of the customers in terms of the demand-weighted travel distance. Eq (2.18) guaranties that each customer can only be serviced by one facility. Eq (2.19) and (2.20) set the limit for number of facilities and allows located facilities to serve customers, respectively. Eq (2.21) is the integrity constrain for binary variables.

In [129], the P-median model is used to find switching centers in communication networks, [25] used the P-median formulation to locate HRSs in Beijing, China by combining information of the existing petrol station network, traffic network, population and regional economic. A hybrid-solution approach is adopted in [25], where genetic algorithm is integrated with greedy algorithm to speed-up convergence and annealing algorithm to avoid converging to local optimums. Simulation results showed that the greedy algorithm can effectively reduce the solution space and the computational complexity. For more information, in [130] a detailed review of P-median problem and its variations in location science was provided.

2.7.1.3 P-center problem

The integer programming model for the P-center problem is as follows:

$$\min z, \tag{2.22}$$

subject to

$$\sum_j D_{ij} a_{ij} \leq z, \forall i, \tag{2.23}$$

$$\sum_j a_{ij} = 1, \forall i \tag{2.24}$$

$$\sum_j x_j \leq P, \tag{2.25}$$

$$a_{ij} \leq x_j, \forall i, \forall j, \tag{2.26}$$

$$a_{ij}, x_j \in \{0, 1\}, \forall i, \forall j. \tag{2.27}$$

The objective function (2.22) and constrain (2.23) together minimize the maximum distance between any given demand location and the facility that services it, which is why the P-center problem is classified as a minmax problem [118]. Constrains (2.24)-(2.27) are exactly the same as constrains (2.18)-(2.21) for the P-median problem.

The goal of the P-center problem is to improve the worse case scenario for all customers [121]. Thus, it is well suited for public/emergency services. For instance, in the original paper [129] P-center problem was solved to locate police stations and hospitals. Due to the NP-hard nature of the P-center problem, obtaining exact solutions may not always be practical and heuristic approaches are adopted [121]. A detailed review of different exact and heuristic approaches used to solve P-center problems can be found in [131].

For locating refueling stations for AFVs, in [132] the core idea of P-center problem, improving the worst case scenario , was combined with flow based demand modelling to form a "p-center flow-refueling problem". The model is designed to locate P refueling stations while trying to minimize the maximum percentage of deviation for each driver. An Implicit enumeration algorithm is employed to find exact optima. The numerical results showed that for the save level of deviation there exists different equally optimal solutions. Additionally, small increase in either vehicle range or number of stations does not always lower the maximum deviation.

In [133], the P-center problem was integrated with robust optimization to solve the reliable facility location problem. In the reliable facility location problem the allocated facilities need to provide service to all customers even if some of the facilities has been disrupted by, for example, nature disasters. The authors formulated a two-stage robust location model and applied three different solution methods. Extensive numerical tests are carried out to examine the performance of the solution methods as well as to compare the proposed model with other reliable location models. The simulation results showed that the proposed reliable the P-center problem can achieve better coverage in the worst case scenarios while other methods have better average performance among all cases.

2.7.2 Flow based models

In point demand models the demands are located at or aggregated to nodes of the network and demands are met via node to node travel [134]. However, in some cases the main goal of a customer is not to obtain a service but to travel between a predefined origin-destination (OD) pair and if a facility happens to be located along the corresponding path the customers may choose to visit it [135], some examples of this type of business include fast food shops, automatic teller machines (ATMs) and fuel stations. To better encapsulate the characteristics of flow based demand, location models that "intercept" traffic flow have been developed, namely the Flow Capturing Location Model(FCLM) [136] and Flow Refueling Location Model(FRLM) [137].

2.7.2.1 Flow Capturing Location Model(FCLM)

The integer programming formulation of FCLM require the following notations:

i	Index of facility locations
q	Index of paths
x_i	Binary variable equal to 1 if a facility is built at location i, 0 otherwise,
y_q	Binary variable equal to 1 if there is a facility on path q, 0 otherwise,
f_q	Flow of traffic on path q,
I_q	Set of potential facility locations on path q,
P	Limit for number of facilities.

The objective is:

$$\max \sum_{q} f_q y_q, \tag{2.28}$$

subject to

$$\sum_{i} x_i \leq P, \tag{2.29}$$

$$\sum_{i \in I_q} x_i \geq y_q, \forall q \tag{2.30}$$

$$x_i, y_q \in \{0, 1\}, \forall i, \forall q. \tag{2.31}$$

As shown in the objective function (2.28), this model aims to maximize the total captured flow. Eq (2.29) limits the total number of facilities to be located. Eq (2.31) ensures that the flow on path q can only be captured if at least one facility is built along q.

Similar to other facility location models, the FCLM is also NP-hard [138]. Therefore, solutions are often obtained with heuristic methods [139,140] or approximation approaches [56,141]. There have been many different extensions of the FCLM that consider different factors such as limited facility capacity [142], drivers taking detours to refuel [143] or to avoid check points [144]. In [145,146] a more generalized formulation for FCLM was provided and it is proved that many extensions are just special cases of the generalized model.

The FCLM was extended by Wu and Sioshansi [56] into a two stage model that consider the uncertain nature of traffic flow as well as the fact that drivers may take detours from their intended path to refuel their cars. However, the resulting model is intractable, hence, the authors proposed a ample-average approximation method to tackle this issue. A case study using data from Central Ohio, US was carried out. The case study showed that optimal solution of the introduced model can increase the percentage of BEVs that can complete their daily tours. In addition, the case study also showed that the stochastic model can achieve better demand coverage that its deterministic version.

2.7.2.2 Flow Refueling Location Model(FRLM)

In the FCLM it is assumed that drivers can complete their trip with just one facility along the desired path. Yet for AFCs, especially in the early stages of AFCs deployment, their limited range means that several refueling stations may be needed along the desired path. To address this concern the FRLM was proposed by Kuby and Lim [137]. The following additional notation is needed to convert FCLM to FRLM:

j	Index of combinations of facility locations
a_{ij}	Binary variable equal to 1 if a facility i is built in combination j , 0 otherwise,
b_{jq}	Binary variable equal to 1 if facility combination j can service path q, 0 otherwise,
l_j	Binary variable equal to 1 if all facilities in combination j is built, 0 otherwise,

The model is

$$\max \sum_{q} f_q y_q, \tag{2.32}$$

subject to

$$\sum_{j} b_{jq} l_j \geq y_q, \forall q, \tag{2.33}$$

$$a_{ij} x_i \geq l_j, \forall j; i | a_{ij} = 1, \tag{2.34}$$

$$\sum_{i} x_i \leq P, \tag{2.35}$$

$$x_i, l_j, y_q \in \{0, 1\}, \forall i, \forall j, \forall q. \tag{2.36}$$

Similar to FCLM, the objective of FRLM (2.32) is to maximize the serviced traffic flow. However, instead of requiring one facility to be located along path q to capture the flow, constrain (2.33) requires at least one combination of facilities, that satisfies the range requirements of AFVs, to be build along path q in order to capture the traffic. Constrain (2.34) sets l_j to one if and only if all facilities in combination j are built. Constrains (2.35) and (2.36) serve the same purpose as (2.30) and (2.31) in the FCLM.

As noted in [137], the FRLM requires all of the combinations of facility locations to be generated, which is infeasible for practical applications. To address this issue various reformulations of FRLM have been brought forward, see [147–149] for these reformulations.

Table 2.3: Summary of Facility location literature covered in this section

Demand type	Model	References
Point-based	SCP	[122,123,125]
	MCLP	[38,126,127]
	P-median	[25,38,129]
	P-center	[129,133]
Flow based	FCLM	[56,142–144,146]
	FRLM	[132,137,147–150]

For example, in [150] the problem of locating wireless charging stations for BEVs was studied while the drivers' routing behaviours was modeled with stochastic user equilibrium. The authors of [150] formulated the modified FRLM as a mixed-integer nonlinear program (MINLP). Different linearization methods were deployed to convert the MINLP to a mixed-integer linear program (MILP), then a commercial solver is used to obtain the final solution. Simulation studies showed that the developed model resulted in different EVCS locations and traffic flow patterns comparing with another model that assumed drivers' will choose the shortest route.

In contrast to the original FCLM and FRLM, which are both based on the maximal covering approach, a P-center formulation of FRLM was implemented in [132], where he objective is to minimize the maximum detour of each driver. For more examples of the different extensions of flow based models, one can refer to [151, 152] and the references therein.

The location models covered in this section are summarized in Table 2.3. So far this section has only been discussing single objective location models. It is worth noting that all of the facility location models can be extended to multi-objective optimization models. One classical approach is the scalarization method where different objective function is added together as a weighted sum. For example, in [153] the FCLM and P-median model was combined, and the objective function is a weighted sum of the two objectives. A different approach can be seen in [154], where the objective of maximal coverage, P-median, and P-center problems were considered, a pareto optimal method was adopted to find the non-dominated solutions. Another example of the pareto frontier approach is [45]. In [155] the different heuristic techniques for multi-objective optimization was reviewed , more examples of multi-objective location problem can also be found inside.

2.8 Fuel cell technologies

At the final step of hydrogen's life cycle, hydrogen is converted to heat and electrical energy in fuel cells. According to [12], the fuel cell technologies are mainly classified by the electrolyte they use to carry charges between cathodes and anodes. However there are fuel cells that are classified by their fuel types, e.g.direct methanol fuel cells.

In this section, we will review the different types of fuel cell technologies and their limitations. The major types of fuel cells and some of their suitable applications are given in Table 2.4, note that Biofuel cells (BFCs) are excluded from Table 2.4 as they are designed for more niche applications.

2.8.1 Alkaline Fuel Cells (AFCs)

AFCs,also known as Bacon fuel cells. were first developed by Francis Thomas Bacon, and saw practical use by NASA in the Apollo program and later in the space shuttle program for generating electricity and drinkable water [156]. AFCs typically use potassium hydroxide (KOH) solution as electrolyte, with the OH^- ion being the charge carrier.

AFC is one of the most mature and the most efficient fuel cell technologies. In AFCs between 60 to 70% of the energy stored in hydrogen is converted to electricity [157]. Another advantage the AFCs have is that the catalysts on the electrodes can be made from a variety of relatively inexpensive metals [13], such as nickel and sliver. This flexibility in catalyst material also leads to the AFC being the cheapest fuel cell type. Furthermore, operating temperature of AFCs is around 100°C leading to fast start time [12].

The main drawback of the AFC is that it is susceptible to CO_2 poisoning. The mechanism for poisoning is that first CO_2 will react with the KOH in the electrolyte thus reducing its

Table 2.4: Fuel cell types and their suitable applications.(Compiled from [12–16])

Category	Applications	AFC	PAFC	PEMFC	SOFC	MCFC	DAFC
Transportation	Passenger vehicles	✓		✓			✓
	Trucks			✓	✓		
	Forklifts			✓			✓
	Buses		✓	✓			
	Logistic vehicles	✓		✓	✓		✓
	Aviation			✓			
	Marine	✓	✓	✓	✓	✓	
	Locomotive		✓	✓	✓		
	E-bikes			✓			✓
Stationary power	Combined heat and power (CHP)	✓	✓	✓	✓	✓	
	Uninterruptible power systems (UPS)	✓		✓			✓
	Distributed Power Generations	✓	✓	✓	✓	✓	
Other	Portable power	✓		✓	✓		✓
	Unmanned Aerial Vehicles (UAVs)			✓			

conductivity, then the K_2CO_3 formed will deposit on the catalyst site and further reduce the performance of the cell. In fact the 0.04% CO_2 in air [158] is enough to significantly reduce the efficiency and life span of the cell. In practical applications the vehicles usually need to use pure hydrogen and either carry pure oxygen on board or have a extra device to remove CO_2 from air for the AFCs to function properly. Moreover, the electrolyte solution in AFC is highly corrosive, leading to issues with the seal of the fuel cell and reduced life span.

Due to the above mentioned issues research interest in AFCs have dwindled since the 1990s after the advancement of PEMFC [2]. But in recent years, there has been a renewed interest in AFCs particularly anion-exchange membrane fuel cells (AEMFCs), which uses solid electrolytes and hops to alleviate much of the issues with traditional AFCs [159]. However currently the AEMFCs still have several problems that need to be addressed before commercial application. For instance, performance stability issues caused by chemical degradation [159].

Examples of EVs using AFCs includes the 1966 GM Electrovan [160], which is the first fuel cell powered vehicle.

2.8.2 Phosphoric Acid Fuel Cells (PAFCs)

PAFC is the first commercial fuel cell type and is the most widely used fuel cell type before the 21 century [161]. As its name suggests PAFCs use liquid phosphoric acid (H_3PO_4) as electrolyte. The common usage for PAFCs is for stationary Combined Heat and Power (CHP) generation. As a result of having low energy density PAFCs require more space, thus can only be fitted into larger vehicles such as buses [162,163] and trains [164]. Apart from having low power density, one other issue the PAFC faces is its low electrical efficiency. Although the efficiency of PAFCs for CHP is around 80% [164], when generating electricity alone PAFC is only $30-45\%$ efficient [13], which sits narrowly above the energy efficiency of ICE ($20-30\%$ [165, 166]). Moreover, PAFCs use platinum as catalyst and have a higher catalyst loading, resulting in the price being high [12]. Similar to AFCs, the liquid electrolyte of PAFCs is also highly corrosive, resulting in limited cell life. As PAFCs operate between 160 – 220°C, they have a relatively slower start time.

The main advantage of PAFC is its ability to handle impurities in both hydrogen and the oxygen sources [167]. Since PAFC uses acidic electrolyte the presence of CO_2 does not affect cell performance. thus air is usually the oxygen source. Unlike PEMFC, PAFC can also tolerate up to 1.5% of carbon monoxide (CO) content, leading to it's wide adoption [168].

2.8.3 Proton Exchange Membrane Fuel Cells (PEMFCs)

Unlike AFCs or PAFCs which use liquid electrolytes, PEMFCs use solid PEMs as electrolytes. The polymer membrane is the most important part of the PEMFC and contribute to around 30% of the component cost for the cell [167]. Since PEMFCs do not use corrosive liquid electrolyte, they have a longer cell life. PEMFCs have been the focus of fuel cell research since the 1990s [13] because it is highly modular and have high power density. In fact PEMFCs have the highest power density among all of the fuel cell technologies [12], making them particularly suitable for applications such as automobiles where space is of concern. Moreover, start time of PEMFCs is short since the operating temperature of is between 50 – 100 °C. The use of acidic electrolyte in PEMFCs makes them indifferent to the presence of CO_2 , thereby ambient air can be used as oxygen source. The energy efficiency of PEMFCs is 40 – 60% which is lower than AFCs but much higher than ICEs.

Similar to PAFCs, PEMFCs also require expensive platinum catalyst at its electrodes leading to high cost, nevertheless, the catalyst loading of PEMFCs is lower than that of PAFCs [169]. In addition the platinum catalyst in PEMFCs is very susceptible to CO poisoning [170]. Currently the limit for CO concentration in hydrogen for vehicle use is 0.2 ppm [171], which is well above the CO content in reformed hydrogen [172]. Furthermore, PEMFCs require complex water and heat management systems. In a PEMFC too much water accumulated in the cell will cause flooding, while too little water will make the PEM to dry up, both of these conditions will reduce the performance of the cell [173].

Examples of FCEVs using PEMFCs include the Toyota Mira [174], which is the first commercially available FCEV.

2.8.4 Direct Alcohol Fuel Cells (DAFCs)

As their name suggests DAFCs uses alcohol as fuel. Most of DAFCs are based on PEM technology, while alkaline cells have also been developed [14]. There are currently two major variants of DAFCs that have seen some commercialization, Direct Menthol Fuel Cells (DMFCs) that use menthol as fuel, and Direct Ethanol Fuel Cells (DEMCs) that use ethanol as fuel. There also have been attempts to develop Direct Ethylene Glycol Fuel Cells (DEGFCs), but DEGFCs are yet to be commercialized [175]. DAFCs are considered as newer types of fuel cells with DMFC being first invented in 1990s. The reasoning for developing DAFCs are very straight forward: alcohols can be produced from a variety of sources(fossil fuels or biomass) [14], all of them are already being produced in large quantities [176–178], all of them have high volumetric energy density [179], and they are in liquid state at room temperature resulting in straightforward storage and transportation methods.

However, currently DAFCs require expensive catalysts and high catalyst loading. For instance DEFCs also uses platinum catalyst and the loading is higher than PEMFCs [180]. Another hurdle that DAFCs face is the slow reaction kinetics at the anode [181] which limits the maximum power output. Moreover, all of the DAFCs suffer from fuel crossover where the fuel will pass though the membrane resulting in problems like reduced performance and lower energy efficiency [182]. For example, the current DMFCs are only $20-30\%$ efficient [183] which is at the same level as ICE. In addition DAFCs will form side products, e.g. CO, aldehydes and acids, that will cause complications like catalyst poisoning and electrode corrosion during operation [15].

As a result of the aforementioned limitations DMFCs and DEFCs have only seen commercialization in portable electronic devices, such as mobile phones and laptops [184,185] and DMFCs have also been used in small vetches like forklifts [186]. Please note that most methanol fuel cell vehicles, like the Gumpert Nathalie [187], are not using DMFCs. Instead methanol fuel cell vehicles actually have on board reformers to convert methanol to hydrogen and use the hydrogen in PEMFCs.

Apart from alcohols, other liquid or liquid solutions,such as formic acid [188], dimethyl ether [189], borohydride [190] and hydrazine [191], have also been considered for direct fuel cell applications. But they are still purely experimental.

2.8.5 Solid Oxide Fuel Cells (SOFCs)

In SOFCs the electrolytes are zirconia-based ceramic that conducts oxide ions (O2-). Most SOFCs operates near 1000°C but there have been newer models where the operating temperature is reduced to $500-800$°C [192], nevertheless all SOFCs are considered as high temperature fuel cells. One major advantage of SOFCs is fuel flexibility. As a result of the elevated operating temperature SOFCs have the ability to use light hydrocarbons [193] and CO as fuel directly or by internally reforming them into hydrogen [194]. Furthermore, the elevated temperature also eliminates the need of expensive catalyst [195]. Additionally the efficiency of SOFCs for generating electricity alone is $50-65\%$ [196], the overall fuel efficiency can be further boosted (80%) if SOFCs are coupled with gas turbines or used for CHP [197,198].

The high operating temperature of SOFCs also brings a set of problems. To begin with, SOFCs requires adequate thermal shielding in order to maintain the high temperature and achieve high energy efficiency, resulting in increased size and lower power density [13]. Another issue of SOFCs is that the start up time is slow [199] partly caused by the high temperature. The other factor contributing to the slow start up of SOFCs is that, if the heat is supplied too quickly or unevenly, the solid ceramic electrolytes might crack under thermal stress [200]. Currently SOFCs also have durability issues caused by processes like electrode corrosion [201,202], carbon deposition [203] and thermal cycling [204]. Despite the fact that expensive catalyst is not required, the overall cost of SOFCs are still high due to strict material requirement and complicated manufacturing process [205]. SOFCs are also sensitive to sulfur contaminates [206].

One way to extend the cell life of SOFCs is to reduce the frequency of start ups and shut downs, thereby reducing the thermal stress the stack experiences. This, coupled with the long start up time, means SOFCs are usually considered as an option for stationary power generation [207] or for heavy duty vehicles such as trains [208]. However companies have tried to adapt SOFCs to power automobiles, with Nissan unveiling the first prototype SOFC car in 2016 [209].

2.8.6 Molten Carbonate Fuel Cells (MCFCs)

MCFCs use liquid alkali carbonate salts, a binary or ternary mixture of Li_2CO_3, Na_2CO_3 and K_2CO_3, as the electrolyte and operates at $600-700$ °C (the melting point of carbonate salts). MCFCs are also categorized as high temperature fuel cells and share some of the strengths and weaknesses with SOFCs, such as high energy efficiency [210], fuel flexibility [211, 212], inexpensive catalyst [213], long start time, durability issues [214], low power density [156] and intolerance of sulfur compounds [206]. In addition, as MCFCs operate at a lower temperature, MCFCs have less strict material requirement than SOFCs [13]. Like other fuel cells that uses corrosive liquid electrolytes, MCFCs also have seal issues [215]. However, MCFCs also have drawbacks that are unique to them. For example, there is a net transfer of CO_2 from the cathode to the anode during operation of MCFCs [216], thus additional auxiliary systems are need to inject more CO_2 to the cathode either by recycling CO_2 from anode [157] or from another CO_2 source [217]. Further more, catalyst dissolution is another issue that reduces the life span of MCFCs [213].

Due to the low power density, long start up time and the need for auxiliary systems, MCFCs are not satiable for FCEV applications. But MCFCs are useful in applications where space and start time is of less concern, for example stationary power generation and large watercraft [156]. More recently, MCFCs have been investigated as a tool to concentrate CO_2 in CCS systems for fossil fuel power plants [218].

2.8.7 Biofuel Cells(BFCs)

BFCs uses biological processes to convert fuel (usually organic compounds) to electricity. There are two different types of BFCs: Enzymatic Fuel Cells (EFCs) that uses immobilized protein catalysts (enzymes) at its electrodes and Microbial Fuel Cells (MFCs) that have living organisms (often bacteria) act as catalysts. One of the proposed usage for BFCs is for powering medical implants [219] due to BFCs mild operating temperatures and PH level. The application that is closet to commercialization is using MFCs for waste water treatment [220, 221].

Currently, BFCs are still being actively developed and researched with several barriers to over come, such as very low power density [222] and current output [223], slow conversion rate [224], high manufacturing cost [225], poor understanding and optimization of the electron transfer mechanisms [226] and strict operational conditions [13].

2.9 Conclusion

Due to the growing concerns regarding the climate emergency, more and more countries begin implementing policies and investments to accelerate the electrification of transportation in order to reduce GHG emission. Hydrogen and FCEVs are considered by many as important tools to achieve this transformation. In this chapter various topics that are critical to using hydrogen as a energy carrier for transportation, namely hydrogen production methods , hydrogen storage and transport methods, fuel cell technologies and HRS planning models, are reviewed. The strengths of each technology/method/model are disused as well as the challenges each of them faces and their short comings. These challenges and short comings can serve as focus points for future researches. This review covers literature spanning the last several decades. However due to the large number of 6 topics covered in this review, it is not possible to cover every detail of each topic, thus additional references are provided should the readers require more information.

Chapter 3

Data-driven Planning of Electric Vehicle Charging Infrastructure: A Case Study of Sydney, Australia

3.1 Relationship to the Thesis

In Chapter 1, one of the research gaps that have been identified is that there lacks a market-based planning approach for EVCSs. In this chapter a data-driven competitive planning framework for EVCSs is developed and validated with a real-world case study of Sydney, Australia.

This Chapter is written from: C. Li, Z. Dong, G. Chen, B. Zhou, J. Zhang, and X. Yu, "Data-driven planning of electric vehicle charging infrastructure: A case study of Sydney, Australia," IEEE Transactions on Smart Grid, pp.1–1,2021.

This chapter has been edited to incorporate thesis reviewers' comments.

Nomenclature

Set	
$\hat{\mathcal{A}}_q$	the set of arcs on path q in the expanded TN
$\hat{\mathcal{H}}$	the set of hours
$\hat{\mathcal{I}}_q$	the set of nodes on path q in the expanded TN
$\hat{\mathcal{M}}$	the set of months
$\mathcal{E}$	the set of edges between nodes
$\mathcal{I}$	the set of nodes in the TN
$\mathcal{M}$	the set of companies in the competitive market
$\mathcal{Q}$	the set of paths
$\mathcal{X}_m$	the set of feasible budget allocation domains for company m
$\mathcal{V}$	the set of nodes
Functions/Operators	
$\mathbb{F}(x)$	the fixed-point map
$\mathbf{f}_m(\cdot)$	the payoff function for company m
$\mathcal{F}(\cdot)$	the nonlinear prediction function
$\phi(\cdot)$	the function to stack all adjacency matrices
$\Phi : (\mathcal{X} \times \mathcal{X}) \to \mathbb{R}$	ρ-regularized *Nikaido–Isoda* function
$\Psi(\cdot)$	the charging serviceability function
$\sigma(\cdot)$	the activation function
$C_i(\cdot)$	the cost function of the construction cost of EVCS as well as the cost associated with waiting time
$SIM(\cdot)$	the cosine similarity function
$tanh(\cdot)$	the tanh function
$tr(\cdot)$	the trace of a matrix
Parameters of Matrix Factorization	
α, β	the l_2 regularisation parameters
γ_g	the graph regularization parameter
$\mathbb{S}$	the temporal traffic flow matrix

$\hat{\mathbb{S}}$	the spacial traffic flow matrix
$\hat{s}_j^n$	the summed traffic flow for node n at the j-hour
$\mathcal{G} = (\mathcal{V}; \mathcal{E})$	the relation network that includes nodes and edges
A_g	the adjacency matrix describing relation g
a_{ij}^1	the spatial proximity between zone i and j
a_{ij}^2	the region similarity between zone i and j
a_{ij}^3	the TN connections between zone i and j
D_g	the degree matrix for graph g
L_g	the Laplacian for graph g
$P \in \mathbb{R}^{N \times K}$	the matrix of size $\mathbb{R}^{N \times K}$ used for the low rank K approximation in spatial matrix factorization
$Q \in \mathbb{R}^{K \times H}$	the matrix of size $\mathbb{R}^{K \times H}$ used for the low rank K approximation in spatial matrix factorization
$U \in \mathbb{R}^{M \times K}$	the matrix of size $\mathbb{R}^{M \times K}$ used for the low rank K approximation in the temporal matrix factorization
$V \in \mathbb{R}^{K \times H}$	the matrix of size $\mathbb{R}^{K \times H}$ used for the low rank K approximation in the temporal matrix factorization
s_{ij}	the traffic flow at hour j in month i
Parameters of Deep Neural Network	
$\hat{\mathcal{Y}}_{t+\kappa}$	the κ-step-ahead predicted traffic flow volume at time t of all nodes
$\hat{A}$	the adjacency matrix with a self-loop connection
$\hat{D}$	the diagonal node degree matrix
$\mathrm{H}^{l,p} \in \mathbb{R}^{1 \times P} (P \leq 3)$	the kernel of 1D convolution at layer l for graph g matrix
$h_t^{'}$	the current memory at time t
h_t	the final memory at time t
l	the layer index
W^l	the weight matrix of layer l
X_t^{l+1},X_t^l	the output and input matrices of layer l at time t
X_{t+Z}	the observed features of N nodes at time $t+Z$
z_t	the update gate at time t

r_t	the reset gate at time t

Parameters of Game Model

Γ	Cournot competition game
μ_m	the utility parameter regarding the charging time
ν_i	the construction cost parameter for zone i
π_i	the service benefit basic price at the ith zone
ρ	the regularization parameter
τ, ζ	the precondition parameters of the accelerated fixed-point map
S_i	the charging demand
θ_i	the parameter related to waiting time, given S_i
B_m	the budget of company m
$E_i^{\max}$	the capacity constraint of the DN
$E_i^{\min}$	the policy constraint

Parameters of Optimal Sizing

η_i	the income coefficient at zone i
$\hat{n}_{i,k}^m$	the maximum number of level-k EV charging post at the ith zone
$\hat{x}_{m,i}$	the budget of company m for constructing EVCS and charging posts at zone i
λ_{ij}^q	the fraction of charging demand on path q from node i to j
λ_{OD}^q	the fraction of unsatisfied charging demand on path q from node O to D
$\overline{I}_{s,t}$	the upper limit of current for line s, t
$\underline{V}_s/\overline{V}_s$	the lower/upper limit of nodal voltage at bus s
ς_s	the square of the magnitude of the nodal voltage at bus s
ϑ	the phase angle between EV charging voltage and current
$\xi_{s,t}$	the impedance of line s, t
$\xi_{s,t}^*$	the conjugate of $\xi_{s,t}$
c_e	the electricity cost caused by EV charging demands
c_p	the penalty cost due to unsatisfied charging demand
$F_{s,t}$	the power flow in line s, t from bus s to bus t

f_s	the nodal power injection at bus s
$l_{s,t}$	the square of the magnitude of the current in line s,t from bus s to bus t
p_k	the charging power of the Level-k EV charging posts
r_k	the revenue generated by Level-k EV charging post
S_q	the traffic flow on path q
Decision Variables	
$\mathbf{x}_{-m}$	the variable describing the strategies of companies beside m
$\mathbf{x}_m$	the variable describing the strategy of company m
$\mathbf{y}_m$	the strategy variable of ρ-regularized *Nikaido–Isoda* function given $\mathbf{x}_m$
$\zeta_{i,k}^m$	the binary variable indicating whether an EVCS containing Level-k EV charging posts is built at zone i
$n_{i,k}^m$	the integer variable corresponding to the number of the Level-k EV charging posts in the EVCS at zone i built by company m
$x_{m,i}$	the allocated budget on zone i from company m

3.2 Introduction

The modern world continues to recognise EVs' advantages to the society and environment [227]. Additionally, technological advancements continue to increase EVs' range while reducing their cost, an increasing number of people are viewing EVs as a viable choice of transportation. As a result, the market share of EVs continues to grow in Australia, which means that the need for EVCSs is also increasing.

The current studies on EVCS planning fall into two categories [228], namely point demand models and flow demand models. In point demand models, the charging demand is located at individual points or polygons, while flow demand models consider demand to be the flow between points [229]. For instance, in FCLM [136], the EV charging demand is represented by the drivers seeking for a EVCS during the journey between origin-destination (OD) pairs. An OD matrix is required to estimate the distribution of EV charging demand

and locate EVCSs to maximise the captured traffic flows [230]. In [228], the CFRLM is proposed by including DN constraints and deploying queuing theory to determine the locations of EVCSs. In point based models, it is assumed that EV charging demand is concentrated at certain point of interest, and the demand is estimated based on nearby traffic flow counts over a period of time [231]. Usually the time cost is the primary concern of such models and the objective is to minimise the travel time while maximising the covered demand for a given number of EVCSs [232]. In [233], a multi-period fast charging location planning model, that can adjust to varying charging demands, is developed by incorporating demand dynamics.

Yet, without a deep knowledge of the TN and the corresponding traffic flow data, it is difficult for the Australian energy sector to have an accurate estimate of EV charging demands, resulting in the sub-optimal deployment of EVCSs. In a recent report, Australian Electric Vehicle Council [227] pointed out that the number of Australian EVCSs is far fewer than other developed nations like U.K. and U.S., with inadequate government funding being the primary reason. In addition, if government investment led the EVCS development plan, it will likely result in a monopoly market which causes various inefficiencies [234]. Hence, private investments should be allowed in the market of EVCS construction and management [235]. To be a successful company, EVCS providers must deliver high-quality services while competing in a free-market [236]. Therefore, to encourage private service providers to invest in EVCSs, it is necessary to design a market-based planning framework. A versatile game-theoretic model is employed in [237] to model the competitive market for EVCS providers. In this model each EVCS provider seeks to maximise their profit by optimally sizing and sitting EVCSs as well as setting charging prices. In [238], the competitive charging behaviors are studied and a charging congestion game is developed to locate EVCSs. Further, Global Positioning System (GPS) data of each vehicle cannot be given to third parties, as per Australian data privacy regulations, thereby limiting one's ability to determine EV charging demand. Theoretically, one can obtain travel profiles by crowdsourcing mobile data [239]. However, in Australia, estimating EV charging demand from GPS data of individual vehicle is difficult due to aforementioned privacy regulations. The spatial-temporal distribution of EV charging demands can estimated using GIS and household travel survey (HTS) information with a probabilistic model [240]. Additionally, a practical market mechanism should also include local economic elements in the planning of EVCSs.

Here are the three main contributions of this chapter.

i) A data-driven framework for optimal planning of EVCSs is developed in the perspective of private companies, adopting a market-based mechanism in a competitive environment. The introduction of a predict-then-optimize diagram aims to forecast the future traffic flow by neural network methods. Then, the EVCS planning strategy for each company is optimised based on the projected traffic flow.

ii) Developed a spatial-temporal missing data imputation method which utilised data-based analysis of the publicly-available TN data in Sydney. The missing data issue, which often exists in real-world data sets, is then addressed by imputing the missing traffic data. In the state of New South Wales (NSW), Australia, the traffic counter data are open for public access. Consequentially, EV charging demand estimation can be based on traffic count data and the optimal budget allocation of EVCSs can can be obtained with a point demand model. To deal with various relations among different nodes, a graph convolutional network (GCN) based on multi-graph fusion is constructed by capturing the spatial information from the traffic flow.

iii) The Cournot competition amongst multiple EVCS providers is described with a game-theoretical model. There is few research focusing on EVCS planning from a competitive market perspective. In a competitive market, private companies compete to allocate EVCS by focusing on maximising their profits and limiting the capital expense. Additionally, from a micro perspective, an MILP model is utilised to size individual EVCSs for each company with for individual zone considering the DN constraints.

The organisation of the remaining sections of this chapter are as follows. A data-driven framework for optimal planning of EVCSs is presented in Section 3.3. The data-based

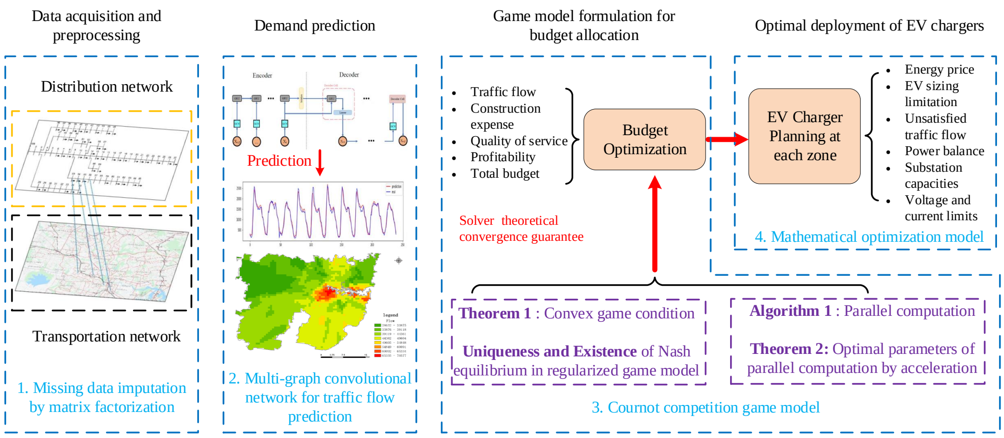

Figure 3.1: Flow chart of the data-driven framework for EVCS planning

approach for EV charging demand estimation is detailed. A data imputation method is proposed. The demand prediction method is given. The Cournot competition model is explained in Section 3.4. This model is then used for allocating EVCS budget to each planning zone. A parallel algorithm is developed to derive the Nash equilibrium. Further, the EVCSs are sized optimally with respect to three charger levels. The experimental results for the optimal planning of EVCSs are given in Section 3.5. Finally, Section 3.6 gives the conclusion of this chapter.

3.3 Data-driven Model on EV charging infrastructure planning

It is assumed that different private companies have a competitive relationship in the planning of EVCSs. In addition, each of the companies seeks to maximise overall profit while operating with fixed budgets. To this end, a data-driven method is developed with the goal of maximising the profit of EVCS provider while minimising the overall cost. The discomfort of EV drivers is also penalised in the form of additional cost to maximise the captured traffic flow. As shown in Fig. 3.1, the solution to EVCS planning includes a *Predict, then Optimize* diagram, in which the EV charging demand is first projected with big data analysis. Afterwards, the EVCS planning result is optimised by the game theory model based on the predicted charging demand.

In the first step, which is data acquisition and pre-processing, DN and TN data are gathered from NSW public services for Sydney. This resulted in adequate data sets for subsequent machine learning steps.

In the prediction step, the EV charging demand of Sydney is estimated via the traffic flow. The EV charging demand estimation is improved by extracting deep insight from economic activities, which represents the people's behaviours to a certain degree. In particular, to address the absence of TN data, a spatial-temporal data imputation method is developed. As [122] pointed out, the EV charging demand is correlated to the daily traffic flow. By thoroughly utilising the spatial-temporal understanding [241], a novel multi-relation GCN is proposed for uncovering the many spatial relations within TN. The projected traffic flow of the whole city is derived in this step. The EV charging demand is then evaluated according to the projected traffic flow.

Next, a Cournot competition model is developed for the budget allocation step. The allocation of EVCS budgets for each company and each zone is determined by the competition model. A conceptual analysis of the competition model is given such that the readers can have a better comprehension on the optimal sizing and sitting of EVCSs. An efficient parallel algorithm is also developed to find the Nash equilibrium in a timely manner. At the end of this step, the optimal budget allocation for each EVCS provider will be decided for all the planning zones.

Lastly, in the optimal sizing of EVCS step, an MILP model is adopted for acquiring the optimal EVCS sizing result by including local DN constraints and serviceability constraints. The optimised EVCS deployment plan that can service the projected EV charging demand is obtained at the end of this step.

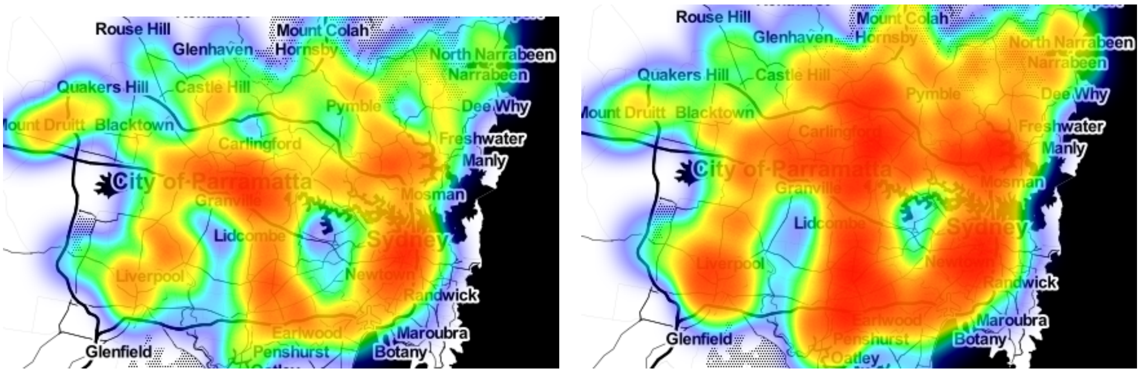

(a) 2008 (b) 2018

Figure 3.2: The average daily traffic flow for 2008 (a), and 2018 (b). High volumes of traffic flow are depicted in red.

3.3.1 Data set for predicting EV charging demand

As mentioned above, to predict future EV charging demand, a new GCN is proposed to describe the spacial and temporal relationship of TN.

The TN data over last twelve years were collected for NSW, Australia. The data set contains the daily traffic volume and the TN structure of the Greater Sydney area. Particularly, the traffic flow data are made of bidirectional vehicle volume count from sensors in 1 hour intervals from 2008. As shown in Fig.3.2, the change in the average daily vehicle count between 2008 and 2018 is considerable. Moreover, economic activities also play an important role in the prediction of EV charging demand. When planning EVCS deployments, it is essential to design a novel prediction model that can accommodate projected traffic conditions and economic factors.

3.3.2 Data Pre-processing

Raw TN data often contains many missing entries, as a result of routine maintenance or sensor failures, that will limit the accuracy of predicted future traffic flow. Hence, a data pre-processing step is necessary to impute the missing data before building a new GCN to conduct the times series prediction of traffic flow. In this chapter, a two-stage method is developed to impute the absent data through the incorporation of the spatial and temporal correlations of TN data sets. The goal of EVCS planning is to achieve long-term social benefit and profit. Consequently, it is within reason to accumulate daily traffic flows from each node into yearly traffic flow to predict traffic flow in the long-term. The raw TN data are collected 24-hours a day and grouped in to calendar months over multiple years. For more information see NSW traffic flow[1]. The data imputation starts with the estimation of temporal missing data for each sensor and each month.

3.3.2.1 Temporal matrix factorisation

Let $\mathbb{S} = [s_{ij}] \in \mathbb{R}^{M \times H}$ be a traffic flow matrix, which represents the traffic flow of node $n \in \mathcal{V}$ for all the months in a given year. $i \in \hat{\mathcal{M}}$ where $\hat{\mathcal{M}} = \{1, 2, 3, ..., 12\}$ is the month index. $j \in \hat{\mathcal{H}}$ where $\hat{\mathcal{H}} = \{1, 2, 3, ..., 24\}$ is the hour index. s_{ij} is the recorded traffic flow at hour j of month i for this particular sensor. It is assumed that the occurrence of missing data is entirely random and can happen at any combination of i and j. The missing data is denoted by $s^0_{ij} = 0$. To reconstruct the original matrix $\mathbb{S}$ without missing data, the formulation of the matrix factorisation is

$$\min_{U,V} \quad \|\mathbb{S} - UV\|_F^2 + \frac{\alpha}{2}(\|U\|_F^2 + \|V\|_F^2), \tag{3.1}$$

where the product of $U \in \mathbb{R}^{M \times K}$ and $V \in \mathbb{R}^{K \times H}$ is the approximation of $\mathbb{S}$ with a low rank K. $\|\cdot\|_F$ is Frobenius norm. α is the l_2 regularisation parameter. The estimated values of missing data $\hat{s}^0_{ij}$ can be obtained by using the Alternating-Least-Squares algorithm (ALS) to solve (3.1). In other words, after solving (3.1) with ALS, the matrix UV would contain the values of $\hat{s}^0_{ij}$ that corresponds to s^0_{ij}.

[1]https://www.rms.nsw.gov.au/about/corporate-publications/statistics/traffic-volumes/aadt-map/#/?z=6

3.3.2.2 Spatial matrix factorisation

To thoroughly encapsulate the spatial features of TN, the approximated $\hat{\mathbb{S}}$ of sensor n is the accumulated sum for each hour in 24-hour format, i.e., $\hat{\mathbb{S}}^n = [\hat{s}_1^n, \hat{s}_2^n, ..., \hat{s}_{24}^n](n \in \mathcal{V})$. Thus, for all sensors within the TN, the traffic flow matrix $\hat{\mathbb{S}} = [\hat{s}_j^n] \in \mathbb{R}^{N \times H}$ is for all months of a specific year.

Spatial dependency modelling: There can be several different spatial relationships between two sensors. Hence, different graphs are needed to describe these relationships.

Definition 1 (Traffic Graph): *A traffic graph is modelled by a weighted, undirected graph, denoted as $\mathcal{G} = (\mathcal{V}; \mathcal{E})$. $\mathcal{V}$ is a set of nodes while $\mathcal{E}$ is a corresponding set of edges. Each edge represents a relationship between two nodes. The spacial inter-dependencies are expresses as an adjacency matrix $A \in \mathbb{R}^{N \times N}$.*

There are three different kinds of relationships modelled in this chapter:

Geographical neighbours Spatial proximity is used to construct the first graph $\mathcal{G}_1$. The corresponding adjacency matrix $A_1 = [a_{ij}^1] \in \mathbb{R}^{N \times N}$ is defined by

$$a_{ij}^1 = \begin{cases} e^{-\frac{Dis_{ij}^2}{\sigma^2}}, & \text{if} \quad e^{-\frac{Dis_{ij}^2}{\sigma^2}} \geq \epsilon, \\ 0, & \text{otherwise}. \end{cases} \tag{3.2}$$

where Dis_{ij} denotes the distance between nodes i and j. The thresholds for the connectivity of the graph are denoted by σ and ϵ, and are set to 20 and 0.5, respectively.

Region similarity Region similarity is used to define the second graph $\mathcal{G}_2$. In this context, a Region is defined as an area on the map that have the same postcode. Traffic nodes located in similar regions are more likely to have similar traffic flow patterns. For example, similar sized shopping malls located within different commercial zones will attract comparable traffic flows. Therefore, the connection between two nodes is given by their similarity. The corresponding adjacency matrix $A_2 = [a_{ij}^2] \in \mathbb{R}^{N \times N}$ is

$$a_{ij}^2 = SIM(\text{Region}_i, \text{Region}_j), \tag{3.3}$$

where the similarity between two regions (a number between 0 and 1) is measured by the function $SIM(\cdot)$. The function $SIM(\cdot)$ is defined by the cosine similarity as

$$cosine(\text{Region}_i, \text{Region}_j) = \frac{< \text{Region}_i, \text{Region}_j >}{\|\text{Region}_i\| \times \|\text{Region}_j\|}, \tag{3.4}$$

where $< a, b >$ denotes the inner product of a and b.

Transportation network Another layer of relationship among the nodes stems from the real-world TN connections. In other words, a connection exists between geographically reachable regions. Hence, the corresponding adjacent matrix is

$$a_{ij}^3 = \begin{cases} 1, & \text{if nodes } i \text{ and } j \text{ are connected in TN,} \\ 0, & \text{otherwise.} \end{cases} \tag{3.5}$$

Note that all graph Laplacian $L_g = D_g - A_g$ where $g = \{1, 2, 3\}$ and D_g is a degree matrix, i.e., $d_{ii}^g = \sum_{j=1}^N a_{ij}^g$.

Thus, the spatial matrix factorisation is formulated as

$$\begin{aligned} \min_{P,Q} \quad & \|\hat{\mathbb{S}} - PQ\|_F^2 + \frac{\beta}{2}(\|P\|_F^2 + \|Q\|_F^2) \\ & + \sum_{g=1}^{3} \gamma_g \text{tr}(P^\top L_g P), \end{aligned} \tag{3.6}$$

where, similar to the temporal factorisation case, $P \in \mathbb{R}^{N \times K}$ and $Q \in \mathbb{R}^{K \times H}$ are used to approximate $\hat{\mathbb{S}}$ by $P \times Q$. γ_g is the graph regularization parameter. β is the l_2 regularisation parameter. $\text{tr}(\cdot)$ is the trace of a matrix. Likewise, this problem can be solved by the ALS algorithm. The resulting matrices P and Q from ALS are used to compute the missing value by computing PQ and finding the entries corresponding to the missing values. The absent data is imputed by taking the temporal and spatial relationships into account over the TN from different times.

3.3.3 Graph Convolutional Network for Traffic Flow Prediction

Multiple graph relations are utilised to predict EV charging demands by developing a new GCN. Similar to deep load forecasting [242], traffic flow at $(t+1), \cdots, (t+Z')$, is foretasted based on past traffic data until (t), using a traffic flow prediction model $\mathcal{F}$. The foretasted traffic flow can then be used to estimate the projected EV charging demand. Using the graph inputs, the forecast model with a lag of $Z+1$ is

$$\begin{aligned} \hat{\mathcal{Y}}_{t+\kappa} &= \mathcal{F}(X_t, X_{t-1}, \cdots, X_{t-Z+1}, X_{t-Z}) \\ &= \mathcal{F}(\mathcal{Y}_{t-Z:t}; \mathcal{G}), \end{aligned} \tag{3.7}$$

where $\hat{\mathcal{Y}}_{t+\kappa}$ is the κ-step-ahead predicted traffic flow at time slot (t). By simultaneously predicting future traffic flows for $\kappa \in \{1, \cdots, Z'\}$, $X_{t+1}, ..., X_{t+Z'-1}, X_{t+Z'}$ from $(t+1)$ to $(t+Z')$ are obtained. All the past information $\mathcal{Y}_{t-Z:t}$ are incorporated in these predictions for all nodes.

Problem 1 (Prediction): *Traffic flow prediction is a typical time-series forecasting problem. For instance, maximising the conditional probability of prediction results (e.g. traffic flow) for the next Z' time stamps, given the previous $Z+1$ time stamps' traffic flow, that is*

$$\begin{aligned} & X_{t+1}, ..., X_{t+Z'-1}, X_{t+Z'} = \\ & \arg\max_X \log \mathcal{P}\Big(X_{t+1}, ..., X_{t+Z'-1}, X_{t+Z'} | X_{t-Z}, \\ & X_{t-Z+1}, \cdots, X_t\Big), \end{aligned} \tag{3.8}$$

where X_t is the observed features of N nodes at time stamp t. Each feature records all the observed values for a single node.

In this prediction model, it is assumed that the training data set is generated from a stationary process. This means that the probability density function (PDF) of traffic flow does not vary over time. It should be noticed that, if the PDF of the traffic flow varies from year to year, the input data sets need to be processed with re-scaling methods to satisfy the stationary requirement.

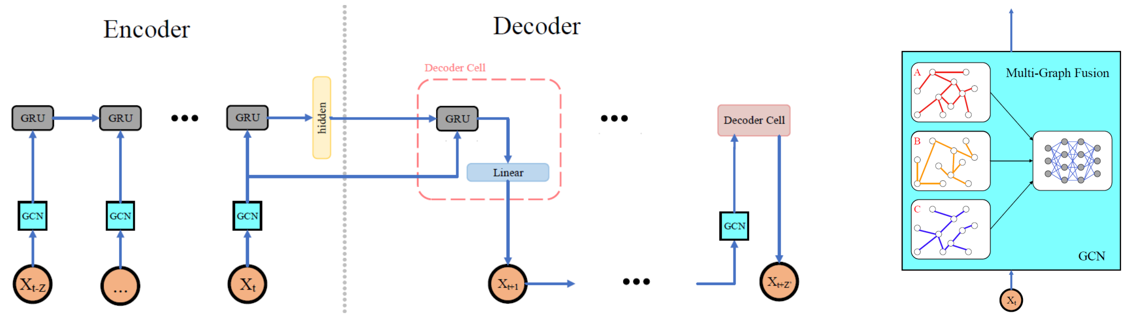

Figure 3.3: (a) The encoder-decoder architecture that is developed for the multi-step demand prediction. (b) the illustration of the multi-graph fusion GCN layer.

3.3.3.1 Network architecture

The architecture of the proposed demand prediction network is given in Fig. 3.3(a). This architecture involves a series of steps, from the multi-graph fusion-based GCN layer to the Gated Recurrent Unit (GRU). An encoder-decoder network is deployed to extract the spatial-temporal characteristics related to the yearly changes in traffic flow and economic activity over the planning area.

GCN Layer. Given data in graph format for day t, the spectral graph convolutional operator is defined as

$$X_t^{l+1} = \sigma\Big(\hat{D}^{\frac{1}{2}} \hat{A} \hat{D}^{\frac{1}{2}} X_t^l W^l\Big), \tag{3.9}$$

where X_t^{l+1} and X_t^l are the matrices for the output and input data at layer l ($l = 1, ..., L$), respectively. The row number of these matrices corresponds to the index of nodes whereas the column number corresponds to the index of features. At time instance t, each element in these matrices represents traffic flow or economic indicator of a specific month. With I being the identity matrix, the adjacency matrix $\hat{A} = A + I$ contains a self-loop connection. $\hat{D}$ is the normalised version of diagonal node degree matrix D. The normalisation aims to re-scale the information from the neighbours of a node. $\sigma(\cdot)$ denotes an activation function. W^l is a weight matrix, the elements of which are trained. A new graph convolutional layer is added to deal with distinct types of relations with corresponding weights. Different from the traditional GCN, a graph convolutional operator is introduced with a trainable filter so as to fuse different sub-graphs. As presented in Fig. 3.3(b), these sub-graphs are learned from a similarity model. Given a kernel $\mathrm{H}^{l,p} \in \mathbb{R}^{1\times P}(P \leq 3)$ at layer l, the formulation of the graph convolutional layer is as below.

$$\begin{aligned} \bar{X}_t^p &= \mathrm{H}^{l,p} * \phi^k(\hat{A}^g X_t^l), \\ X_t^{l+1} &= \sigma\Big(\Big[X_t^l\Big|\bar{X}_t^1, ..., \bar{X}_t^P\Big]W^l\Big), \end{aligned} \tag{3.10}$$

where $\phi(\cdot)$ is used to stack the products of $\hat{A}_g$ and $X_t^l \in \mathbb{R}^{N\times F}$, following a top-$k$ selection rule. The number of features is denoted with F.

GRU Layer The recurrent neural network (RNN) is a powerful tool for predicting sequential data. After the fusion process of the multi-graph $GCN(\cdot)$, the temporal dependency is modelled by the standard GRU as follows

$$z_t = \sigma\Big(W_z\mathrm{GCN}(X_t) + u_z h_{t-1} + b_z\Big), \tag{3.11}$$

$$r_t = \sigma\Big(W_r\mathrm{GCN}(X_t) + u_r h_{t-1} + b_r\Big), \tag{3.12}$$

$$h_t^{'} = tanh\Big(W_h\mathrm{GCN}(X_t) + u_h(r_t \odot h_{t-1}) + b_{h^{'}}\Big), \tag{3.13}$$

$$h_t = (1 - z_t) \odot h_{t-1} + (1 - z_t) \odot h^{'}, \tag{3.14}$$

where $\odot$ is the Hadamard product. $\sigma(\cdot)$ is a nonlinear activation function. z_t and r_t are the gates for updating and resetting at time stamp t, respectively. $h_t^{'}$ and h_t are the present and final memories.

Decoder Cell A GRU is constructed as the output layer to further extract the temporal information. This GRU linearly maps the outcomes from the previous GRU unit to the next decoder cell. The prediction of traffic flow for N nodes is derived by a linear transformation, which is formulated as

$$\hat{X} = ReLU(wz + b)$$

where w is a weight vector. b is a bias. z is the prediction result obtained from the previous GCN and GRU layers. The loss function is defined as

$$L(\hat{X}) = \Big\|\mathcal{F}(\mathcal{Y}_{t-Z:t}; \mathcal{G}) - \mathcal{Y}_{t+1}\Big\|^2, \tag{3.15}$$

Table 3.2: Australian EV Charging Station Configuration

Commercial EV Charging Station List					
Charging Modes	Nominal Supply Voltage (Volts)	Current (Amps)	Fully Charged Time	Charging Rate	Installation Cost
Level 1	120 VAC, single phase	10 $\sim$ 15 Amp	12 $\sim$ 18 hours	10$\sim$20 km of range per hour	\$ 400 $\sim$ 800
Level 2	208 $\sim$ 240 VAC, single phase	32 Amp	1 $\sim$ 3 hours	up to 40 km of range per hour	\$500 $\sim$ 2,200
Level 3	600 VDC, three phases	40 $\sim$ 500 Amp	15 $\sim$ 30 mins	up to 150 km of range per hour	\$50,000+

where $\mathcal{Y}_{t+1}$ is the ground truth at $(t+1)$. Similarly, $\hat{\mathcal{Y}}_{t+\kappa}$ can be obtained for all κ.

Remark 1. *In the prediction network [243], an LSTM layer is used to capture the temporal information. After that, a GCN layer is adopted for obtaining the spatial information. Whereas in this chapter, the multi-graph GCN is used at each time stamp for the extraction of spatial information among various nodes. Then, the output from the GCN layer is passed to a GRU-based encoder-decoder architecture. Additionally [243] used the weighted summation to handle the multi-graph information fusion through the attention mechanism. In contrast, this chapter proposed the use of a trainable 1D convolutional operator for fusing the multi-graph information.*

3.4 Game Theoretical Model of EV Charging Infrastructure Deployment

The focus of this section is the deployment of commercial EVCSs for multiple companies. These companies aim to provide the charging service in the same area.

3.4.1 Cournot Competition Model

The objective of the Cournot competition model is to give the optimal planning guideline for individual company to achieve the maximal profit. The profit refers to the difference between the revenue from serving EV charging demand and the cost. Different from the existing approaches that are based on integer programming [244], the deployment of EVCSs is solved in a resource-allocation manner. That is, there are competitive relations between service providers in the same market.

Here are a few of assumptions applied to the model.

i) The EV chargers provided by the same company are of the same type. Moreover, each company has an exclusive right to use a certain charging mode. The available charging modes are presented in Table 3.2. The lifespan of each charging post is no less than 10 years.

ii) An entire charging operation is without interruption. In order to maximize the battery lifespan, a charging operation results in the **SoC** increasing from 20% to 80%.

iii) For a specific zone, there is a linear mapping between the EV charging demand and the traffic flow.

Assume that a city is partitioned into I zones. M is the number of companies that build EVCSs. $\mathbf{x}_m = [x_{m,1}, ..., x_{m,i}, ..., x_{m,I}]^\top$ denotes the optimal planning strategy of a service provider m at the ith zone. $\mathbf{x}_{-m}$ is the service providers in the same zone except m. π_i is the basic price at zone i. The setting of this price is linked with the local consumption level. B_m is the budget for service provider m. The projected EV charging demand of the ith zone is S_i while its corresponding cost function of the charging post deployment is written as $\mathbf{C}_i(\cdot)$. The cost consists of the quality of service as well as construction expenses.

Construction Expense According to [228], the installation cost and the land-use cost account for a large portion of the investment of an EVCS. These costs are proportional to the average real-estate price and the business activities at zone i, and are modelled by $\nu_i x_{m,i}$. ν_i is the construction expense at the ith zone, including the cost of labour, space and installation.

Quality of Service High investment input always accompanies high-quality service. To fulfill the EV charging demand, desirable service means shorter charging time and waiting time. Often, the charging time is dependent on the power of the provided charging posts. The length of waiting queue determines the waiting time. Specifically, the queue length is highly related to the charging demand of zone i. The measure of the service quality is modelled as the summation of $-\frac{1}{\mu_m}x_{m,i}^2$ [245] and $\theta_i S_i x_{m,i}$. θ_i is the parameter associated with the waiting time, given charging demand S_i. The calculation of the final cost is as below

$$C_i(x_{m,i}) = -\frac{1}{\mu_m}x_{m,i}^2 + (\nu_i + \theta_i S_i)x_{m,i}. \tag{3.16}$$

Problem 2 (Game Model) *The service-provider-based planning problem is formulated by the Cournot competition model.*

$$\begin{aligned}
\max_{\mathbf{x}_m} \quad & \mathbf{f}_m(\mathbf{x}_m, \mathbf{x}_{-m}) && (3.17)\\
&= \sum_{i=1}^{I} \Big\{ \pi_i \Big(1 - \frac{x_{m,i} + \sum_{j=1, j\neq m}^{M} x_{j,i}}{S_i} \Big) x_{m,i} - C_{m,i}(x_{m,i}) \Big\}, \\
\text{s.t.} \quad \mathcal{X}_m = \Big\{ \mathbf{x}_m | \quad & \sum_{i=1}^{I} x_{m,i} \leq B_m, && (3.18)\\
E_i^{\min} \leq & \sum_{m=1}^{M} x_{m,i} \leq E_i^{\max}, && (3.19)\\
0 \leq & \, x_{m,i} \quad \Big\}. && (3.20)
\end{aligned}$$

Eq.(3.17) is the payoff function associated with individual service provider m. The objective of this payoff function is to maximise the demand coverage while achieving the maximal profit at the minimal cost. The competitive relations between service providers are described by the Cournot competition model. In this model, if all the service providers develop high-value investment plans in the same zone, the benefit of individual demand coverage falls. In addition, this Cournot model allows multiple players. This may result in multiple Nash equilibria due to the joint constraint. Eq.(3.18) gives the allocated-budget constraint of service provider m at all the zones. B_m is the total budget of service provider m. Eq.(3.19) discusses the availability of EV charging posts at a specific zone. $E_i^{\min}$ is the minimum EV charging posts required by the government. The upper limit of the availability, $E_i^{\max}$, is determined by the capacity of the local DN. To avoid the non-existence of Nash equilibrium caused by integer variables, the deployment strategy is modelled with a continuous variable. A large number of EVs charging simultaneously might degrade the frequency stability of the power system, and cause a voltage imbalance in the power grid. Even though the uptake of EVs in Sydney is still at a low level, it is necessary to take actions in advance to cope with the massive adoption of EVs in the future. Therefore, a capacity constraint is introduced to guarantee a reliable EVCS deployment at zone i. The constraint in Eq.(3.20) is for ensuring a non-negative EVCS deployment strategy.

Cournot Competition Game To maximize the benefit of each service provider, individuals will choose their own optimal planning strategy of EVCS. Thus, the optimisation problem of individual service provider in a Cournot competition game model is formulated as $\Gamma = \left\{\mathcal{M}, \{\mathcal{X}_m\}_{m\in\mathcal{M}}, \{\mathbf{f}_m(\mathbf{x}_m, \mathbf{x}_{-m})\}_{m\in\mathcal{M}}\right\}$ in which

- Players: $\mathcal{M}$ is a set of service providers;
- Strategy set: $\mathcal{X}_m$ is nonempty, compact and convex, for each $m \in \mathcal{M}$;
- Payoff function: for each $m \in \mathcal{M}$, $\mathbf{f}_m(\mathbf{x}_m, \mathbf{x}_{-m})$ is shown in (3.17).

Definition 2 (Optimal Planning Strategy): *Let* $\Gamma = \left\{\mathcal{M}, \{\mathbf{x}_m\}_{m\in\mathcal{M}}, \{\mathbf{f}_m(\mathbf{x}_m, \mathbf{x}_{-m})\}_{m\in\mathcal{M}}\right\}$ *be the Cournot competition model for EVCS planning.* $\mathbf{x}^* = (\mathbf{x}_m, \mathbf{x}_{-m})$ *is a Nash equilibrium of* Γ*, if and only if:*

$$\mathbf{f}_m(\mathbf{x}_m^*, \mathbf{x}_{-m}^*) \leq \mathbf{f}_m(\mathbf{x}_m, \mathbf{x}_{-m}^*), \forall m \in \mathcal{M}. \tag{3.21}$$

The final allocation of budgets for each company is called the optimal planning strategy.

3.4.2 Cournot Competition Equilibrium

In game theory, a Nash equilibrium refers to the case where no player can further their objective by changing their strategy. In this chapter, the Nash equilibrium is the same as the Cournot competition equilibrium. The existence of Cournot competition equilibrium needs to be verified before a parallel computation algorithm is developed to find the equilibrium.

Theorem 1 *If* $4(\frac{\pi_i}{S_i} - \frac{1}{\mu_m}) \geq \frac{1}{I-1}\sum_{j=2}^{I}\frac{\pi_j}{S_j}, \forall i \in \{1, 2, \cdots, I\}, \forall m \in \{1, 2, \cdots, M\}$, *then there is at least one equilibrium for the Cournot competition model (3.17).*

3.4.3 Parallel Computation for Cournot Equilibrium

To deal with the real-world scenario where a large number of zones exist, an efficient competition model is required to solve the Cournot competition model. This section introduces a parallel best response dynamics algorithm to obtain the Cournot competition equilibrium by using a *Nikaido–Isoda* function. Firstly, the ρ-regularized *Nikaido–Isoda* function $\Phi : (\mathcal{X} \times \mathcal{X}) \to \mathbb{R}$ is defined as

$$\begin{aligned}\Phi(\mathbf{x}, \mathbf{y}) \quad = \quad & \sum_{j=1}^{M}\Big(\mathbf{f}_m(\mathbf{x}_m, \mathbf{x}_{-m}) - \mathbf{f}_m(\mathbf{y}_m, \mathbf{x}_{-m}) \\ & -\frac{\rho}{2}\|\mathbf{x}_m - \mathbf{y}_m\|^2\Big) \end{aligned} \tag{3.22}$$

where $\mathcal{X} = \Pi_{m=1}^{M}\mathcal{X}_m$ is the joint constraint. $\mathbf{y}_m = [y_{m,1}, ..., y_{m,i} \;, ..., y_{m,I}]^\top \in \mathcal{X}$. The ρ-regularized *Nikaido–Isoda* function is uniformly concave with respect to $\mathbf{y}_m$ for $\rho \geq 0$ as a fixed parameter.

Given $\min_{\mathbf{y}\in\mathcal{X}} \Phi(\mathbf{x}^*, \mathbf{y}) = 0$, $\mathbf{x} \in \mathcal{X}$ is a Cournot competition equilibrium. Then, the best response dynamics is a convex combination of the current strategy $\mathbf{x}(n)$ and the best response strategy $\mathbf{y}$:

$$\begin{cases} \mathbf{y} := \text{argmin}_{\mathbf{y}\in\mathcal{X}}\Phi(\mathbf{x}^*, \mathbf{y}), \\ \mathbf{x}(n+1) = \tau\mathbf{x}(n) + (1-\tau)\mathbf{y}, \end{cases} \tag{3.23}$$

where $\tau \in [0, 1)$ is used to reconstruct a new best response strategy $\mathbf{x}$ at the $n + 1$th iteration. The best response dynamics (3.23) can be viewed as the fixed-point mapping $\mathbb{F}(x) = \mathbf{y} - \mathbf{x}$ which resulting in a normalized Nash equilibrium.

The results from the classic best response dynamics algorithms linearly converge to a normalized Nash equilibrium. In **Algorithm 1**, a momentum method is employed to speed up the convergence.

Algorithm 1 Accelerated Best Response Dynamics for Cournot Competition Equilibrium

for $m \in \{1, 2, \cdots, M\}$ and $i \in \{1, 2, \cdots, I\}$ **do**
  Initialise an EVCS budget allocation $\mathbf{x}_{m,i}$;
  Randomly initialize $\mathbf{y}_{m,i}$;
end for
$n = 1$;
while $\|\mathbf{x} - \mathbf{y}\| \leq \epsilon$ **do**
  Best response of company m:
    Parallel computation $\mathbf{y}_m = \text{argmin}_{\mathbf{y}_m \in \mathcal{X}} \Phi(\mathbf{x}_m^*, \mathbf{y}_m)$;
  New EVCS budget allocation is determined by

$$\mathbf{x}(n+1) = \mathbf{x}(n) + \tau\Big(\mathbf{y} - \mathbf{x}(n)\Big) - \zeta\Big(\mathbf{x}(n) - \mathbf{x}(n-1)\Big); \tag{3.24}$$

  $n++$;
end while
Output: Optimal budget allocations $\mathbf{x}$ for all companies;

Theorem 2 *If*

$$\tau = \left(\frac{2}{\sqrt{\lambda_{\max}(\partial\mathbb{F}(\mathbf{x}^*))} + \sqrt{\lambda_{\min}(\partial\mathbb{F}(\mathbf{x}^*))}}\right)^2, \tag{3.25}$$

$$\zeta = \left(\frac{\sqrt{\lambda_{\max}(\partial\mathbb{F}(\mathbf{x}^*))} - \sqrt{\lambda_{\min}(\partial\mathbb{F}(\mathbf{x}^*))}}{\sqrt{\lambda_{\max}(\partial\mathbb{F}(\mathbf{x}^*))} + \sqrt{\lambda_{\min}(\partial\mathbb{F}(\mathbf{x}^*))}}\right)^2, \tag{3.26}$$

where $\lambda_{\max}(\cdot)$ *and* $\lambda_{\min}(\cdot)$ *denote the maximal and minimal eigenvalues of the matrix regarding the subgradient*

$$\partial\mathbb{F}(\mathbf{x}^*) = \nabla\mathbf{y}^\top(\mathbf{x}^*) - E \tag{3.27}$$

at the Cournot competition equilibrium $\mathbf{x}^*$. *E is the identical matrix with a proper dimension, Then,* ***Algorithm 1*** *can superlinearly converge to a Cournot competition equilibrium.*

Note that step 7 of **Algorithm 1** is a standard convex optimisation problem which can be easily solved by the existing algorithms, i.e. quadratic programming.

3.4.4 Optimal Sizing of EVCSs

After the optimal budget allocations are obtained for each zone, the final optimal sizing of EVCSs for each provider is modelled as an MILP.

According to charging powers, there are three types of EV charging posts. They are Level-1, 2 and 3 in ascending charging power. $\zeta_{i,k}^m$ is a binary variable, indicating whether an EVCS, that contains Level-k charging posts, is built at zone i. For instance, $\zeta_{5,3}^m = 1$ means there is an EVCS with Level-3 charging post at zone 5 built by company m. The cost of building an EVCS varies according to the type of charging post. $c_{1,i,k}$ denotes the expense of building an EVCS that contains Level-k charging posts at zone i. $c_{2,i,k}$ is the expense of building individual Level-k charging posts in the EVCSs at zone i. $n_{i,k}^m$ is an integer variable corresponding to the number of the Level-k charging post in the EVCS at zone i for company m.

Problem 3 (Optimal Sizing) A new CFRLM is developed to maximise the profit of each node. The optimal sizing of EVCSs takes various types of charging posts into account as follows:

$$\max_{\{\zeta_{i,k}^m, n_{i,k}^m\}} \quad \Bigg\{ \sum_{m \in \mathcal{M}} \sum_{i \in \mathcal{I}} \sum_{k=1}^{3} \Big(\Delta T \eta_i (r_k - c_e) p_k n_{i,k}^m - c_{1,i,k} \zeta_{i,k}^m - c_{2,i,k} n_{i,k}^m \Big) - \sum_{q \in \mathcal{Q}} c_p \lambda_{OD}^q S_q \Bigg\} \tag{3.28}$$

subject to

$$\sum_{\{j|(i,j)\in \hat{A}_q\}} \lambda_{ij}^q - \sum_{(j|(j,i)\in \hat{A}_q)} \lambda_{ji}^q = \begin{cases} 1, & i = O \\ -1, & i = D \\ 0, & i \neq O, D \end{cases} ,\forall q \in \mathcal{Q}, \forall i \in \hat{\mathcal{I}}_q, \tag{3.29}$$

$$\lambda_{ij}^q \geq 0, \forall q \in \mathcal{Q}, \forall (i,j) \in \hat{A}_q, \tag{3.30}$$

$$\sum_{q\in\mathcal{Q}}\sum_{\{j|(j,i)\in A_q\}} T_q\lambda_{ji}^q \le \sum_{m\in\mathcal{M}}\sum_{k=1}^{3}\Psi(n_{i,k}^m), \forall i\in\mathcal{I}, \tag{3.31}$$

$$n_{i,k}^m \le \zeta_{i,k}^m \hat{n}_{i,k}^m, \forall i\in\mathcal{I}, k\in\{1,2,3\}, \tag{3.32}$$

$$\sum_{k=1}^{3}(c_{1,i,k}\zeta_{i,k}^m + c_{2,i,k}n_{i,k}^m) \le \hat{x}_{m,i}, \tag{3.33}$$

$$F_{s,t} = f_s + \sum_{u\in\mathcal{U}_{\to s}}(F_{u,s} - \xi_{u,s}l_{u,s}), \tag{3.34}$$

$$0 = f_0 + \sum_{u\in\mathcal{U}_{\to 0}}(F_{u,0} - \xi_{u,0}l_{u,0}), \tag{3.35}$$

$$\varsigma_s - \varsigma_t = 2Re(\xi_{s,t}^* F_{s,t}) - |\xi_{s,t}|^2 l_{s,t}, \tag{3.36}$$

$$|F_{s,t}|^2 \le l_{s,t}\varsigma_s, \tag{3.37}$$

$$l_{s,t} \le |\overline{I}_{s,t}|^2, \tag{3.38}$$

$$|\underline{V}_s|^2 \le \varsigma_s \le |\overline{V}_s|^2, \tag{3.39}$$

$$f_s = -f_s^{EV} - f_s^B, \tag{3.40}$$

$$f_s^{EV} = p_s^{EV} + J\tan\vartheta p_s^{EV}, \tag{3.41}$$

$$p_s^{EV} = \sum_{m\in\mathcal{M}}\sum_{i\in\mathcal{I}_s}\sum_{k=1}^{3} p_k n_{i,k}^m, \tag{3.42}$$

$$n_{i,k}^m \in \mathbb{Z},\ \zeta_{i,k}^m \in \{0,1\}, \forall i\in\mathcal{I},\ k\in\{1,2,3\}. \tag{3.43}$$

By assuming the average life span of an EV charging post is 10 years, the planning horizon ΔT in hours is calculated as

$$\Delta T = 10 \times 365\text{days/year} \times 24\text{hours/day}. \tag{3.44}$$

The profit modeling recognises that the same service has a higher price in high-income areas. Thereby, the adjusted profit is calculated as the product of base profit i.e. $r_k - c_e$ and the income coefficient η_i at the ith zone. c_p is introduced to penalise the unsatisfied EV charging demand.S_q is the total charging demand on path q. λ_{OD}^q is the fraction of unsatisfied charging demand on path q. λ_{ij}^q is the fraction of charging demand on path q from node i to j. $\mathcal{I}$ is the set of nodes of the traffic network. $\hat{\mathcal{I}}_q$ is the set of nodes of the expanded TN on path q. $\hat{A}_q$ is the set of arcs of the expanded TN on path q. $\mathcal{Q}$ is the set of paths. $\Psi(\cdot)$ is the function of charging serviceability. The expression of $\Psi(n_{i,k}^m)$ is

$\Psi(n^m_{i,k}) = \alpha_k n^m_{i,k}$, where α_k is a parameter based on the type of EV charging posts. $\hat{n}^m_{i,k}$ is the maximum number of Level-k EV charging posts at the ith zone. $\hat{x}_{m,i}$ is the budget for building the EVCS and EV charging posts at zone i for company m.

$F_{s,t}$ denotes the power flow in line s,t from bus s to bus t. f_s is the nodal power injection at bus s. $\xi_{s,t}$ is the impedance of line s,t. $\xi^*_{s,t}$ is the conjugate of $\xi_{s,t}$. $l_{s,t}$ is the square of the magnitude of the current in line s,t from bus s to bus t. ς_s is the square of the magnitude of the nodal voltage at bus s. $\overline{I}_{s,t}$ is the upper limit of current for line s,t. $\underline{V}_s/\overline{V}_s$ is the lower/upper limit of nodal voltage at bus s. Bus 0 is the transmission substation that connects to the transmission network.

The term $\Delta T \eta_i (r_k - c_e) p_k n^m_{i,k}$ in Eq.3.28 includes the electricity cost c_e and the revenue r_k from Level-k EV charging posts over ΔT. The charging power of the Level-k EV charging post is denoted as p_k. The revenue r_k is set as $1.5c_k$. The operation cost c_k is obtained by Eq.(3.45).

$$c_{1,k}/\bar{n} + c_{2,k} + p_k c_e t = p_k c_k t, \quad \forall k \in \{1,2,3\}, \tag{3.45}$$

where $\bar{n}$ is the average number of charging posts per EVCS. $c_{1,k}$ and $c_{2,k}$ are the base cost of building one Level-k EVCS and EV charging post, respectively.

The objective function Eq.(3.28) is to maximise profit while maximising the captured charging demand. The term $c_{1,i,k}\zeta^m_{i,k} + c_{2,i,k} n^m_{i,k}$ in Eq.(3.28) is the total cost of building EVCSs. This cost includes the expense of each EVCS and a variable expense determined by the number of EV charging posts and the location. Term $\sum_{q\in\mathcal{Q}} c_p \lambda^q_{OD} S_q$ in Eq.(3.28) is the penalty cost for unsatisfied charging demand. Eqs.(3.29) and (3.30) are traffic flow constraints. Eq.(3.31) guarantees that the charging demand at each node is less than its serviceability. Eq.(3.32) gives the upper limit of the number of EV charging posts, and ensures that EV charging posts can only be built given a corresponding EVCS at the node. The budget constraint is represented with Eq.(3.33), in which $\hat{x}_{m,i}$ is derived from the budget allocation step in the previous section.

Eqs.(3.34)-(3.37) are DN constraints with the SOCP relaxation. Futher details can be found in [246] and [247]. Eqs.(3.38) and (3.39) are the capacity constraints of line currents

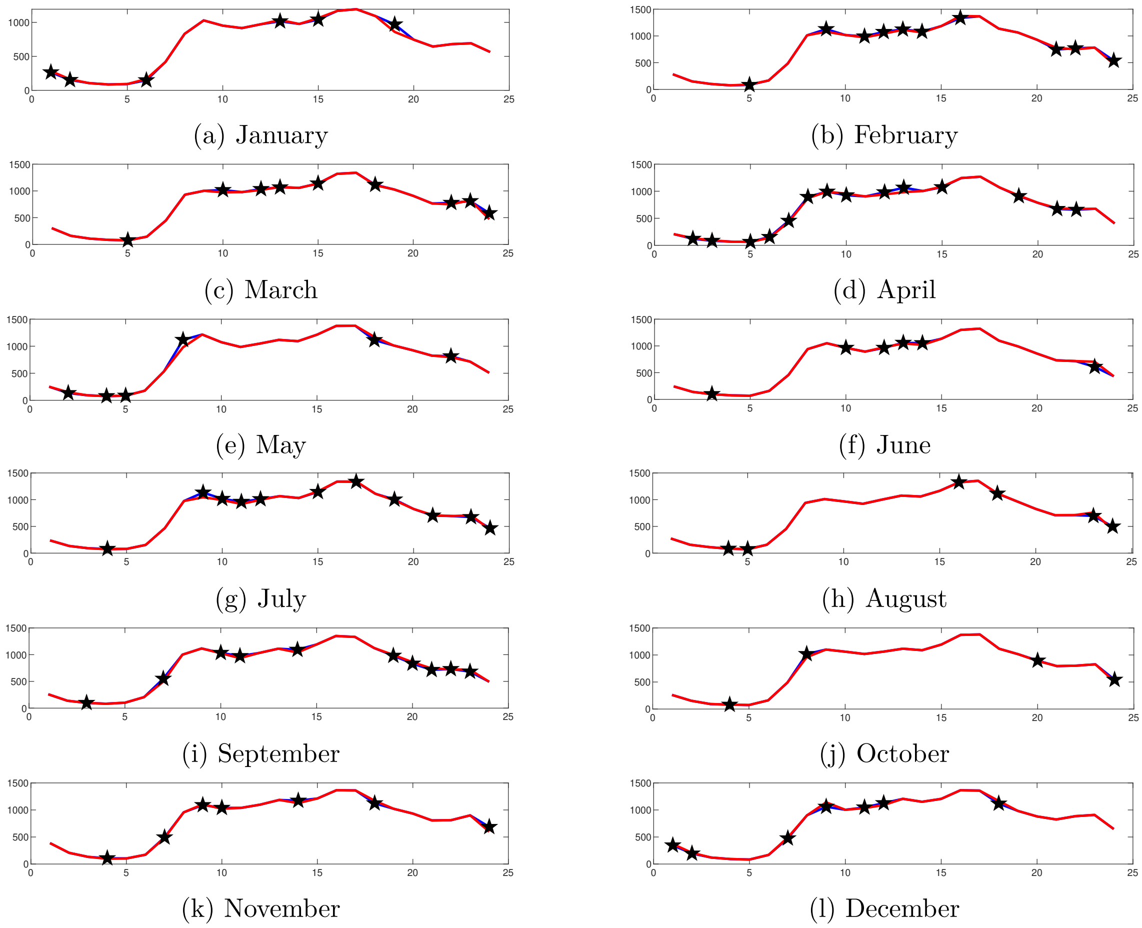

(a) January (b) February (c) March (d) April (e) May (f) June (g) July (h) August (i) September (j) October (k) November (l) December

Figure 3.4: The missing traffic flow imputation in 2018.

and nodal voltages. Moreover, Eqs.(3.41) and (3.42) calculate the EV charging loads at nodes of DN, where ϑ is the phase angle between EV charging voltage and current. The power factor is $\cos\vartheta$. Since the power factor of EV charging posts are very close to 1, then $\cos\vartheta = 1$ and $\tan\vartheta = 0$.

3.5 Experiments and Results

This section uses the real-world data set of Sydney, Australia to validate the proposed framework. The TN data were collected by the hourly traffic volume sensors. The distribution of sensors covers the CBD area and its neighbouring suburbs. The economic

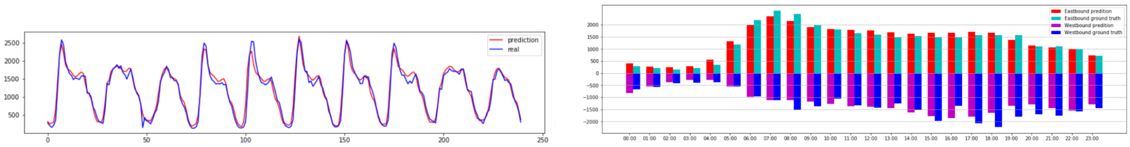

(a) 10-day prediction of one direction traffic flow (b) 1-day prediction of bi-direction traffic flow

Figure 3.5: Traffic flow prediction by the multi-raltion GCN-GRU architecture.

indicators were collected by the Australian Bureau of Statistics[2]. The experiments in this section are implemented with Python 3.6 and Pytorch 1.2 on a Ubuntu computer with 64 GB RAM and a RTX 2080 Ti GPU. The optimization simulations are conducted with Matlab R2018b and CPLEX through Yalmip toolbox.

3.5.1 Missing Traffic Flow Imputation

In this subsection, the effectiveness of the proposed data imputation approach is demonstrated with a simulation. First, for a chosen node, 30% of the daily traffic flow data in a 12 month period are randomly set to 0. Then the temporal matrix factorisation method introduced in Section 3.3.2.1 is applied to the set with missing data. Let $K = 12$ and $\alpha = 0.1$. The imputed daily average traffic flow on a monthly basis is shown in Fig.3.4. The ground truth is plotted in blue while the recovered values are plotted in red. The black stars represent the instances of the artificially induced missing values. The discrepancy, the absolute value of the difference, between the original set and the set with missing data is 5547.4. The discrepancy between the original set and the recovered set is 198.4.

3.5.2 EV Charging Demand Prediction

To demonstrate the effectiveness of the EV charging demand prediction method, 164 TN nodes, located in the Sydney region, are used to construct the multiple relationship graphs as defined in Section 3.3.2.2, namely the geographical neighbours (3.2), the similarity of regions (3.3) and the transportation network (3.5). The parameters for the encoder-decoder

[2]https://www.abs.gov.au/AUSSTATS/abs@.nsf/mf/1345.0?opendocument

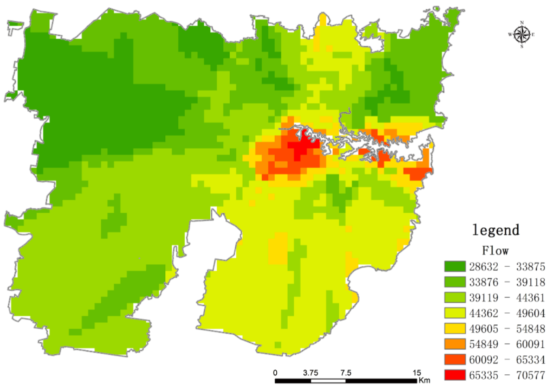

Figure 3.6: The prediction result over the whole city of Sydney.

Table 3.3: Key parameters for the neural network

Parameter name	Value
Layers of GCN	3
Layers of GRU	2
Learning rate	0.001
Batch size	128
Epoch	200
Dropout	0.2
Weight decay	0.0001
Time step	24
Dimension of input	34

architecture are determined by the grid search method. Table 3.3 lists parameter setting for the GRU-GCN architecture. The following metrics are used to evaluate algorithm performance

$$\mathbf{MAE} = \frac{1}{N}\sum_{n=1}^{N}|Y_n - \hat{Y}_n|,$$

$$\mathbf{MAPE} = \frac{1}{N}\sum_{n=1}^{N}\frac{|Y_n - \hat{Y}_n|}{Y_n},$$

$$\mathbf{RMSE} = \sqrt{\sum_{n=1}^{N}\frac{(Y_n - \hat{Y}_n)^2}{N}}$$

where Y_n is the original value. $\hat{Y}_n$ is the predicted value. N is the number of samples.

The input is one-week (7×24 hours) traffic flow data. The output is the predicted traffic flow for the next day. The predicted result of a single node is shown in Fig.3.5. In

Table 3.4: Comparison Results of Different Prediction Algorithms

Model	MAE	MAPE	RMSE
ARIAM	256.8677	24.36%	421.3162
RF	234.8679	21.03%	390.3182
XGboost	165.4877	16.86%	230.3527
LSTM	203.9898	20.55%	331.9577
DeepAR	188.6075	18.62%	249.8043
T-GCN	183.0239	15.45%	217.2420
Ours	165.1412	14.88%	206.4713

Fig.3.5(a), a 10-day prediction result of the traffic node is presented, with the true values in blue and the predicted ones in red. The aforementioned metrics for this experiment are as follows: RMSE is 235.7, MAE is 119.3 and MAPE is 21.39%. An example of bidirectional hourly traffic flow prediction is presented in Fig.3.5(b). In this case, the total RMSE is 198.8, MAE for each direction is 149.2 and 104.2, MAPE for each direction is 34.03% and 13.3%.

For the EVCS planning, it is desirable to cover the maximal EV charging demand. It can be concluded from Fig. 3.4 that the traffic flow of the same day in various months oscillates around a fixed value. Hence, the future maximum monthly traffic flow can be predicted solely based on the present maximum monthly traffic flow. From this predicted maximum traffic flow, the EV charging demand can be estimated with high confidence. The monthly maximum traffic flow for the next five years is projected based on the economic features in NSW and the traffic flow data from the last sever years. The traffic flow projection for all nodes in 2025 is shown in Fig.3.6. It takes $6,153$s to train the proposed deep network while the prediction time is 32s.

The following state-of-art algorithms are selected as references in the comparison:

- **ARIAM** [248] is one of the most established time series prediction methods.
- **Random forests (RF) model** [249] is an ensemble decision tree algorithm, and has been widely adopted in the field of machine learning.

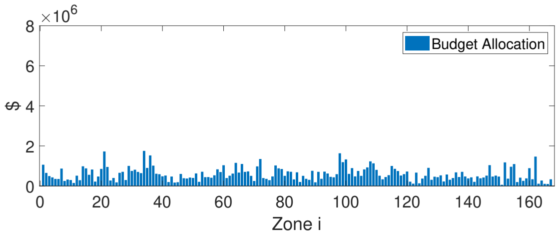

(a) Service provider $m = 1$ with Budget $B_1 =$ $\$100,000,000$

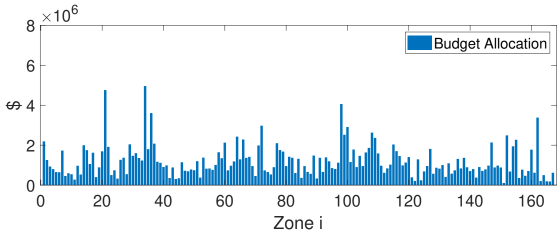

(b) Service provider $m = 2$ with Budget $B_2 =$ $\$200,000,000$

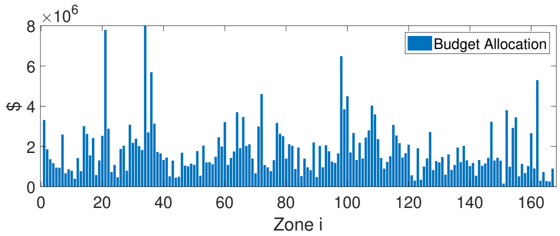

(c) Service provider $m = 3$ with Budget $B_3 =$ $\$300,000,000$

Figure 3.7: The optimal strategy of budget allocation on each zone for EV charging infrastructure over the city of Sydney.

- **XGboost** [250] is a decision tree algorithm based on the technique, gradient boosting. It has the ability of fast training, low memory consumption and high efficiency.
- **LSTM** [251] is a RNN architecture featuring feedback connections.
- **DeepAR** [252] is a RNN-based approach. It is the most applicable in the situations where the time series in the data set are highly correlated.
- **T-GCN** [253] has a hybrid GCN and GRU architecture, being able to extract the spatial and temporal distributions of traffic flow.

The result of the comparison experiment in Table 3.4 illustrates that the proposed algorithm achieved better prediction results than the other methods in the aforementioned metrics.

3.5.3 The Optimal Strategy of Budget Allocation

This experiment assumes that there are three private companies ($m = 1, 2, 3$) competing in the task of EVCS construction. The corresponding budget for each company is 100, 200, 300 million AUD, respectively. Additionally, it is assumed that the serving capabilities of a Level-1, a Level-2, a Level-3 charging posts are 3, 12 and 72 EVs per post per day, respectively. Let the charging time parameter μ_m be 1000 for all three companies. Based on the postcodes of TN nodes, Sydney is partitioned into $I = 167$ zones. Let the waiting time parameter $\theta_i = 0.01S_i$. This means that the traffic flow will have a notable effect on the waiting time. The construction expense parameter ν_i at zone i is calculated from the base installation cost and commercial property sale price. The service benefit basic price π_i is extrapolated from the average property rent. $E_i^{\min}$ is set to 0. $E_i^{\max}$ is set by the maximal capacity of surrounding DN. To obtain the different budget allocations for individual company, **Algorithm 1** was run for each company. Fig. 3.7 illustrates the optimal budget for each service provider. As expected, all companies allocate majority of their budget in urban nodes.

3.5.4 Optimal Sizing of EVCSs

This section investigates the effect of DN constraints on EVCS planning with a subset of nodes. The DN is a simplified version for west side of Sydney. Fig. 3.8a shows the distributions of these substations and the feeders connecting them. The TN is made of 41 transportation nodes. Fig. 3.8b also plots the connections between TN nodes. It is assumed that the EVCSs at each TN node draw power from their nearest zone substation.

Two simulations are carried out in this experiment. The first takes the DN constraints Eqs.(3.34)-(3.39) into account. In Figs.3.9(a)-3.11(a), with DN constraints, all providers built Level-1 EV charging post the most. This is due to the fact that the available capacities at several substations are not able to support Level-2 and 3 EV charging posts. Therefore, only Level1 charging posts can be built in surrounding TN nodes, as a result of Level1's low power consumption. Company $m = 1$, under the lowest budget, builds the

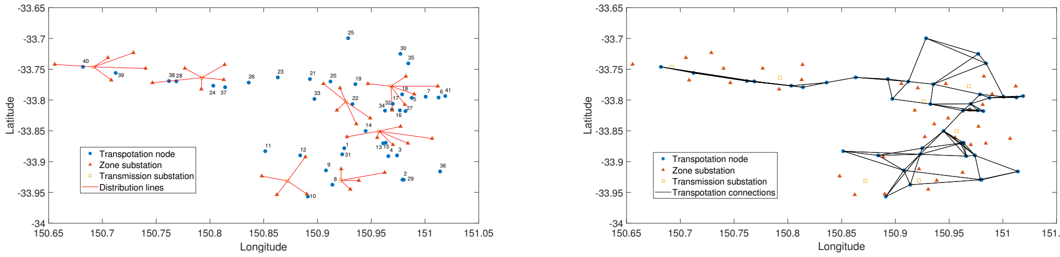

(a) Connections between transmission substations and zone substations

(b) Connections between transportation zones

Figure 3.8: Topology of DN and TN used for the simulation

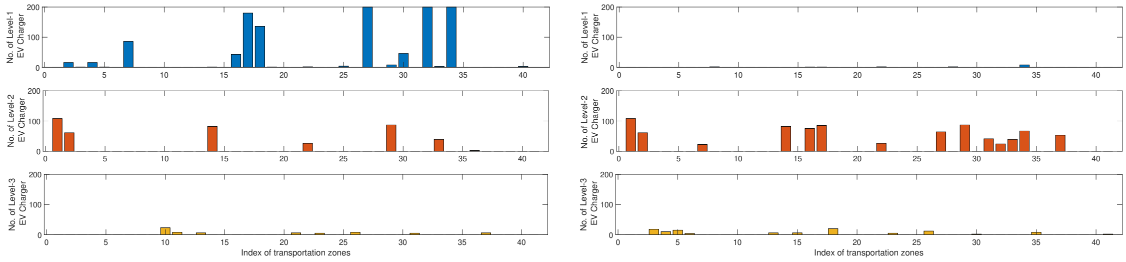

(a) With DN constraints

(b) Without DN constraints

Figure 3.9: Comparison result: the number of different EV charging posts built by company $m = 1$ at each TN node

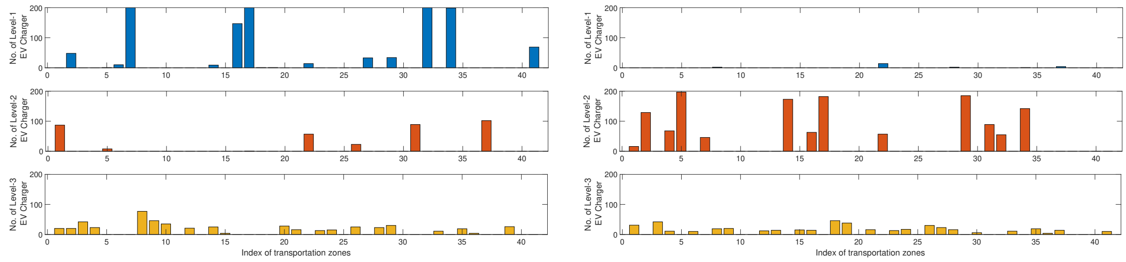

(a) With DN constraints

(b) Without DN constraints

Figure 3.10: Comparison result: the number of different EV charging posts built by company $m = 2$ at each TN node

least number of Level-3 EV charging posts amounting at 108. Conversely, company $m = 3$ has the largest amount of investment. Thereby, the most number of Level-3 charging posts are installed by company $m = 3$.

In Figs. 3.9(b)-3.11(b), when DN constraints are ignored, both companies $m = 1$ and 2

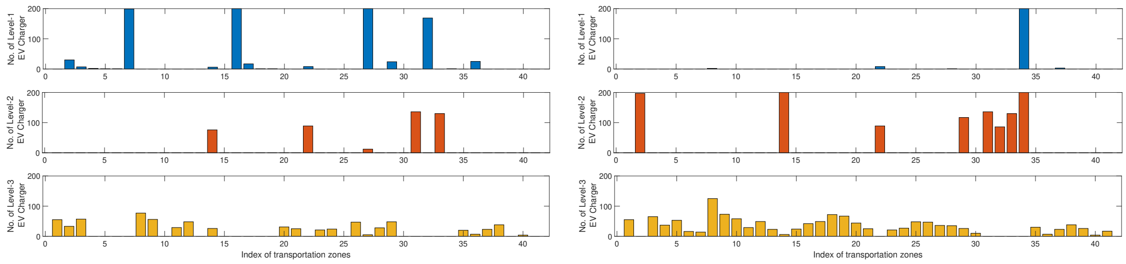

(a) With DN constraints (b) Without DN constraints

Figure 3.11: Comparison result: the number of different EV charging posts built by company $m = 3$ at each TN node

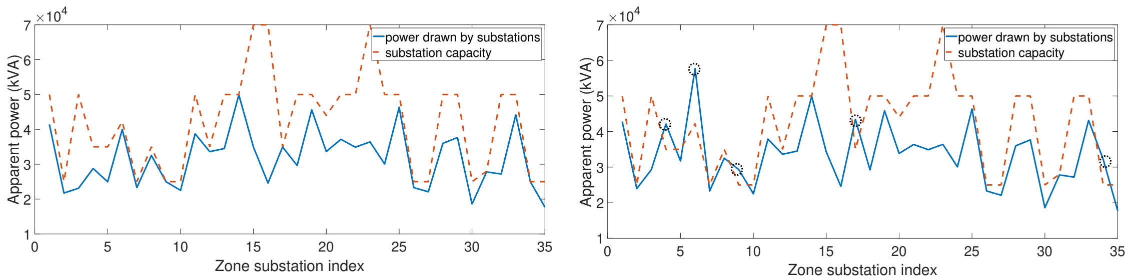

(a) (b)

Figure 3.12: Comparison result between with and without DN constraints. Power drawn at substation is plotted with solid line. The capacity is drawn with dashed line at each zone substation. (a) is simulation results for power consumption at each substation with DN constraints. (b) is simulation results withou DN constrains.

choose to allocate most of their budgets for construction of Level-2 EV charging posts. This is because, the service ability of Level-2 EV charging posts is around the half of Level-3, with only 1/20th of the cost. Consequently, both companies $m = 1$ and 2 operating under smaller budgets are incentivised to deploy Level-2 EV charging posts. Whereas, company $m = 3$, with a more generous budget, puts a considerable amount of its resource into building Level-3 EV charging posts. This is a result of the increased serviceability of Level-3 charging posts, enabling company $m = 3$ to capture more charging demands and generate increased profits in the process.

Figs. 3.12(a) and (b) show that, when the planning is carried out with DN constraints, the loads at all the zone substations are within their capacity. This means the current DN is able to support the obtained EVCS planning results. However without including

DN constraints in the planning phase, the capacity of 5 zone substations is exceeded, indicating that additional investments are needed to upgrade the DN to accommodate for the planned deployment of EVCSs.

3.6 Conclusion

This chapter proposed a data-driven framework for addressing the EVCS planning problem in a competitive market environment through a predict-then-optimize diagram. The missing traffic data are imputed through a spatial-temporary analysis of the TN,leveraging the matrix factorisation technique. Moreover, the EV charging demand is projected by an encoder-decoder architecture, in which the multi-relation GCN is utilised. This deep learning technique lead to a better prediction result. To obtain the optimal budget allocations for individual companies, a Cournot competition model is introduced after the data pre-processing steps. A parallel algorithm is developed to find the Cournot competition equilibrium in a timely manner. Moreover, the optimal sizing problem of EVCS at each zone is formulated as an MILP, in which local DN constraints are considered to make the model more realistic. The effectiveness of the proposed framework is validated through a series of simulation experiments.

3.7 Appendix

3.7.1 Proof of Theorem 1

Proof: Convexity check of payoff functions is performed by minimising the negative payoff function of each company as follows

$$\begin{aligned}\mathrm{Rev}_m &= -\sum_{i=1}^{I}\Big\{\pi_i(1-\frac{x_{m,i}+\sum_{j=1,j\neq i}^{M}x_{j,i}}{\mathbf{S}_i}))x_{m,i} \\ &\quad -C_{m,i}(x_{m,i})\Big\},\end{aligned} \tag{3.46}$$

The Hessian matrix is

$$\nabla^2\mathrm{Rev}_m = \begin{bmatrix} 2(\frac{\pi_1}{\mathbf{S}_1}-\frac{1}{\mu_m}) & \frac{\pi_2}{\mathbf{S}_2} & \cdots & \frac{\pi}{\mathbf{S}_I} \\ \frac{\pi_2}{\mathbf{S}_2} & 2(\frac{\pi_2}{\mathbf{S}_2}-\frac{1}{\mu_m}) & \cdots & \vdots \\ \vdots & \vdots & \ddots & \vdots \\ \frac{\pi_I}{\mathbf{S}_I} & \cdots & \cdots & 2(\frac{\pi_I}{\mathbf{S}_I}-\frac{1}{\mu_m}) \end{bmatrix}.$$

Considering the positiveness of the Hessian matrix $\nabla^2\mathrm{Rev}_m$, following condition holds

$$4(\frac{\pi_i}{\mathbf{S}_i}-\frac{1}{\mu_m}) \geq \frac{1}{I-1}\sum_{j=2}^{I}\frac{\pi_j}{\mathbf{S}_j}, \forall i \in \{1,2,\cdots,I\}, \forall m \in \{1,2,\cdots,M\}. \tag{3.47}$$

Thus, all payoff functions are strongly convex, implying the existence of Cournot competition equilibrium. ■

3.7.2 Proof of Theorem 2

Proof. In view of the new best response dynamics, the fixed-point mapping 3.23 is accelerated by the momentum. Note that $\zeta\Big(\mathbf{x}(n)-\mathbf{x}(n-1)\Big)$ involves in the difference operators which is the approximation of the gradient $\partial_{\mathbf{x}}\mathbb{F}(\cdot)$. Thus, the gradient is given by $\nabla\mathbf{y}^{\top}(\mathbf{x}^{*}) = G^{-1}H - G^{-1}J(J^{\top}G^{-1}J)^{-1}J^{\top}G^{-1}H$ where

$$
\begin{aligned}
G &:= -\nabla^2_{\mathbf{yy}}\Phi(\mathbf{x},\mathbf{y}(\mathbf{x})) \\
&= 2A^{\dagger}\otimes E^{M} + \rho E^{IM}, \\
H &:= \nabla^2_{\mathbf{xy}}\Phi(\mathbf{x},\mathbf{y}(\mathbf{x})) \\
&= \rho B^{\dagger}\otimes E^{M}, \\
J &:= \nabla g(\mathbf{y}(\mathbf{x})), \\
A^{\dagger} &= \begin{bmatrix} \frac{\pi_1}{\mathbf{S}_1}-\frac{1}{\mu_m} & 0 & \cdots & 0 \\ 0 & \frac{\pi_2}{\mathbf{S}_2}-\frac{1}{\mu_m} & \cdots & \vdots \\ \vdots & \vdots & \ddots & \vdots \\ 0 & \cdots & \cdots & \frac{\pi_I}{\mathbf{S}_I}-\frac{1}{\mu_m} \end{bmatrix}, \\
B^{\dagger} &= \begin{bmatrix} 0 & \frac{\pi_2}{\mathbf{S}_2} & \cdots & \frac{\pi}{\mathbf{S}_I} \\ \frac{\pi_2}{\mathbf{S}_2} & 0 & \cdots & \vdots \\ \vdots & \vdots & \ddots & \vdots \\ \frac{\pi_I}{\mathbf{S}_I} & \cdots & \cdots & 0 \end{bmatrix}.
\end{aligned}
$$

$\otimes$ is Kronecker product. $g(\mathbf{y}(\mathbf{x}))\leq 0$ is the constraint set of Eqs. (3.18)-(3.20). The optimal preconditions of the multi-step update (3.24) to accelerate the best response dynamics are given in (3.25) and (3.26) according to the heavy ball method. ■

Chapter 4

Planning of Electric Vehicle Charging Stations and Distribution System with High Renewable Penetrations

4.1 Relationship to the Thesis

As noted in Chapter 1, current methods in probabilistic modelling of EV charging behaviours require MCSs and time consuming scenario reduction steps. In this chapter a multi-objective EVCS planning model is developed while a novel scenario generation approach is deployed to skip the scenario reduction step entirely.

This Chapter has been published.

This chapter has been edited to incorporate thesis reviewers' comments.

4.2 Abstract

With the increasing prevalence of Electric Vehicle (EV), the EV Charging Station (EVCS) and power distribution have been becoming a coupled physical system. In this chapter, a multi-objective planning model is developed for the sizing and sitting of EVCSs and the expansion of power distribution network with high wind power penetrations. The objectives of the planning model are to minimize the total cost of investment and energy losses of the distribution system while maximizing the total captured traffic flow. The uncertainties associated with wind power sources are considered. Additionally, the uncertainties in EV daily charging loads are also important concerns in the optimisation of the planning model. To model the EV load uncertainties, a recent Scenario Generation (SG) method is adopted. Further, a multi-objective optimization tool, Multi-Objective Natural Aggregation Algorithm (MONAA), is introduced to obtain the final solutions of the planning model. The simulations based on coupled 54-node distribution network and 25-node traffic network systems are conducted to verify the efficiency of the proposed model and the effectiveness of SG-based MONAA.

Nomenclature

N^D, N^T	The node set of distribution network and transportation network;
N_{EV}	Total number of EVs;
T	Set of the time steps;
Ω^{DL}	Set of the feeders;
Ω^{SR}, Ω^{SE}	Set of existed substations with and without reinforcement;
Ω^{TL}, Ω^{SC}	Set of traffic network links and candidate location of substations;
Ω_a, Ω^I	Set of different feeder types and candidate location of EVCSs;
Ω^b, Ω^c	Set of substation capacity with reinforcement/construction;

Ω_q^I	Set of candidate EVCSs that can capture the traffic flow on path q;
Q_{rs}	Set of paths connecting O-D pair rs;
Parameters	
m	Year index;
C_{ap}	EV battery capacity;
ω	The power consumption of EV battery per 100 km;
S_{SOC0}, S_{SOC1}	The initial state of charge (SOC) and end state of charge of the EV battery capacity;
η	EV charging efficiency;
$f_{1,m}$	The total annual cost of the investment and energy losses of year m;
$P_{i,t}^{CP}$	Total charging demand of ith charging station at time t;
$P_{i,t}^D, Q_{i,t}^D$	Active power and reactive power of node i at time t;
$P_{i,t,m}^{Total}$	Total load of ith node at time t of year m;
$c_{i,j}^L, l_{i,j}$	Construction cost and length of feeder ij;
c_i^{SC}, c_i^{SR}	Construction and reinforcement cost of new substation i;
$z^{\min}, z^{\max}$	Size limits of EVCSs;
$\overline{S_t^{SR}}$; $\overline{S_t^o}$	Apparent power of the substation with and without reinforcement at node i;
$\overline{s_t^{SC}}$, $\overline{s_{lj}}$	Apparent power of candidate substation at node i and feeder ij;
$g_{ij,b_{ij}}$	Conductance and susceptance of feeder ij;
G_{ij}, B_{ij}	Real and imaginary parts of the admittance matrix;
$U_t^{\min}, U_t^{\max}$	Upper and lower voltage limits of node i;
c^E, d^{annual}	Energy cost and the number of the days for one year;
c^{CH}	Capital cost of each charging pile;
c_i^F, c_i^{other}	Initial investment cost of ith EVCS and other costs according to the size of EVCS;
n^{DS}, n^{Sub}	Total nodes numbers of distribution system and substation;
$N_{wind}, P_{w,t}^{wind}$	Number of wind turbine units and wind power output of wth wind turbine units at time t;
μ_s, σ_s	Expectation and standard deviation value for EV start charging time;
μ_d, σ_d	Expectation and standard deviation value for EV travel distance.

4.3 Introduction

The optimal planning of Electric Vehicles (EVs) charging infrastructure will play an irreplaceable role for better catering for the increasing number of EVs. An effective planning strategy will help the network operator to reduce cost, allow the policy makers to make informed decisions, and provide EV users with more places to charge their vehicles. However, the planned EV Charging Stations (EVCSs) will inevitably add stress to the existing distribution network. Some papers can be found to consider the expansion planning of the distribution network and EVCSs simultaneously.

Table 4.2 presents the comparison of a few of these works with this chapter. [32] proposed a planning strategy for distribution network, EVCSs and wind power, and was expanded in [33] to also consider solar and battery energy storage. In [26, 32, 33], the EV charging demand was calculated based on historical data of fossil-fuelled cars, under the assumption that EVs and fossil-fuelled cars have similar driving patterns. However, in cases where the driving patterns are different, probabilistic models might be more suitable. Furthermore, [32–37] utilized commercial solvers to obtain the final solutions. But it has been shown in various applications that genetic algorithms can achieve comparable results in similar or less time [254–256] Some examples of using genetic algorithm in the context of distribution network and EVCSs are [26–31]. The distribution network and EVCSs planning were often considered in absence of a corresponding transportation network [27, 31–33, 257]. But the EV charging demand is inevitably affected by flow of traffic, which is in turn correlated to the layout of the transportation network. A joint planning strategy of EVCSs together with distribution network expansion was introduced in [28], by considering the impact of traffic flows. Though, [28] did not consider the stochastic nature of EV driving patterns. In work [29], the planning of EVCSs and distribution network was proposed by considering the uncertainty of EV charging behaviours as well as captured traffic flow, yet the load increments over multiple years were not taken into account. Moreover, [28, 29, 31] did not include the penetration of renewable generation, which is a non-negligible consideration in modern distribution networks.

Table 4.2: Comparison of joint planning approaches of EVCSs and distribution network expansion

Approach	Renewable energy source	EV demand modelling	Solver/Optimization algorithm	Case study
[32]	Wind	Historical data	CPLEX	24-node distribution system
[33]	Wind & Solar	Historical data & K-means++ clustering	CPLEX	54-node distribution system
[26]	Solar	Historical data	NSGA-II	Hybrid AC/DC 38-node system
[34]	None	Robust optimisation	CPLEX	18-node and 54-node distribution system
[35]	Wind & Solar	Probalistic model & MSCS	CPLEX	18-node distribution system
[36]	Solar	Probalistic model & Queuing theory	Gurobi	Coupled 4×4-node distribution and 39-node transportation system
[37]	None	Deterministic model	GAMS	Coupled 33-node distribution and 14-node transportation system
[27]	Wind	Probabilistic model & MCS	NSGA-II	9-node distribution and 33-node distribution system
[28]	None	Deterministic model	MOEA/D	1) Coupled 23-node distribution and 20-node transportation system 2) Coupled 54-node distribution and 25-node transportation system
[29]	None	Probabilistic model & MCS	MOEA/D	Coupled 54-node distribution and 25-node transportation system
[30]	Wind	Probabilistic model & MCS	ICA	33-node distribution with a logistics distribution system connected
[31]	None	Probabilistic model & 2 stage estimation	NSGA-II	33-bus distribution system
Proposed approach	Wind	Probabilistic model & SG method	MONAA	Coupled 54-node distribution and 25-node transportation system

Additionally, for the randomness of EV driving behaviours and wind generation, [30] presented a scenario-based stochastic program to model the uncertain nature of EV charging demand. In [27, 29, 30, 35] the EV charging model is based on Monte-Carlo Simulations (MCS) of multi-dimensional joint probability distribution, and the representative scenarios with high precision results can only be obtained when the size of initial generated scenarios is large enough. Yet, the large initial scenario set will considerably raise the computational cost of the scenario reduction procedure, thus decreasing the efficiency of stochastic optimization planning. To address this issue, a recent work [258] developed a high efficiency Scenario Generation (SG) method to generate a small number of representative scenarios to accurately model real-time uncertain variations from PV power generation and loads. However, it has not been used for modelling the EV charging uncertainties. In contrast to the isolated distribution systems in [26, 27, 31–35], this chapter considers a coupled system, which consists of a traffic network and a power distribution network. Unlike [28, 29, 31, 34] , the power distribution network in this chapter takes high wind power penetration into account. A multi-objective joint planning model of EVCSs and distribution network expansion is developed based on this coupled system, as follows. Firstly, the wind power generation is modelled. The uncertainty of wind generation based on Markov Chain Monte-Carlo (MCMC) method is proposed in this study. Secondly, different from the literatures listed in Table 4.2, the SG method is adopted for modelling the uncertain charging duration and start charging time of the EV slow charging, thereby the stochastic EV charging demand is predicted. Thirdly, the joint planning model is formulated to determine the location and sizing of EVCSs and the expansion of distribution network. Lastly, the optimal solutions to the joint planning model are obtained by a multi-objective optimization tool which is called Multi-Objective Natural Aggregation Algorithm (MONAA).

The main contribution of this chapter is the investigation of a new approach to solve the joint planning problem of EVCSs and distribution network expansion while considering the effect of traffic and wind generation. In this approach, the SG-based MONAA is proposed to obtain the final solutions to the joint planning problem. To efficiently generate a small number of representative scenarios of EV charging profiles, the SG method is used. Given

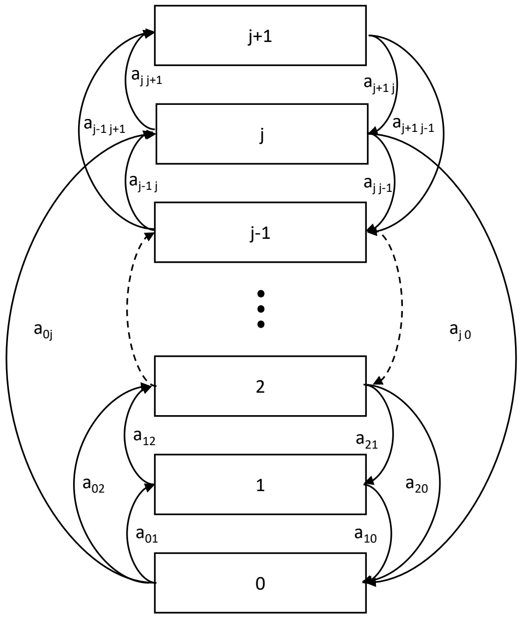

Figure 4.1: Representation of transitions between different states of wind speed

these scenarios and other inputs, MONAA is adopted for optimization. The efficiency and effectiveness of SG-based MONAA are validated by comparison experiments.

The rest of this chapter is organized as follows: Section 4.4 presents the stochastic modelling of wind power; the scenario-based EV charging demand prediction model is introduced in Section 4.5; Section 4.6 presents the planning model of coupled distribution and EVCSs; Section 4.7 presents the MONAA algorithm used for solving the planning model; the case study and comparison experiments are given in Section 4.8; Section 4.9 gives the conclusions and Section 4.10 provides some directions for future works.

4.4 Stochastic Wind Power Model

In this study, the EV charging energy is provided by both wind and thermal energy sources. The wind power can be treated as a stochastic model, and an MCMC approach is used in this study to obtain the temporal series of wind power output. The application of MCMC method involves two steps, discretising the random process (e.g., wind speed) into different states and calculating the transition probabilities between these states [259].

Fig. 4.1 illustrates the states of wind speed and their transitions between different states, where $\alpha_{j-1,j}$ represents the transition probability from state $j-1$ to j. [260] noted that the representation in wind speed domain is complicated due to the large number of possible states. To alleviate this problem, [260] proposed to transform from wind speed domain to wind power domain and managed to achieve a considerably lower uncertainty in the matrix entries without losing any information in the transformation process. Therefore, the historical wind speed data are used to estimate the wind power $p_w(v)$ in our work. Wind speed can be transformed to $p_w(v)$ according to the wind turbine curve which results in a general accuracy of the uncertainty model [260]. Wind power $p_w(v)$ is estimated with Eq. (4.1):

$$\begin{cases} 0 & v < v_{in}, v > v_{out} \\ \frac{v-v_{in}}{v_r-v_{in}} P_{rated} & v_{in} \leq v \leq v_r \\ P_{rated} & v_r \leq v \leq v_{out} \end{cases} \tag{4.1}$$

where P_{rated} represents the rated power of the wind turbine; v, v_{in} and v_{out} are the wind speed, the cut-in wind speed, cut-out wind speed and rated wind speed, respectively. Therefore, a Markov chain of wind power can be expressed by an associated transition probability matrix A, which is defined by Eq.(4.2)-(4.4).

$$A = \begin{bmatrix} a_{11} & \cdots & a_{1m} \\ \vdots & \ddots & \vdots \\ a_{m1} & \vdots & a_{mm} \end{bmatrix} \tag{4.2}$$

where a_{ij} denotes the transition probability between states i and j. The entries of a certain row sum up to one because the sum represents the transition probability from a certain state to any states. a_{ij} is calcualted by Eq. (4.3) and satisfies Eq. (4.4).

$$a_{ij} = \frac{n_{ij}}{\sum_{j=1}^{m} n_{ij}} \quad i, j = 1, 2, \ldots m \tag{4.3}$$

$$\begin{cases} a_{ij} \geq 0 \\ \sum_{j=1}^{m} a_{ij} = 1 \\ i, j = 1, 2, \dots m \end{cases} \tag{4.4}$$

where n_{ij} denotes the number of the transitions between state i and j.

For a given A, we can build a cumulative probability transition matrix A_{cum} as

$$A_{cum,i,i} = \sum_{j=1}^{m} A_{ij}. \tag{4.5}$$

A standard normal random variable u can be used for sampling. u is compared to the elements in row i of A_{cum}. If u sits between the elements from $j-1$ to j, i.e.:

$$A_{cum,i(j-1)} \leq u \leq A_{cum,ij} \tag{4.6}$$

state j is selected as the next state. The wind power of state j is computed as

$$X = X_{i,\min} + u(X_{j,\max} - X_{i,\min}) \tag{4.7}$$

where X is the estimated power of state j, $X_{j,\max}$ and $X_{j,\min}$ are the bounding values of wind power corresponding to state j, calculated according to Eq.(4.1). The same sampling procedure is repeated until enough samples have been generated.

4.5 EV Charging Demand Prediction

In this chapter, the slow charging station serves as the main charging facility due to its low cost and small size. The location and size of the charging stations are determined by the charging demand. In this chapter the EV charging demand is predicted in a probabilistic manner, in which two variables are considered, namely EVs' charging duration and start charging time. The SG method [258] is employed to discretise each variable into scenarios, due to its efficiency and simplicity. Joint states are constructed by pairing up the discretised charging duration and start charging time. Given these joint states, the charging demand at each time interval can be derived.

4.5.1 Probabilistic modelling

For the charging duration, it is associated with vehicle daily travel distance which is subject to the lognormal distribution [261]:

$$f_\delta(\delta) = \frac{1}{x\sigma_\delta\sqrt{2\pi}} \exp(-\frac{(\ln\delta - u_\delta)^2}{2\sigma_\delta^2}) \tag{4.8}$$

where δ denotes the distance that the EV travelled. Sequentially, the charging duration can be calculated based on Eq. (4.9).

$$t_{cs} = \frac{\delta\omega}{p_{\text{slow}}\eta} \tag{4.9}$$

The EV start charging time (t_{ss}) follows the subnormal distribution [262]:

$$f_{ss}(t_{ss}) = \begin{cases} \frac{1}{\sigma_s\sqrt{2\pi}} \exp(-\frac{(t_{ss}-u_s)^2}{s\sigma_s^2}), u_s - 12 < t_{ss} < 24 \\ \frac{1}{\sigma_s\sqrt{2\pi}} \exp(-\frac{(t_{ss}+24-u_s)^2}{s\sigma_s^2}), 0 \le t_{ss} \le u_s - 12. \end{cases} \tag{4.10}$$

4.5.2 SG method

Given the probabilistic modelling of charging duration and start charging time, the SG method is deployed in this chapter to generate a small set of representative scenarios for these two variables.

For EV start charging time t_{ss}, the SG method discretises t_{ss} into V states. Each state v has a lower bound $\underline{t}_{ss,v}$ and an upper bound $\overline{t}_{ss,v}$. The occurrence probability corresponding to each state v is

$$\rho_{ss,w} = \int_{\underline{t}_{ss,v}}^{\overline{t}_{ss,v}} f_{ss}(t_{ss}) dt_{ss}, v = 1, 2, \ldots, V. \tag{4.11}$$

Thus, the EV charging start time is modelled within these states: for a specific state v, the probability of start charging time between $\overline{t}_{ss,v}$ and $\underline{t}_{ss,v}$ is $\rho_{ss,v}$ over the whole planning horizon.

Similarly, for the charging duration, the SG method begins with discretising the uncertain daily travel distance d into W states. For each state w, the lower and uppder bound are

$\underline{\delta}_w$ and $\overline{\delta}_w$, respectively. The occurrence probability $\rho_{\delta,w}$ for the interval between $\underline{\delta}_w$ and $\overline{\delta}_w$ can be calculate by the integral of Eq. (4.8). Then based on Eq. (4.9), the mean value of each charging duration state can be calculated as:

$$t_{cs,w} = \frac{\omega \int_{\underline{\delta}_w}^{\overline{\delta}_w} \delta f_\delta(\delta) d\delta}{p_{\text{slow}} \eta \int_{\underline{\delta}_w}^{\overline{\delta}_w} \delta f_\delta(\delta) d\delta}, w = 1, 2, \ldots, W. \tag{4.12}$$

For a specific charging duration state w, the mean value δ represents the uncertain daily travel distance between $\overline{\delta}_w$ and $\underline{\delta}_w$; state w would occur with the probability of $\rho_{\delta,w}$ over the whole planning horizon.

4.5.3 Construction of joint state

These states of start charging time and charging duration can be combined to construct $R(= V \times W)$ joint uncertainty states $\{(t_{ss,v}), t_{cs,w}, \rho_r\}$. Each joint state consists of a pair of $t_{ss,v}$ and $t_{cs,w}$ as well as the occurrence probability ρ_r. The joint uncertainty state is constructed by following steps. Firstly, the charging start time and charging duration make up two separate state sets Ψ^{ss} and Ψ^{cs}:

$$\Psi^{ss} = t_{ss,v}, \Psi^{cs} = t_{cs,W} \tag{4.13}$$

Secondly, the start charging time and charging duration states are paired by computing the Cartesian product of Ψ^{ss} and Ψ^{cs} as Eq. (4.14). The probability ρ_r of the occurrence of each joint uncertain state is then derived by Eq.(4.15).

$$\{(t_{ss,v}, t_{cs,w})\} = \Psi^{ss} \times \Psi^{cs} \tag{4.14}$$

$$\rho_r = \rho_{ss,v} \times \rho_{\delta,w} \tag{4.15}$$

These joint uncertainty states represent the probability distribution characteristics of the uncertain EV charging start time and charging duration. According to probabilistic function given above, the total charging load at each time interval can be calculated by:

$$P_t^{cp} = \frac{\lambda_i \sum_{k=1}^{N} \sum_{t=1}^{24} (\rho_r N_{\text{EV}} P_{\text{slow}})}{N} \tag{4.16}$$

where ρ_r is sampled based on the MCS; N denotes the total number of samples. λ_i denotes the ratio of the charging demand on ith node, of which the EV total charging demand can be computed based on the objective function in [28]. The number of charging posts which should be deployed at ith station (μ_i, $i \in \Omega^I$) could be determined accordingly:

$$Z_i = \frac{\lambda_i}{\gamma} \tag{4.17}$$

where γ represents the average service capability of a charging post.

4.6 Stochastic Joint Planning Model

The planning model for EVCS and distribution network expansion proposed can be expressed with two objectives, namely minimization of annual investment cost and energy losses as well as maximization of captured EV traffic flow.

4.6.1 The first objective: Annual investment Cost and energy losses Minimization

$$\min f_1 = \frac{f_{1,1}}{(1+\epsilon)} + \frac{f_{1,2}}{(1+\epsilon)^2} + \dots \frac{f_{1,m}}{(1+\epsilon)^m} \tag{4.18}$$

$$\begin{aligned} f_{1,n} = & \sum_{(i,j)\in\Omega^{DL}} \sum_{a\in\Omega^a} c_{ij}^L x_{ij} l_{ij} + \left(\sum_{(i,j)\in\Omega^{DL}} \sum_{a\in\Omega^b} c_i^{SR} y_i^{SR} + \sum_{(i,j)\in\Omega^{DL}} \sum_{a\in\Omega^c} c_i^{SC} y_i^{SC} \right) \\ & + \sum_{i\in\Omega^I} \{\mu_i (c^{CH} z_i + c_i^{\text{other}} z_i + c_i^F)\} \\ & + d^E d^{\text{annual}} \sum_{(ij)\in\Omega^{DL}} \sum_{a\in\Omega^a} \sum_{t\in\Omega^T} [g_{ij} x_{ij} (U_{i,t}^2 + U_{j,t}^2 - 2U_{i,t}U_{j,t}\cos(\theta_{ij,t})] \end{aligned} \tag{4.19}$$

$$P_{i,t,m}^{\text{Total}} = \left(P_{i,t}^D + \sum_{i\in\Omega^I} P_{i,t}^{CP} \right) (1+\tau)^m \tag{4.20}$$

subject to:

$$P_{i,t,m}^S = P_{i,t,m}^{\text{Total}} - \sum_{w=1}^{N_{\text{wind}}} P_{w,t} + U_{i,t} \times \sum_{j\in N^D} U_{j,t} (G_{ij}\cos\theta_{i,j,t} - B_{ij}\sin\theta_{i,j,t})$$

$$\forall i \in N^D, \forall t \in T' \tag{4.21}$$

$$Q^S_{i,t,m} = Q^D_{i,t,m} + U_{i,t} \sum U_{j,t}(G_{ij}(x_ij) \sin\theta_{i,j,t} - B_{ij}(x_{ij} \cos\theta_{i,j,t})$$
$$\forall i \in N^D, \forall t \in T' \tag{4.22}$$

$$z^{\min} \leq z_i \leq z^{\max} \quad \forall i \in \Omega^I \tag{4.23}$$

$$\sum_{ij \in \Omega_{DL}} x_{ij} = n^{DS} - n^{\text{Sub}} \tag{4.24}$$

$$U_i^{\min} \leq U_{i,t} \leq U_i^{\max} \tag{4.25}$$

$$P^2_{i,j,t} + Q^2_{i,j,t} \leq (x_{ij}\overline{S_{ij}})^2 \forall ij \in D^{DL}, \quad \forall t \in T' \tag{4.26}$$

$$P_{i,j,t} = x_{ij}\left[U^2_{i,t} g_{ij} - U_{i,t}U_{j,t}(g_{ij \cos\theta_{ij,t} + b_{ij} \sin\theta_{ij,t}})\right] \tag{4.27}$$

$$Q_{i,j,t} = x_{ij}\left[-U^2_{i,t} b_{ij} - U_{i,t}U_{j,t}(g_{ij \sin\theta_{ij,t} - b_{ij} \cos\theta_{ij,t}})\right] \tag{4.28}$$

$$0 \leq P_{w,t} \leq P_{\text{rated}} \tag{4.29}$$

Objective (4.18) calculates the present value of the total cost of investment and energy losses over the m years planning horizon. Considering the effect of inflation, the present value of cost in the k-th year is depreciated by $(1+\epsilon)^k$, where ϵ denotes the interest rate. In year n the annual investment cost and energy losses are given by Eq. (4.19), the investment cost of feeder, substation construction cost, and EVCS investment cost are represented by the first three terms, respectively. The cost of annual energy loss is the 4th term.. In Eq. (4.19), the investment cost of feeder, substation construction cost, and EVCS investment cost are represented by the first three terms, respectively. The cost of annual energy loss is the 4th term. The total active power is given in Eq. (4.20). The EV Charging power demand is computed as described in Section 4.5. All the decision variables can be found in Table 4.3.

The final planning solutions should satisfy DN constrains which are formulated as Eq.(4.21)-(4.29). Eq.(4.21) and (4.22) represent the network power flow constraints. The wind power generation of wth wind turbine of time t, $P_{w,t}$ can be found according to the stochastic wind power model in Section 4.5. Eq.(4.23) corresponds to the size constraint of EVCSs. Eq.(4.24) is the radiation topology constraint of power distribution network. Eq.(4.25) is upper and lower voltage constraints for buses. The constraints of transmission power of

Table 4.3: Variables overview

Variable	Definition
$x_{ij}, u_i, y_i^{SC}, y_i^{SR}$	Binary decision variables; value of 1 means construction of feeder, EVCS, new substation, and reinforcement of existing substation.
$P_{i,j,t}, Q_{i,j,t}$	Active power and reactive power on feeder ij at t;
$P_{i,t,m}^S, Q_{i,t,m}^S$	Active power and reactive power supplied by ith substation at time t of year m;
$U_{i,t}, U_{j,t}$	Voltage on bus i and bus j at time t
$\theta_{ij,t}$	Phase distribution on feeder ij at time t

feeders are represented in Eqs.(4.26)-(4.28). Eq.(4.29) limits the wind power generation of the wth wind turbine unit not exceeding the rated capacity.

4.6.2 The second objective: Captured EV Traffic Flow Maximization

A desirable EV charging system should meet as many EV charging demands as possible. For this purpose, the second goal is to maximize the captured traffic flow by EVCSs, which is expressed as the following equation:

$$\max f_2 = \sum_{t \in N^t} \sum_{s \in N^t} \sum_{q \in Q^{rs}} T^{rs} q, \text{annual} \tau_q^{rs} \tag{4.30}$$

subject to:

$$\sum_{k \in \Omega_q^K} u_k \geq \tau_q^{rs} \tag{4.31}$$

$$T_{q,\text{annual}}^{rs} = d^{\text{annual}} \sum_{t \in T} f_{q,t}^{rs} \tag{4.32}$$

Eq.(4.31) ensures there is at least one EVCS on path q to capture its traffic flow, where path q is the path connection an O-D pair rs. τ_q^{rs} is the binary decision variable indicating if the traffic flow can be captured. $T_{q,\text{annual}}^{rs}$ in Eq. (4.32) is the annual traffic flow of each path and $f_{q,t}^{rs}$ denotes the traffic on path q at time t, the FISK's traffic model is used to find its numerical value [263].

4.7 Solving Approach

In this study, a multi-objective optimization algorithm, MONAA, is deployed to solve the proposed joint planning model. MONAA is based on the stochastic migration model, Natural Aggregation Algorithm (NAA) [264]which allows individuals to migrate in sub populations. For each generation, the probability of an individual leaves its present shelter s, Q_s can be calculated as follows:

$$Q_s = \frac{\overline{\theta_s}}{1 + (\frac{x_s}{Cp^S})^2}. \tag{4.33}$$

where $\overline{\theta_s}$ denotes the standardised quality for shelter s. x_s represents the number of individuals; the maximum number of individuals the shelter can contain is represented by the capacity Cp^S. The individual chooses if to leave the present shelter or not based on Q_s. For an individual outside any shelters, it chooses a shelter s randomly and calculates the possibility of its entry as below:

$$R_s = (1 - \overline{\theta_s})(1 - \frac{x_s}{Cp^S}) \tag{4.34}$$

An individual then decides to enter the chosen shelter or not based on R_s. After the migration decisions are made, individuals that are inside a shelter can conduct a location search. However, the individuals outside of all shelters conduct a generalized search. In NAA, following strategy is used to calculate the normalized quality of shelter $s(\overline{\theta_s})$:

$$\theta_s = \text{fitness}(\text{site}_s^S) - fn_{\text{base}} \tag{4.35}$$

$$\overline{\theta_s} = \begin{cases} \frac{1}{N^S} & \sum_{j=1}^{N^s} \theta_j = 0 \\ 1 - \frac{\theta_s}{\sum_{j=1}^{N^S} \theta_J} & \text{otherwise} \end{cases} \tag{4.36}$$

where site_s^S represents the position for shelter s; fn_{base} denotes the fitness value of the corresponding individual with minimum fitness value of $(N^S + 1)$th; fitness() is the fitness calculation function. For K-objective optimization, the fitness of the ith individual can be represented as an array $fn_i = [fn_{i,1}, \ldots, fn_{i,K}]$, where the item $fn_{i,k}$ represents the fitness value of the kth objective of the ith individual. In MONAA, the distance calculation in

Eq.(4.35) is therefore changed as:

$$\theta_s = \mathrm{Eucli}(\mathrm{fitness}(\mathrm{site}_s^S), fn_{\mathrm{base}}) \tag{4.37}$$

where $\mathrm{Eucli}(a, b)$ denotes the Euclidean distance between two K-dimension points a and b.

In MONAA, after each generation, a new set of positions for individuals will be generated. Only when the fitness values of every objective in the new position are better than the ones in the previous position, will the individual move to the new position. Fig. 4.2 demonstrates the key steps of MONAA algorithm. To begin, all decision variables in Table 4.3 are coded as an individual of MONAA, indicating a possible solution. Next, the wind power generation, EV charging profiles, the traffic network and distribution network are input into the proposed planning model. MONAA algorithm is then used to obtain all the nondominate solutions and Pareto frontier. In order to guarantee that the EVCSs provide service to at least a certain number of EVs, the nearest solution which is above a predefined minimum captured traffic flow (8.5×10^7Veh) is chosen as the final solution. The MONAA algorithm is terminated either the maximum iteration number is reached, or the nondominated solutions do not change for a set number of successive iterations.

4.8 Simulation Study

4.8.1 Case Description

A 54-node distribution system [265] coupled with a 25-node transportation system [136] is used as the case study to test the proposed model. The cost of EVCSs investment and the cost of feeders, substations reinforcement and construction can be found in study [28]. Table 4.4 lists the key parameters used in this simulation. The graphical structure of combined distribution network and transportation network is shown in Fig.4.5. Additionally, there are 13020 vehicles in the studied metropolitan area based on the survey [262]. The EV penetration rate is 35%. The upper and lower voltage are set to ±5%. In this study

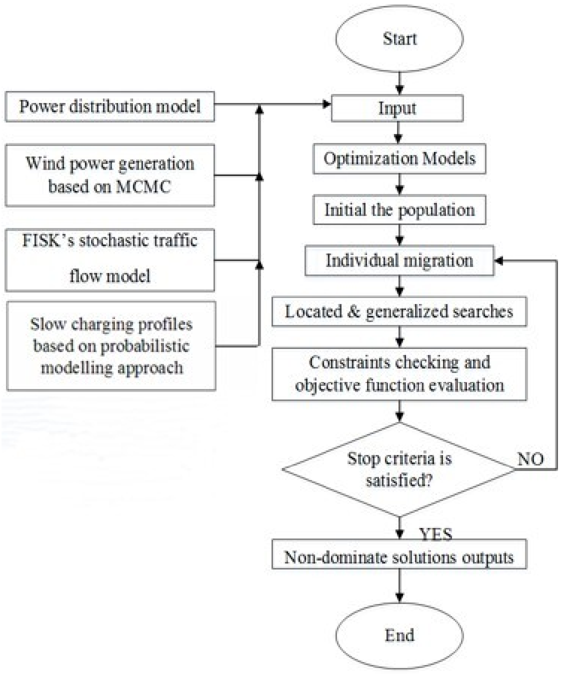

Figure 4.2: Flow chart of the solving process

the placement (node 4 and 30) and sizing (550MW and 800MW) of wind power sources are chosen as an example to investigate the effect of wind power on the joint planning model. The maximum wind penetration level is nearly 20%. Each wind energy source consists of Vestas V52 – 850kW wind turbines, the rated speed of which is 17 m/s. This simulation uses the wind data set from the National Renewable Energy Laboratory (NREL) [266] and the width of states for discretising the wind speeds is set to 1m/s, resulting in 35 states. The increasing rate of charging demand is set to 10% per year within the 20-year planning horizon considered. There is yet to be an industry-wide or national standard for EV charging power, let alone a unified plan for EV charging standards in the future. Thus, in this sturdy it is assumed that the charging power of a single charging post does not vary within the planning horizon.

Table 4.4: Values of key parameters

Parameter	Value	Parameter	Value
p_1	3.5kW	p_2	35kW
η	0.9	β	80%
ω	15km·h	$z^{\max}$	10
$z^{\min}$	6	n^{FCS}	20
P_{rated}	0.85MW	v_{in}	4 m/s
v_{out}	25 m/s	$c^{\text{CH}}[10^8\text{US\$}]$	8

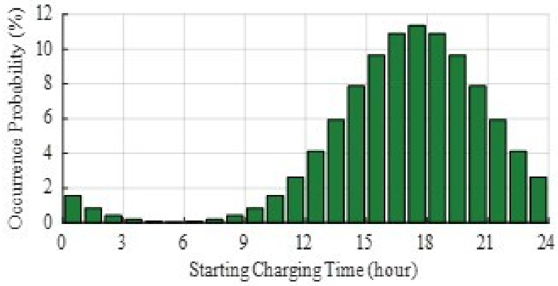

Figure 4.3: Starting Charging Time (hour)

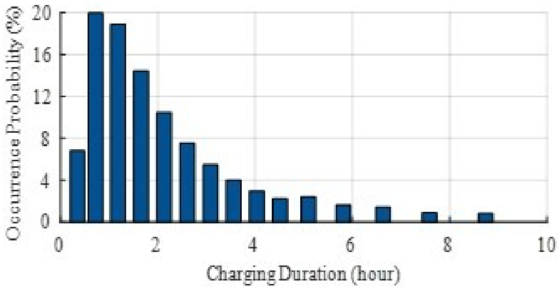

Figure 4.4: Charging Duration (hour)

4.8.2 Comparison Results of SG and Other Methods

The probabilistic models of the uncertain EV start charging time and charging duration for the slow charging are established according to the methodology detailed in Section 4.5. The charging start time and charging duration are divided into 24 and 15 states, respectively. The modelling results are shown in Fig. 4.3 and 4.4. By applying Eq.(4.13) and (4.14), 360 joint uncertainty states are constructed, which are used to model the EV uncertainty and calculate the daily charging demand.

Table 4.5: Comparison among FFS, BR and the SG method

Approaches	FFS		BR		SG method
Number of scenario groups	1	2	3	4	5
Initial scenario number	500	1000	500	1000	N/A
Scenario reduction time (s)	175	574	161	543	0.31
Approximated cost of investment and energy losses (10^7US$)	7.20	7.01	7.13	6.96	6.95
Approximated error	8.50%	5.57%	7.52%	4.97%	4.71%
Computation time (s)	3321	4451	3234	4325	2057

To measure the performance of the SG method, we compared it with two conventional MCS based scenario generation methods: Backward Reduction (BR) and Fast Forward Selection (FFS). Table 4.5 shows the comparison results. MCS is used to generate four scenario groups (denoted as group $1-4$). The groups are then used for constructing joint probability states of start charging time and charging duration; then, the reduced scenario set (R) is constructed by applying BR and FFS algorithms. Group 5 is constructed by the SG method. In this test, R is set as 50 for the scenario groups.

The time required to build reduced scenarios is represented by scenario reduction time in Table 4.5. As shown in Table 4.5, the SG method only costs 0.31s, which is much more efficient than MCS based FFS and BR. This is due to the fact that the SG method directly generates a small number of representative scenarios, thus eliminating the need for a scenario reduction step. It also shows that for Group $1-4$, the time required for FFS and BR calculations increased significantly as the number of initial scenarios increases, when original scenarios vary from 500 to 1000, the time rises from 175s to 574s and 161s and 543s, respectively.

We then input the predicted EV charging profiles into the joint planning model and use MONAA to solve the model. In Table 4.5, the approximated error represents the difference between "the realistic cost of investment and energy loss" (in which the EV charging profile is obtained by 8000 constructed scenarios from MCS based FFS reduction approach) and the cost from Group $1-5$. The approximated error resulting from the proposed method is 4.71%, suggesting that the uncertainty is well approximated by the constructed representative scenarios. For MCS based BR and FFS approaches, it is clear to see that when the number of random scenarios increased the error rate decreased. However, the SG method still gives a smaller approximated error when compared with the 1000 original scenarios. This is because that the SG-based scenarios tend to cover the whole range of possible values, while MCS-based scenarios might be prone to aggregate to the values with high probabilities, especially with smaller number of initial samples. The computational cost comparison of the proposed EVCS planning model is shown in the last row of Table 4.5. It can be observed that the computation time of SG method is 2057s, which is around half the time of MCS based FFS or BR method. To sum up, using the scenarios generated by the SG method, MONAA can achieve better uncertainty approximation accuracy and require significantly less computation time.

4.8.3 Comparison of Planning Results With/Without Wind Using MONAA

MONAA and curve fitting method are developed to find the Pareto frontier and all non-dominated solutions for the joint planning model. For a non-dominated solution, the value for one of the objectives cannot be improved without negatively impacting the other. Fig. 4.5(a) and (b) show the final planning decisions for the cases without/with wind power. In Fig.4.5, the sizes of EVCSs are given by the numbers under the EVCS icons. As shown in Fig. 4.5 six EVCSs are built in the distribution system considering the wind power penetration, but in the system without wind power, there are only four EVCSs. Also, the number of the charging piles for most EVCSs are increased, which means that the wind power integration allows the system to serve more EVs and thus increase the charging service level of the system.

The final pareto frontiers obtained from the stochastic planning model with and without wind power are shown in Fig. 4.6. The selected solution meets a specified minimum traffic flow (8.5×10^7 vehicles) to make sure that the proposed system can provide satisfied EV charging services to users. Under the final selected planning strategy, the total cost of investment and energy losses is 6.6398×10^7 US$ and the captured traffic flow is 8.50453×10^7 vehicles. The captured traffic flow is in the range between 4.224×10^7 to 8.882×10^7

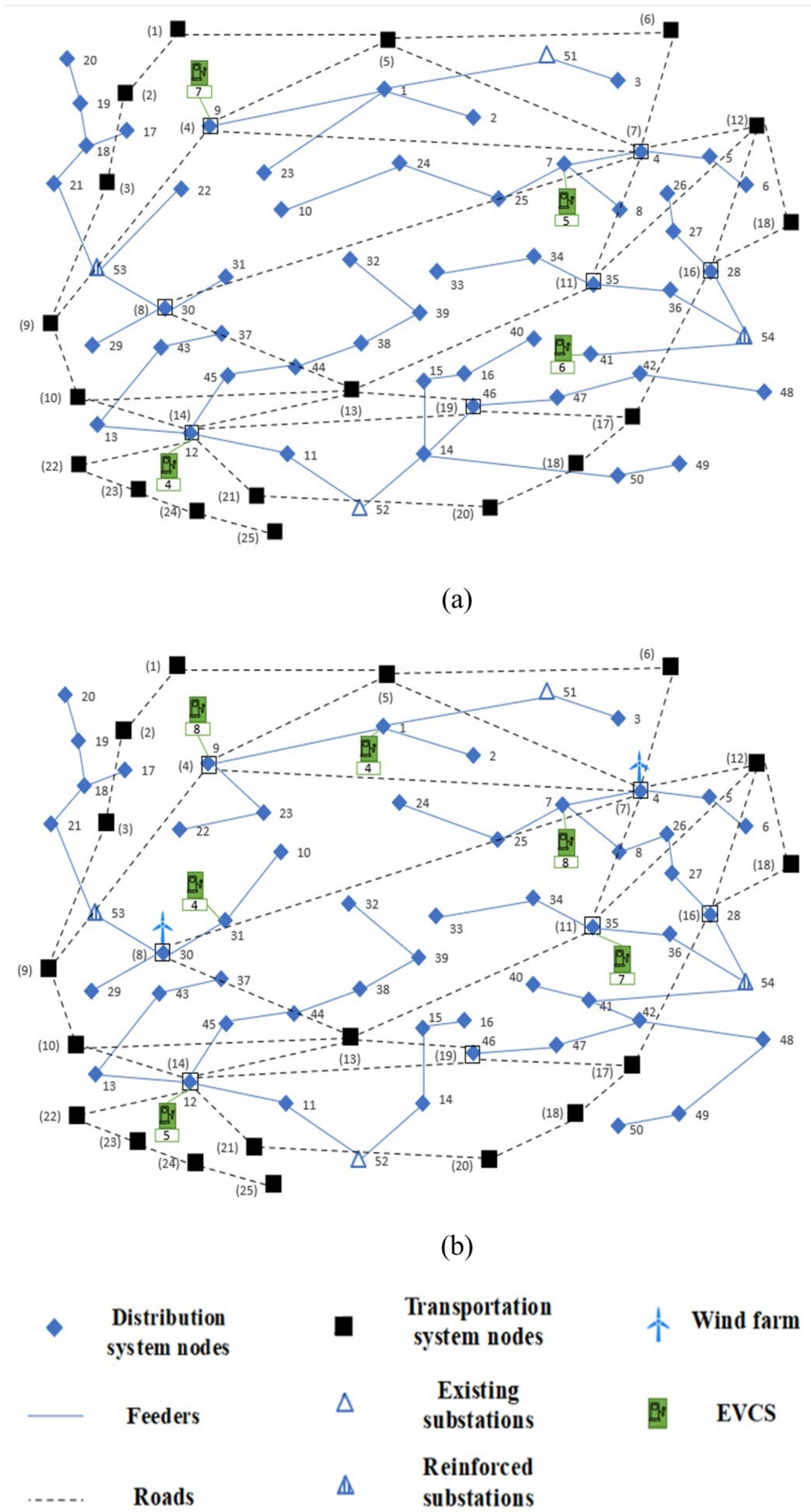

Figure 4.5: The graphical structure of combined distribution network and transportation network (a) case without wind power (b) case with wind power

Table 4.6: Summary of the selected solutions to model with/without wind power

		Wind power	Without wind power
Traffic flow [10^7Veh]		8.50453	8.48711
Costs [10^7US$]	Lines	1.4425	2.1151
	Substations	4.3271	4.6142
	EVCSs	0.2557	0.2031
	Energy losses	0.6145	0.7504
	Overall	6.6398	7.6828

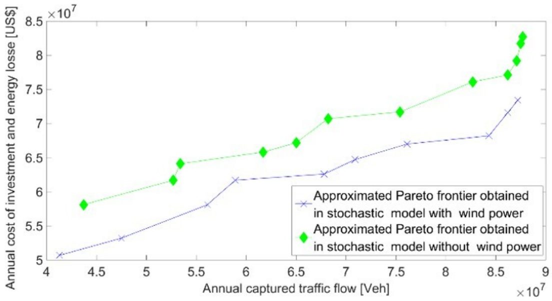

Figure 4.6: Optimization results obtained with and without wind power

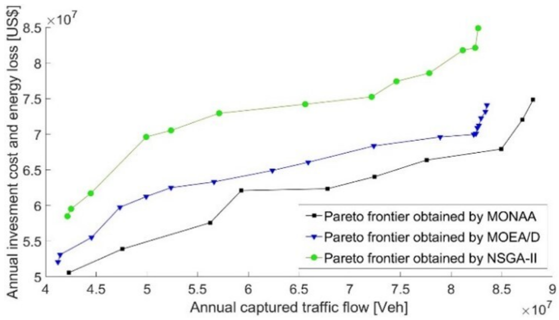

Figure 4.7: Results of MONAA, MOEA/D and NSGA II a lgorithm.

vehicles. In the meantime, the total cost of investment and enerfy losses varies in the range between 5.140×10^7 to 7.212×10^7 US$. It is clearly shown in Fig. 4.6 that inclusion of wind power in the model lowers the investment cost compared to the model without wind power. The main reason for this is that wind farms are located at nodes with high power demand, and supply electricity and serve the local demands directly, consequentially reducing the feeder construction cost. Table 4.6 summarizes the cost and total captured traffic flow within the 20-year horizon, for the layouts of final chosen solutions for model with/without wind power.

4.8.4 Comparison of Planning Results Using MONAA and Other Optimization Algorithms

Finally, the efficiency of MONAA solver on the EVCS model is tested by comparing with two common multi-object optimization solvers, Nondominated Sorting Genetic Algorithm (NSGA-II) [267] and Multiobjective Evolutionary Algorithm Based on Decomposition (MOEA/D) [268]. Fig. 4.7 shows the performance comparison results. It can be concluded that the Pareto frontier obtained by MONAA outperforms those obtained by MOEA/D and NSGA-II due to the higher investment efficiency and EV charging service. In addition, MONAA shows faster convergence speed than the other two algorithms. The average execution time of MONAA is 2147.81s, significantly less than that of MOEA/D (4562.11s) and NSGA-II (4453.71s). The reason that MONAA was able to obtain a better Pareto frontier than NSGA-II might be that MONAA uses a parameter-based diversity preserving mechanism, the maximum shelter size. In terms of execution time, the computational complexity of MOEA/D is $\mathcal{O}(mNT)$ [268], where m is the number of objective, N is the population size and T is the number of solutions. Using the same terminology, the computational complexity of NSGA-II is $\mathcal{O}(mN^2)$ [267]. Compared to MOEA/D and NSGA-II, the computational complexity of MONAA is only $\mathcal{O}(mN)$, resulting in a faster execution time.

4.9 Conclusion

A multi-objective EVCS planning model is suggested in this study, the goal of which is to optimize the size and sitting of the EVCSs and the expansion plans of the distribution system. Wind power penetrations are considered. High efficiency scenario based stochastic models of EV charging demand are established using the SG method. The suggested model is solved with a multi-objective optimization tool, MONAA. As shown in Section 4.8.2, compared to FFS and BR, the SG method not only significantly reduced overall computation time, but also lowered the error in approximating the cost of investment and energy loss. Moreover, Section 4.8.3 demonstrated the benefit of including wind generation, which is that the overall cost was reduced. Furthermore, the efficiency for the developed algorithm is highlighted in Section 4.8.4 where MONNA outperformed the commonly used NSGA-II and MOEA/D. To sum up, the final planning strategy calculated from the proposed model using SG-based MONAA improves computation efficiency and approximation accuracy, increases the charging service level, and reduces the investment cost and energy losses.

4.10 Future Works

Here are some of the aspects in our planning approach that can be improved. 1) Currently, the location and capacity of wind generation is pre-determined. To improve the obtained Pareto frontier, one can include the optimization of renewable generation in the planning. Additionally, more types of renewable generation, e.g., solar and hydro, may also be considered. 2) Battery Energy Storage Systems (BESS) can be used to mediate the stochastic nature of renewable generation and EV charging demand, as well as improve network stability. The optimization model could include the location and sizing of BESS in future iterations. 3) Real-world transportation and distribution network data could be used in the optimization to obtain planning results that are more practically relevant. 4) One might also consider the issues in real-time operation of the EVCSs, such as missing data, data latency and sensor failure. In some cases, these issues might be alleviated by data processing techniques, e.g., deep learning [44].

Chapter 5

Planning of Hydrogen Refuelling Stations in Urban Setting While Considering Hydrogen Redistribution

5.1 Relationship with the thesis

In Chapter 1, it is recognized that there is a lack of studies focusing on the profitability of HRSs during planning phase. In this chapter, a planning model that aims to maximize the captured traffic flow and profit while sizing and sitting HRSs is presented.

This Chapter has been published.

This chapter has been edited to incorporate thesis reviewers' comments.

5.2 Abstract

Electrified transportation systems and renewable energy resources have been recognized as effective environmental-friendly technologies against global warming contributed by greenhouse gas (GHG). Remarkably, hydrogen fuel cell-powered electric vehicles (FCEVs) can outperform battery-powered electric vehicles (BEVs) largely in the sense of the driving range and the refueling time. However, both of them requires a better coordination of infrastructure system and renewable energy resources to achieve a significant reduction of GHG emissions. This chapter aims to maximize the long term profitability for the planning model of hydrogen refueling stations where the Capacitated Flow Refueling Location Model (CFRLM) is leveraged for maximal traffic flow coverage. Furthermore, we discuss various real-world constraints, such as Traffic Network (TN) constraints, Distribution Network (DN) constraints, hydrogen balance constraints, and energy constraints for EVs, to make the planning model more practical. By considering the uncertainty of the short-term refueling demand across the city, an approach for geographically redistributing hydrogen among the stations is also presented where the minimal cost of redistribution is modelled by One-commodity Pickup-and-Delivery Traveling Salesman Problem. A real-life case study of western Sydney is adopted to testify the efficiency of the planning model under current and future cost levels. Finally, a numerical simulation is utilized to demonstrate the validity of the hydrogen redistribution method.

Nomenclature

Parameters

β	Charging/discharging efficiency of BES
c_B	Per kWh cost of BES
c_C	Per kWh penalty of using grid power

$c_{E,t}$	Per kWh cost of buying electricity from the grid at time t
c_{fixed}	Per station fixed cost for hydrogen refuelling stations
c_H	Per kg/h production capacity cost of hydrogen electrolyser
c_p	Penalty cost for unsatisfied traffic flow
c_{PV}	Per kW cost of PV module
c_T	Per kg capacity cost of the hydrogen storage tank
C_{total}	Max budget for capital investment
D	Total number of days in the planning horizon
E_H	Amount of energy required to produce 1 kg of hydrogen
η	PV module efficiency
F_t^q	Traffic flow on path q at time t
$\hat{g}_{B,i}$	Max BES size at node i
$\hat{g}_{H,i}$	Max hydrogen production capacity at node i
$\hat{g}_{PV,i}$	Max capacity of PV size at node i
$\hat{g}_{T,i}$	Max Hydrogen storage tank size at node i
$\overline{I}_{m,n}$	Upper limit of current on feeder m,n
κ	Amount of hydrogen required by each FCEV for a full refill
m_i	Profit modifier at node i
p_{max}^B	Max power output of the BES
r_i	Per kg revenue for selling hydrogen at node i
SI_t	Solar irradiance during time t
$s_{m,t}$	Power injection at bus m during time t
$s_{m,t}^b$	Base-load at bus m during time t
$\underline{V}_m/\overline{V}_m$	Lower/upper limit of nodal voltage at bus mr
$z_{m,n}$	Impedance of feeder m,n
Variables	
$B_{i,t}$	Amount of energy stored by the BES at node i during time t
$g_{B,i}$	BES size at node i
$g_{H,i}$	Production capacity of hydrogen electrolyser at node i
$g_{PV,i}$	Name plate capacity of PV module at node i

$g_{T,i}$	Capacity of the hydrogen storage tank at node i
$H_{i,t}$	Amount of hydrogen produced by the electrolyser at node i during time t
$\lambda^{q}_{ij,t}$	Fraction of traffic travelling from i to j on path q at time t
$l_{m,n,t}$	Square of the magnitude of the current in feeder m, n during time t
μ_i	Binary variable indicating if a station is built at node i
$p^{B}_{i,t}$	Power output of the BES at node i during time t
$p^{H}_{i,t}$	Net power required for hydrogen production at node i during time t
$p^{H}_{i,t}$	Net power for hydrogen production at node i during time t
$p^{PV}_{i,t}$	PV output at node i during time t
$p^{H}_{m,t}$	Active hydrogen production load at bus m during time t
$S_{m,n,t}$	Apparent power flow from bus m to bus n during time t
$s^{H}_{m,t}$	Hydrogen production load at bus m during time t
$T_{i,t}$	Amount of hydrogen in the storage tank at node i during time t
$v_{m,t}$	Square of the magnitude of the nodal voltage at bus m during time t

5.3 Introduction

Almost all world-class metropolises are densely populated which requires a considerable amount of energy to maintain the daily commute and the road traffic contributing to a large proportion of carbon dioxide emissions [269]. Electrified transportation systems and renewable energy resources are considered as one of most effective green technologies to reduce the effect of global warming and climate change attributed to greenhouse gas emissions [270]. In comparison to internal combustion vehicles (ICVs), electric vehicles (EVs) including cars and metro trains not only can bring about better energy efficiency, but also can introduce a great benefit of not emitting any GHGs in driving.

With the high proliferation of EVs, fast-Charging infrastructure is essential. A fast charging station planning strategy is investigated in [228] where the interactions of the traffic and the flows are considered to construct the capacitated-flow refuelling location model (CFRLM). By considering traffic constraint [271], an EV flow capturing location model is introduced for maximizing the traffic flow where the battery capacity is also considered. To further refine the practicality of the fast-charging station planning, the practical constraints of the power network with AC power flow is modeled into a modified CFRLM which can be efficiently solved by the second-order cone programming [247]. A data-driven planning approach is studied in [44] where graph neural network is leveraged for the long-term charging demand forecasting in Sydney city. To achieve the purpose of EV's faster charging, the battery charging/swap stations can be considered as a promising solution When power is collected from renewable energy. In [272], an optimal framework for battery charging/swap stations planning is presented in distribution systems where the life cycle cost is modelled into the battery charging/swap station and renewable energy can be used to charge the battery in advance. A similar idea of battery charging/swap stations planning can be found in [273] where the utilization of solar energy is maximized.

The controversy between battery-powered electric vehicles (BEVs) and hydrogen-powered electric vehicles (HEVs) has lasted more than one decade. Despite being an environmentally favored transportation tool, EVs still pale compared with fossil fuel-powered vehicles in terms of popularity. This is probably because of the inconvenience caused by a short driving range and a long refuelling time. As hydrogen is a high-efficient clean energy source with a higher energy density, both academia and industry are increasingly interested in developing and deploying hydrogen Fuel Cell Electric Vehicles (FCEVs) for electrified transportation systems [274]. Moreover, in terms of the driving range and the refuelling time, FCEVs are advantageous over Battery Electric Vehicles (BEVs). Yet, the planning and profitability of electric vehicles' charging stations [228, 275] have been well studied, less so for hydrogen refuelling stations. To simultaneously provide services for both FCEVs and BEVs, a combo station involving a fast EV charging station and a hydrogen refuelling station is introduced in [42]. Although the concept of the planning approaches of EV charging stations can be used to design Hydrogen refuelling stations, unique attributes of hydrogen refuelling stations should be identified for practicality. There have been several studies focused on the location and size of hydrogen refuelling stations. For example, [38] proposed a multi-stage planning strategy to plan hydrogen stations for South Korea, in which the Maximal Covering Location Problem and the P-median problem are solved in sequence to obtain the final result. In [25] the authors used information from several data sources to estimate the refuelling demand and deployed genetic algorithm to solve the P-median model. In [276], the authors developed a mathematical model to optimize the hydrogen supply system as well as hydrogen refuelling stations. Although the authors compared different hydrogen production methods in [276], certain aspects of electrolysis were overlooked. For instance, the impact [277] on the distribution network contributed by the hydrogen electrolyser where the constraints on distribution network should be considered in the planning. The desirable planning should consider practical constraints, thereby real-world case studies are preferably over synthetic ones.

The optimization objective of [25, 38, 276] are focused on social benefit,like covering the most of demand, minimizing the travel cost for customers, or minimize the overall cost of hydrogen. To promote FCEVs and widely deploy hydrogen refuelling stations, the participation of private companies is essential while profitability is the main concern of private investment. Although centralized hydrogen generation can lower production costs, a significant amount of energy and cost is consumed in the process of hydrogen transportation [278]. It is indispensable to take the long-term profit for private investment into account in the planning. In [38] and [25] the authors do not consider hydrogen production in their model, which may reduce the profitability of the stations due to high hydrogen delivery costs.

Currently, most of the world's hydrogen supply is produced from fossil fuels, with Steam Methane Reforming (SMR) being the most common method [20]. However, these fossil fuel based methods still generate large amount of GHG when producing hydrogen [276]. While water electrolysis does not generate any GHG when producing hydrogen, the electrolyzers does require electricity to run. There for, rather than depending on the fossil fuels to produce hydrogen, FCEV's true success of emission reductions significantly relies on the successful integration of electrolysis with the renewable energy resources and the charging infrastructure systems. Renewable energy resources can be leveraged to power hydrogen production in order to reduce emissions. That is why the electrolyzer capacity around the world is ramping up very quickly. According to a recent report by the International Energy

Agency (IEA) electrolysis capacity becoming operational in 2019 was $25.4MW$, and in 2023 the additional electrolysis capacity becoming operational will be $1143.1MW$ [20]. Therefor, in this chapter we choose on site electrolyzers to be the production method for hydrogen.

In [25, 38, 276] only long term demands are considered in the planning models. However, the short-term demand of hydrogen refuelling can be volatile which leads to an imbalanced distribution of the reserved hydrogen across the city. Eventually it creates a large supply-demand imbalance. It is critical to investigate how to optimally coordinate the renewable energy resources and the charging infrastructure systems for supporting the electrified transportation system. Thus, to maximize the profit, we not only plan for long term demand coverage but also seek to address short term demand uncertainty.

Therefore, the contributions of this chapter address the aforementioned concerns as follows:

1) The profit is considered in the planning of hydrogen fueling station with the coordination of renewable energy resources. To eliminate the transportation cost, in this chapter the hydrogen is generated by an on-site electrolyser.

2) On-site renewable generation, Photostatic (PV), is used to power the hydrogen electrolyser along with Distribution Network (DN). In addition, the economic feasibility of on-site Battery Energy Storage (BES) is also investigated. DN constraints are also included in the optimization model to make the planning results more practical.

3) The proposed planning model is validated with a case study, in which western Sydney transportation data are used for the maximal coverage test.

4) To compensate the discrepancy of the projected and the actual hydrogen demands, a separate redistribution step is considered. For this purpose, the uncertainty of the short-term refuelling demand is addressed as a One-commodity Pickup-and-Delivery Traveling Salesman Problem, and solved by the mixed-integer linear programming.

The system diagram is shown in Fig. 5.1. We organize the rest of this chapter as follows. In

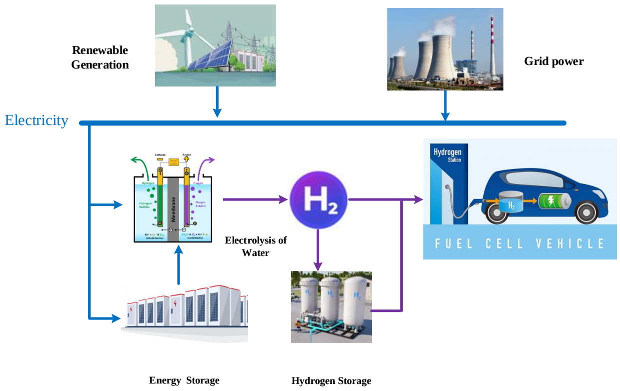

Figure 5.1: System diagram of hydrogen refuelling station with renewable energy resources

Section 5.4, the underlying problem of the planning of hydrogen refuelling stations is first formulated and then the algorithm for the problem is designed. The problem description and formulation of hydrogen redistribution are given in Section 5.5. The experimental settings are given in Section 5.6. Several numerical experiments are displayed in Section 5.7. Section 5.8 concludes this chapter.

5.4 Hydrogen refuelling station planning model

This section introduces a planning model, Capacitated Flow refuelling Location Model (CFRLM) [228], which is modified for sizing and sitting of hydrogen refuelling stations. The CFRLM has the advantage of maximizing serviceability under limited resources. Additionally, we also consider the optimal sizing of hydrogen storage tanks, BES and PV modules, plus DN constraints.

5.4.1 Capacitated Flow refuelling Location Model

To use the CFRLM the Traffic Network (TN) needs to be expanded first. Fig.(5.2) shows an example of TN expansion. The TN in (5.2a) contains one single path from node 1 to

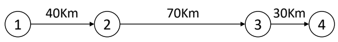

(a) A 4-node traffic network with a single path.

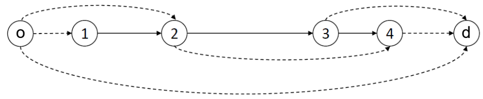

(b) The corresponding expanded traffic network

Figure 5.2: Transportation network expansion example

node 4 with arcs a_{12}, a_{23} and a_{34}. (5.2b) is the corresponding expanded TN of (5.2a), by adding virtual nodes o and d and assuming driving range is 100 km $\forall i < j$ and $d_{ij} \leq 100$, a_{ij} is added if $a_{ij} \notin A$, where A is the set of arcs of the TN. Note that o is considered as node 0 and d is node 5, in the example. For a network with more than one path, the process is repeated for each path.

In this chapter, CFRLM is modified to account for the specific constraints of hydrogen production. Note that Equ. (5.1) is the objective function, which consists of four terms. The first term is the overall investment cost, which is made of BES cost, hydrogen electrolyser cost, PV cost, hydrogen storage tank cost, and a fixed per station cost. The second term is the penalty for unsatisfied traffic flow. The third term is the cost of purchasing electricity from the grid, while the last term captures the gross profit of the hydrogen stations.

$$
\begin{aligned}
\min \Bigg\{ & \underbrace{\sum_{i\in\Psi}(c_B g_{B,i} + c_H g_{H,i} + c_{PV} g_{PV,i} + c_T g_{T,i} + c_{fixed}\mu_i)}_{\text{capital investment}} \\
& + D\sum_{t=1}^{24}(\underbrace{\sum_{q\in Q} c_p \lambda_{od,t}^q F_t^q}_{\text{penalty for unsatisfied traffic}} + \underbrace{\sum_{i\in\Psi}(c_{E,t}+c_C)p_{i,t}^H}_{\text{electricity cost}} \\
& \underbrace{- \sum_{q\in Q}\sum_{\{j|(i,j)\in\hat{A}_q\}} r_i \lambda_{ji,t}^q F_t^q \kappa)}_{\text{total revenue}} \Bigg\}, \quad (5.1)
\end{aligned}
$$

subject to

$$\sum_{\{j|(i,j)\in\hat{A}_q\}} \lambda^q_{ij,t} - \sum_{(j|(j,i)\in\hat{A}_q)} \lambda^q_{ji,t} = \begin{cases} 1, & i=o \\ -1, & i=d \\ 0, & i\neq o,d \end{cases} ,\forall q \in Q, \forall i \in \hat{\Psi}_q, \forall t, \quad (5.2)$$

$$0 \leq \lambda^q_{ij,t}, \forall q \in Q, \forall (i,j) \in \hat{A}_q, \forall t, \quad (5.3)$$

$$0 \leq g_{B,i} \leq \mu_i \hat{g}_{B,i}, \forall i \in \Psi, \quad (5.4)$$

$$0 \leq g_{H,i} \leq \mu_i \hat{g}_{H,i}, \forall i \in \Psi, \quad (5.5)$$

$$0 \leq g_{PV,i} \leq \mu_i \hat{g}_{PV,i}, \forall i \in \Psi, \quad (5.6)$$

$$0 \leq g_{T,i} \leq \mu_i \hat{g}_{T,i}, \forall i \in \Psi, \quad (5.7)$$

$$\sum_{i\in\Psi} \left(c_B g_{B,i} + c_H g_{H,i} + c_{PV} g_{PV,i} + c_T g_{T,i} + c_{fixed} \mu_i \right) \leq C_{total}, \quad (5.8)$$

$$\mu_i \in \{0,1\}, \forall i \in \Psi. \quad (5.9)$$

Equs. (5.2) and (5.3) represent the traffic flow constraints, where the supply and demand must be met. Equs. (5.4)-(5.7) are the size constraints for BES, hydrogen electrolyser, PV panels, and hydrogen storage tanks, respectively, ensuring the size of each of the components does not exceed its limit. Equ. (5.8) is the budget constraint, which is the main limiting factor for a private company.

5.4.2 Additional constraints

5.4.2.1 Hydrogen balance

The following constraints couples the hourly hydrogen production and tank reserve at each station with the traffic flow.

$$\forall i \in \Psi, \forall t:$$

$$T_{i,t} = T_{i,t-1} + H_{i,t} - \sum_{q\in Q} \sum_{\{j|(i,j)\in\hat{A}_q\}} \lambda^q_{ji} F^q_t \kappa, \quad (5.10)$$

$$T_{i,1} = T_{i,24} + H_{i,1} - \sum_{q\in Q} \sum_{\{j|(i,j)\in\hat{A}_q\}} \lambda^q_{ji} F^q_1 \kappa, \quad (5.11)$$

$$0 \leq T_{i,t} \leq g_{T,i}, \tag{5.12}$$

$$0 \leq H_{i,t} \leq g_{H,i}. \tag{5.13}$$

Equ. (5.10) balances the supply and demand of hydrogen at each site over time, ensure that the traffic can only be captured if there is enough hydrogen supply at a given station. . Equ. (5.11) is the special case of Equ. (5.10) introduced to avoid depletion of hydrogen at the end of each day. Equs. (5.12) and (5.13) ensure the storage and production cannot exceed their limit at each site.

5.4.2.2 Battery energy balance constraints

the constraints concerning the charge/discharge of the BES are similar to the hydrogen balance constraints for hydrogen tanks. The energy balance constraints of BES are formulated as Equs. (5.14)-(5.17).

$$\forall i \in \Psi, \forall t :$$

$$B_{i,t} = \begin{cases} B_{i,t-1} - \beta p^B_{i,t}, & p_{i,t} < 0 \\ B_{i,t-1} - \frac{1}{\beta} p^B_{i,t}, & p_{i,t} \geq 0 \end{cases}, \tag{5.14}$$

$$B_{i,1} = \begin{cases} B_{i,24} - \beta p^B_{i,1}, & p_{i,1} < 0 \\ B_{i,24} - \frac{1}{\beta} p^B_{i,1}, & p_{i,1} \geq 0 \end{cases}, \tag{5.15}$$

$$0 \leq B_{i,t} \leq g_{B,i}, \tag{5.16}$$

$$|p^B_{i,t}| \leq p^B_{max}. \tag{5.17}$$

Equ. (5.14) links the BES's energy reserve with the hourly charge/discharge. Equ. (5.15) ensures the BES is not drained at the end of the day. Equ. (5.16) make sure the BES cannot store more energy than its capacity, and it will not create energy. Equ. (5.17) is included such that the charge/discharge power does not exceed the rated power of the BES.

5.4.2.3 DN constraints

In practical settings, the DN is also a limiting factor on the location and size of the hydrogen refuelling stations. Thus the Second-Order Cone Programming (SOCP) modeling of DN constraints [246] is incorporated into the planning model as follows.

$$\forall m, n \in \Phi, \forall i \in \Psi, \forall t :$$

$$S_{m,n,t} = s_{m,t} + \sum_{h \in M_{\to m}} (S_{h,m,t} - z_{h,m} l_{h,m,t}), \tag{5.18}$$

$$0 = s_{0,t} + \sum_{h \in M_{\to 0}} (S_{h,0,t} - z_{h,0} l_{h,0,t}), \tag{5.19}$$

$$v_{m,t} - v_{n,t} = 2Re(z^*_{m,n} S_{m,n,t}) - |z_{m,n}|^2 l_{m,n,t}, \tag{5.20}$$

$$|S_{m,n,t}|^2 \leq l_{m,n,t} v_{m,t}, \tag{5.21}$$

$$l_{m,n,t} \leq |\overline{I}_{m,n}|^2, \tag{5.22}$$

$$|\underline{V}_m|^2 \leq v_{m,t} \leq |\overline{V}_m|^2, \tag{5.23}$$

$$s_{m,t} = -s^H_{m,t} - s^b_{m,t}, \tag{5.24}$$

$$s^H_{m,t} = p^H_{m,t} + j \tan\theta p^H_{m,t}, \tag{5.25}$$

$$p^H_{m,t} = \sum_{i \in I_m} p^H_{i,t}, \tag{5.26}$$

$$p^H_{i,t} = H^P_{i,t} E_H - p^{PV}_{i,t} - p^B_{i,t}, \tag{5.27}$$

$$p^{PV}_{i,t} = \eta n_{PV,i} SI_t, \tag{5.28}$$

$$0 \leq p^H_{i,t}. \tag{5.29}$$

Equs. (5.18)-(5.21) are the AC power flow constraints, in which Equ. (5.21) is a SOC relaxation of the exact constraint. Equs. (5.22) and (5.23) ensure the feeder current and nodal voltage do not violate their limits, respectively. The PV generation, BES output, and electrolyser loads are coupled to the DN as shown in Equs. (5.24)-(5.28). Constraint (5.29) is introduced so that the hydrogen refuelling stations do not feed back to the grid. Note that generally speaking the more standard semidefinite programming (SDP) formulation is a stronger relaxation than SOCP [279]. However, in this chapter the DN is made of radial networks that have unidirectional power flows, therefore the SOCP relaxation is exact [246].

5.5 Hydrogen redistribution

For onsite storage at the refuelling stations, hydrogen can be easily stored and quickly refuelled as a compressed gas [96]. Storing hydrogen as a compressed gas at room temperature also have low energy loss [85] When the projected hydrogen demand during the planning phase and the actual hydrogen refill demand in operation does not match, certain stations may not be able to meet the hydrogen refuel demand while other stations will have an excess of production, thus there would exist a need to redistribute the hydrogen. As an underground hydrogen pipe network connecting all hydrogen stations requires both a large amount of investment and extended period of time to build, the hydrogen tube trailer is the only viable option for the hydrogen redistribution among the refuelling stations in the early stages.

In this chapter, we assume that all of the hydrogen refuelling stations, as well as the tube trailer, are operated by the same entity, thereby allowing coordination among the stations. Moreover, since in the early stages of hydrogen station deployment both the number of stations and the amount of hydrogen requiring pick-up/delivery at each station will be small, it is within reason to assume a single tube trailer will be able to service all the stations. With these assumptions, the redistribution of hydrogen can be formulated as a special case of the traveling salesman problem, known as the "One-commodity Pickup-and-Delivery Traveling Salesman Problem" (1-PDTSP). We use the mixed-integer linear programming (MILP) reformulation in [280] to solve this problem.

Define a set of locations Ψ_d, which contains the depot (denoted as node 0) and all customers (in this case hydrogen refuelling stations). Next, define A_d as the set of arcs connecting the node pairs. Then the 1-PDTSW is defined under a complete graph $G = (\Psi_d, A_d)$, which is a subgraph of the TN. Let e_{ij} denote the distance between node pairs. h_i is the quantity of hydrogen at node i, where a negative value means a surplus of hydrogen for pick-up, and a positive value means a shortage of hydrogen that needs to be filled. $h^{cap}$is the capacity of the tube trailer. Define a binary variable y_{ij}, where $y_{ij} = 1$ means that the tube trailer traveled from node i to j, and zero otherwise. Define a continuous variable x_{ij} which corresponds to the weight of hydrogen onboard the tube trailer when traveling from i to j. Define $o_{ij}$to be the order of arcs the trailer traveled in the solution.

The objective, shown in Equ. (5.30), is to minimize the distance traveled by the tube trailer.

$$\min \sum_{(i,j) \in A_d} e_{ij} y_{ij} \tag{5.30}$$

subject to

$$\sum_{j \in N, i \neq j} y_{ij} = 1, \forall i \in \Psi_d, \tag{5.31}$$

$$\sum_{i \in \Psi_d} y_{ij} = \sum_{i \in \Psi_d} y_{ji}, \forall i \in \Psi_d, \tag{5.32}$$

$$x_{ij} \leq h^{cap} y_{ij}, \forall (i,j) \in A_d, \tag{5.33}$$

$$\sum_{j \in \Psi} x_{ji} - \sum_{j \in \Psi} x_{ij} = h_i, \forall i \in \Psi_d, \tag{5.34}$$

$$\sum_{j \in \Psi} o_{ji} - \sum_{j \in \Psi} o_{ij} = 1, \forall i \in \Psi_d \backslash \{0\}, \tag{5.35}$$

$$o_{ij} \leq n(\Psi_d) y_{ij}, \forall (i,j) \in A_d, \tag{5.36}$$

$$x_{ij}, o_{ij} \geq 0, \forall (i,j) \in A_d. \tag{5.37}$$

Equ. (5.31) ensures that each node is visited once and once only. Constraints (5.32) forces the trailer to leave a node after visiting it. The capacity constraint of the tube trailer is enforced by Equ. (5.33). Equ. (5.34) guarantees the hydrogen demand of each node is met. Equ. (5.35) and (5.36) are used to prevent subtours.

Please note that 1-PDTSP is a special case of Pick-up and Delivery Problems (PDPs), which have many variations and is an area of active research. For example, as the number of hydrogen stations and the hydrogen imbalance increases, multiple tube trailers may be required for the redistribution of hydrogen. In this case, one can either split the planning area as different smaller partitions which can be solved by 1-PDTSP for each partition, or formulate the problem as a multi vehicle PDP (MVPDP). Another variation is when time constraints are added to each pick-up/delivery order, such problems are referred as PDP with Time Window (PDPTW). Interested readers can find a detailed review of PDPs in [281], which include different formulations for both MVPDP and PDPTW.

5.6 Experimental setup

The experiments for validating the optimization models include two parts. Section 5.6.1 describes the case study used to verify the effectiveness of the planning model. Section 5.6.2 gives the detailed settings of hydrogen redistribution simulation.

5.6.1 Case study: hydrogen refuelling station planing

The case study in this chapter uses the real-world TN and DN data of Western Sydney [44]. The data include 24-hour bidirectional traffic flow through each traffic node as well as 24-hour power consumption at each distribution node. The TN consists of 41 transportation nodes with each node being an equally valid candidate for hydrogen refuelling stations. The DN is a simplified version of the Endeavour Energy 33kV network that has 7 transmission substations and 35 zone substations, in the vicinity of the TN nodes. Fig. 5.3 shows the locations of these traffic nodes and substations. The connections of TN and DN nodes are shown in Fig. 5.4. We assume that the hydrogen station at each TN node is supplied by the nearest zone substation. The Time Of Use (TOU) pricing of grid electricity is obtained from [282] for and is shown in Fig. 5.5. It has three levels namely off-peak 0.1 $\$/kWh$, peak 0.43 $\$/kWh$ and shoulder 0.19 $\$/kWh$. Please note that additional costs for using grid power, c_C, is added to simulate the effect of carbon tax, thereby further penalize GHG emissions and incentives the use of renewable energy. However, in this study such penalty is set to 0 $\$/kWh$ as Australia currently does not have a carbon tax scheme. The solar irradiance data used is from [283], we assumed the all the TN nodes have the same

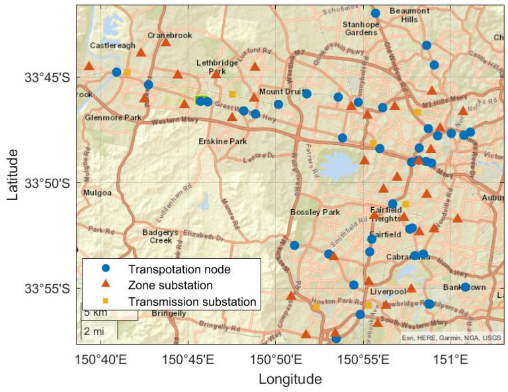

Figure 5.3: Real world location of TN and DN nodes

amount of solar irradiance.

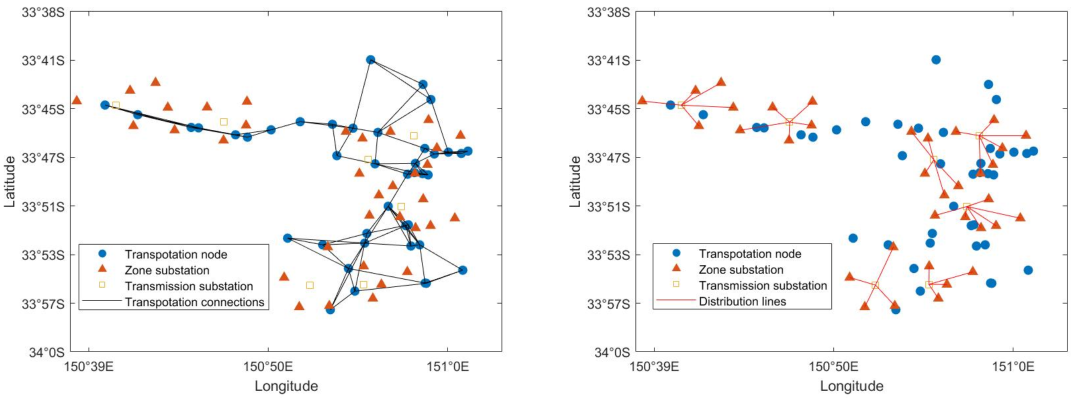

(a) (b)

Figure 5.4: Scatter plot of TN and DN, showing transportation connections (a) and distribution connections (b)

In this experiment, we used the first generation of Toyota Mirai as an example, which has a range of 502 km and the onboard hydrogen tank has a capacity of 5.0 kg [284]. We assume that drivers will refuel their FCEVs every 400 km to avoid range anxiety. Additionally, to account for the non-optimal driving conditions of Sydney, we assume that FCEVs will require 4.5 kg of hydrogen each time they are refilled. The FCEVs enter the transportation network with enough hydrogen to travel 140 km. To study the effect of different parameters (e.g. the cost and the efficiency of electrolyser) on the planning result, two different experiments were conducted, one using the current values while the

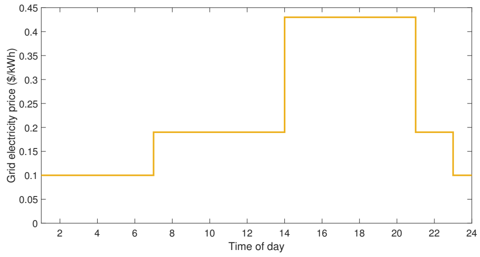

Figure 5.5: TOU pricing of electricity from Ausgrid [6]

Table 5.2: Key parameters for the planning model

	Current value	Projected value
c_{PV}	100 $\$/m^2$ [285]	70 $\$/m^2$ [68]
c_H	123,390 $\$/kg \cdot h^{-1}$ [68]	55,000 $\$/kg \cdot h^{-1}$ [68]
c_B	540 $\$/kWh$ [68]	200 $\$/kWh$ [68]
c_T	400 $\$/kg$ [286]	350 $\$/kg$ [286]
E_H	54 kWh/kg [68]	50 kWh/kg [68]
r_i	23 $\$/kg$ [287]	15 $\$/kg$
c_{fixed}	$ 250,000 [53]	
C_{total}	$ 100 millions	
c_p	1000 $\$/veh$	
η	4%	
β	90%	
$\hat{g}_{B,i}$	300 kWh	
$\hat{g}_{H,i}$	100 kg/h	
$\hat{g}_{PV,i}$	500 m^2	
$\hat{g}_{T,i}$	500 kg	
p^B_{max}	100 kW	

other using projected values that can be achieved by technological development in the next 10-15 years. The planning horizon is set to 25 years in both experiments [68]. The key parameters are summarized in Table.5.2. Note the parameters are for demonstrative purpose only because in real life some of the parameters, such as the size limit for each of the components, are determined by a plethora of factors (national/local regulations, site specific constraints, company policies, etc) while others, such as the cost of components, are constantly changing as a result of development, thus readers can choose and modify the parameters to suit their specific circumstances.

5.6.2 Hydrogen redistribution

Once the planning of hydrogen refuelling stations have been completed under the setup mentioned in the above section, we can then validate the hydrogen redistribution method described in Section 5.5. Firstly the complete graph G is constructed by selecting all the TN nodes with hydrogen refuelling stations built on them (Ψ_d) and connecting them by arcs (A_d) corresponding to the minimum distance between them in the TN. It is worth pointing out that in this step all the intermediate nodes are excluded. For example, if node 1 and node 5 are not directly connected and the path of minimum distance is $1-3-7-5$, then arc a_{15} will be added whose length is equal to path $1-3-7-5$. Node 3 and 7 will not be included in G unless they have hydrogen refuelling stations on them. After constructing G, we randomly assigning hydrogen quantities in the range of -100 to 100 kg to each station and ensure the net request is zero. In other words $h_i \in [-100, 100], \forall i \in \Psi_d$ and $\sum_{i \in \Psi_d} h_i = 0$. We assume the hydrogen tube trailer has a capacity of 200 kg. The trailer will start and end the route at one of the stations that require hydrogen pickup ($h_i \leq 0$), meaning one of the stations is both a customer and the depot.

Both of the models in Section 5.4 and 5.5 are implemented with YALMIP and MATLAB, which are then solved with CPLEX on a desktop computer with a 4-core Intel Core i7-6700K processor and 16 GB of RAM. Each simulation is stopped when the optimization gap is below 5%.

5.7 Simulation Results

The simulation results in this section are based on the experiment setup in the aforementioned Section 5.6. The planning results of hydrogen refuelling stations are given in Section 5.7.1 while Section 5.7.2 presents the validation of the 1-PDTSP model in the context of hydrogen redistribution.

Table 5.3: Comparison of optimization results using current and projected parameters

	Current case	Projected case
Number of stations	11	19
Hydrogen production capacity	766 kg/h	1616 kg/h
Max captured traffic flow	170 veh/h	359 veh/h
PV module	4,820 m^2	7,796m^2
Hydrogen tank capacity	3,064 kg	5,921 kg
BES	0 kWh	0 kWh
Total revenue	\$ 944.5 millions	\$ 1,229 millions

5.7.1 Results of hydrogen refuelling station planning

The comparison of planning results using current and projected parameters is summarized in Table 5.3. Comparing to the current case, the component cost for electrolysers is reduced due to technology development in the next 10-15 years. As a result, there are 7 more hydrogen refuelling stations built in the future with more than double the total production capacities. The increase in production capacities, from 766 to 1616 kg/h, enables the station to refuel additional 189 vehicles per hour in rush hours. Moreover, the lower component cost also leads to the rise in the total area of PV modules and total storage capacity of hydrogen tanks, from 4820 m^2 and 3064 kg to 7796 m^2 and 5921 kg, respectively. The aforementioned changes in the projection contribute to a roughly 30 % increase in total revenue to 1229 million dollars with the same investment budget.

It should be noted that there are zero BES installed at the hydrogen refuelling stations in both cases. In fact, the BESs are only included in the hydrogen stations when we lowered their cost to about 100 $\$/kWh$, which is not a reasonable level that can be achieved in the next 10-15 years, meaning unless the battery technology advances drastically including BES in hydrogen refuelling stations may not viable in a purely economical sense. The BES does offer other benefits such as load leveling and increasing resilience to grid disturbances, but these benefits are not within the scope of this study and thus are not included in the model.

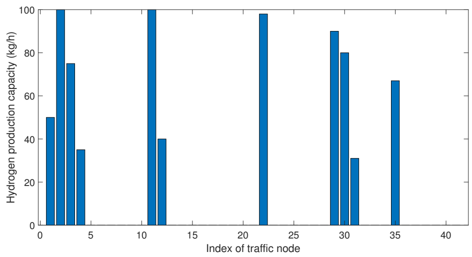

(a)

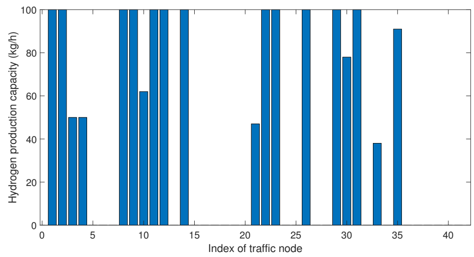

(b)

Figure 5.6: Optimized hydrogen production capacity using current (a) and projected (b) parameters at each traffic node. The node with an electrolyser means that there is a hydrogen refuelling station

Fig. 5.6 and 5.7 show the hydrogen production capacity and size of the hydrogen storage tank at each node after optimization using the current and projected parameters. Note that in Fig. 5.6a only 2 stations at node 2 and 11 have the maximum allowed production capacity installed, while other stations have an electrolyser with production capacity in the range of 31-90 kg of hydrogen per hour. Additionally, all of the stations have hydrogen storage tanks built (see Fig. 5.7a), and the sizes of the tanks are proportional to the sizes of electrolysers where each tank can hold about 4 hours worth of hydrogen produced at the installed capacity. Given the same demand profile, a station with a small electrolyser would need to produce hydrogen continuously and store the hydrogen in its tank to meet rush-hour demand, while a station equipped with a large electrolyser can ramp up/down the production of hydrogen according to demand and/or energy cost. At the current cost level, it seems that it is more economically favorable to build a small electrolyser than a large one. This is confirmed when we plotted the hourly hydrogen production at stations in the current case. All of the stations are production hydrogen near capacity and did not show variation though out the day. One of the example of hourly hydrogen production at node 35 is shown in Fig. 5.8a .

Whereas in the projected case (Fig. 5.6b), 12 out of the 19 stations built are at maximum allowed production capacity as the result of reduced electrolyser cost. More interestingly, in Fig. 5.7b there are a few stations that do not have a hydrogen storage tank built. For instance, as shown in Fig. 5.8b the production of hydrogen at one of the stations without

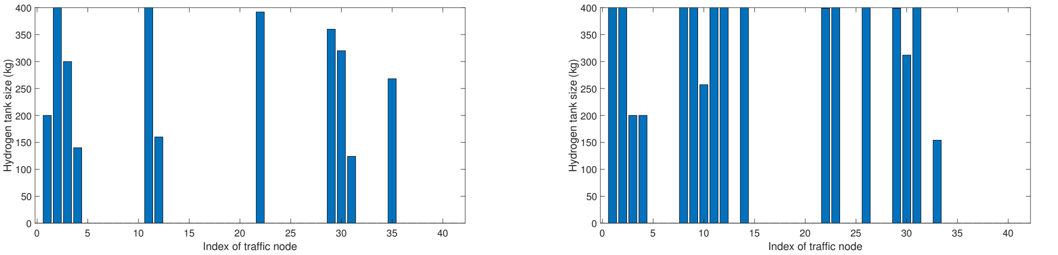

(a) (b)

Figure 5.7: Optimized hydrogen storage tank size using current (a) and projected (b) parameters at each traffic node.

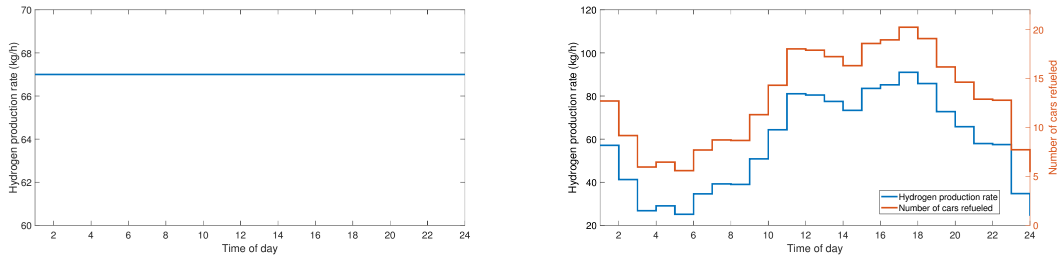

(a) (b)

Figure 5.8: Hourly hydrogen production at the refuelling station on node 35 in the current (a) and projected (b) case.

a tank, still at node 35, is actually varying according to the hydrogen demand which is proportional to traffic flow. This means the reduction in component cost can affect how a hydrogen refuelling station operates. Although at a real-life hydrogen station, a hydrogen buffer tank is always needed to at least temporarily store the hydrogen produced by the electrolyser.

In Fig. 5.9, for both the current and projected cases, the majority of the stations have built the maxim allowed size of PV modules. The economical reason for installing PV modules is that the time window of PV output (around 7:00-20:00) coincides with the peak(between 14:00-21:00) and shoulder (7:00-14:00) TOU pricing of the grid supply, thus significantly offsetting the increase in hydrogen production costs caused by TOU pricing. The amount of money spent buying electricity from the grid with and without PV at the hydrogen refuelling station (node 35) in the current case is shown in Fig.5.10. It can be seen that during 14:00-1500 the PV module reduced the energy cost by around 300 $\$/h$, and the

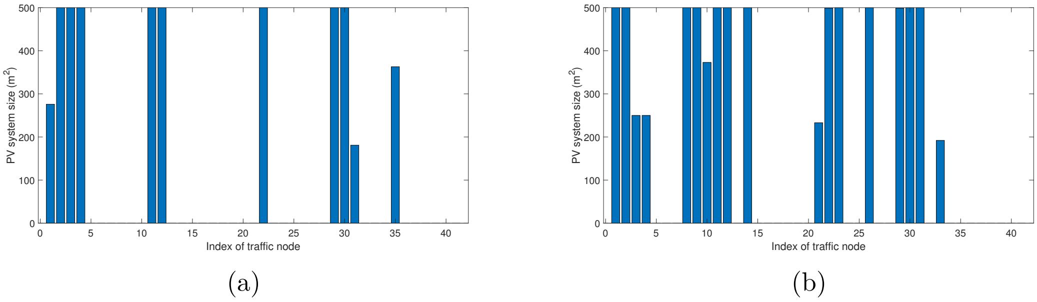

Figure 5.9: Optimized solar module size using current (a) and projected (b) parameters at each traffic node.

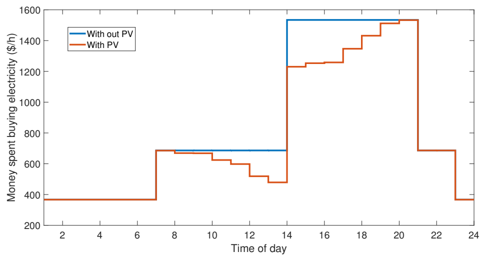

Figure 5.10: Hourly energy cost at node 35 with and with out PV in the current case

over cost saving is about 1750 $ for the entire day. The significance of this offsetting effect is that, even at the current cost level, a private company has a tangible monetary incentive to include PV generation when planning for hydrogen refuelling stations in addition to the social/environmental benefit in reducing carbon emission.

In order to better understand the impact of different component on the total profit. A sensitivity analysis is also conducted based on the cost level of the current case. In this analysis the cost of each of the major component, namely the electrolyzer, PV module, storage tank, BES and the fixed per station cost were increased/decreased by 30% each, the values of the changed cost levels are given in Table 5.4. The impact of varying cost levels on the total revenue is plotted in Fig. 5.11. Please note that since the increase of electrolyzer cost resulted in a 100% reduction of total revenue, we have to truncate the plot to better visualize the effect of other components. As it can be seen in Fig. 5.11, the changes in electrolyzer cost has the most significant effect on the total revenue. For instance, if the electrolyzer cost increase by 30%, hydrogen refuelling stations become

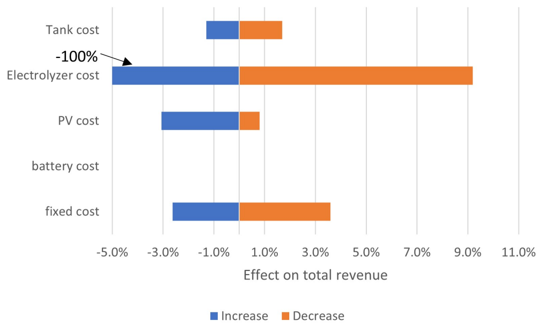

Figure 5.11: Tornado chart of the impact on total profit, with the negative impact of electrolyzer truncated.

Table 5.4: The decreased and increased cost levels of the current case for sensitivity analysis

	Decreased	Base	Increased
c_T	280 $\$/kg$	400 $\$/kg$	520 $\$/kg$
c_H	86,400 $\$/kg \cdot h^{-1}$	123,390 $\$/kg \cdot h^{-1}$	16380 $\$/kg \cdot h^{-1}$
c_{PV}	70 $\$/m^2$	100 $\$/m^2$	130 $\$/m^2$
c_B	380 $\$/kWh$	540 $\$/kWh$	700 $\$/kWh$
c_{fixed}	\$ 175,000	\$ 250,000	\$ 325,000

economically unfeasible under the current setting. This is unsurprising as electrolyzer dominates the total cost of all the hydrogen refuelling stations. In addition, the variation in BES cost does not have any impact on the total revenue. As mentioned before, BES only become financially viable if the cost lowers to 100 $\$/kWh$, thus BESs are still not built this analysis. The effect of PV cost is also notable, as it has the second greatest negative impact on revenue when increased. However, when the PV cost decreased, it has the least effect on revenue. This is due to the fact that in the base case most stations already have the maximum (or near maximum) allowed PV built, thus further reduction in PV cost does not significantly affect total revenue.

An additional comparison experiment is conducted to evaluate the benefit of using SOCP formulation over the more standard SDP formulation for DN constraints. Please note that this part of the experiment is solved using MOSEK under YALMIP and MATLAB, as CPLEX cannot be used to solve SDP. The SDP formulation of DN in [279] is used as

Table 5.5: Comparison of computation time and final result of SOCP and SDP formulations

	SOCP	SDP
Optimization gap	5%	5%
Computation time	$2728s$	$6805s$
Total profit	\$945.2 million	\$945.6 million

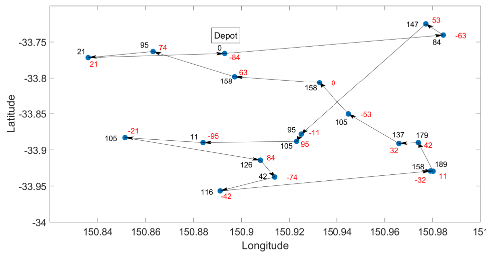

Figure 5.12: Hydrogen redistribution result

an example. The result for this experiment is shown in Table 5.5. It can be seen that the difference in objective value is about 0.05% but the computation time of SDP formulation is more than double that of SOCP formulation. In other worlds the SOCP formulation can achieve comparable results in much less time than SDP formulation.

5.7.2 Results of hydrogen redistribution

The simulation result for hydrogen redistribution in the projected case is shown in Fig. 5.12. The blue dots are the hydrogen refuelling stations. The arrows indicate the path and direction the tube trailer travels. The red numbers are the amounts of hydrogen that need to be picked up/delivered at each station in kg, while the numbers in black are the amount of hydrogen on the tube trailer when it arrives at each of the stations. It is clear that all the pickup and delivery requests have been fulfilled, thus proving the effectiveness of the implemented model. Furthermore, the network of hydrogen refuelling stations acquired greater flexibility and resilience to fluctuations in hydrogen demand. In this case study the amount of hydrogen that needs redistribution is 475 kg/day, or about 15 % of the daily hydrogen production in the current case. Assuming the levelized transportation cost for hydrogen is about $1\$/kg$ [288], then the annual redistribution cost is 173375 $\$/y$.

5.8 Conclusion and Future works

In this chapter, we formulated a planning model for hydrogen refuelling station that can simultaneously optimize the sizing and sitting of the hydrogen stations. The planning model is based on the CFRLM, while considering additional constraints specific to the hydrogen refuelling stations as well as DN constraints. The main components considered when sizing the hydrogen refuelling stations include the electrolyser, the hydrogen storage tank, PV panels, and BES. The main novelty of this chapter is that the planning model also includes the profitability of the stations. Furthermore, this chapter also analyzed the effect of the change in component cost on the profitability of stations. Additionally, during the operation of the hydrogen refuelling stations, a number of factors can cause an imbalance in hydrogen production and demand. For instance, the traffic flow patterns might change after the stations have been built, thus altering the hydrogen demand at each location. In this chapter, the hydrogen redistribution issue is treated as a 1-PDTSP under mild assumptions.

A case study using real-life TN and DN data of western Sydney is conducted to validate the planning model. The validation is performed under two settings. These two settings represent the current level of cost associated with building hydrogen stations and the level of cost that could be reached in the next 10-15 years. Experimental results show that, as expected, the profitability of the hydrogen refuelling stations will increase which is attributed to the reduced cost in the future. In addition, the reduction in cost level may alter how some of the stations operate. Moreover, the experiments revealed that even under current cost levels PV panels can reduce the operational cost of the stations. However, the BES is not economically viable in neither the present nor the future case. The experiment in Section 5.7.2 presents an instance of hydrogen redistribution in the case of an imbalance between hydrogen production and demand.

To sum up, the proposed planning model is able to optimise the sizing and sitting of hydrogen refuelling stations, while considering the TN and DN constraints, by trying to minimize the overall cost and maximise revenue at the same time. Through the case study, the effect of reduced cost on the operation of hydrogen stations is revealed, allowing companies to optimally allocate budget.

There are several areas of our work that can be improved in future works. To begin with, one can study the impact of the composition of different type of demand at each TN and DN node on the planning of hydrogen refuelling stations.

Chapter 6

Conclusion and Future Directions

6.1 Thesis conclusion and contributions

With transportation being the second largest GHG emitting sector [1], reducing emissions from transportation is pivotal in the fight against the climate crisis. Both BEVs and FCEVs are effective tools in reducing GHG emissions from road transport, but the lack of supporting infrastructure, particularly the insufficient number of EVCSs and HRSs, hinders the deployment of BEVs and FCEVs. To address this issue and promote adoption of BEVs and FCEVs, this thesis proposed three EVCS and HRS planning models and frameworks. The major contributions of this thesis are as follows:

The current status of technology and research related to the hydrogen life cycle from the literature is summarised in Chapter 2 (**under review**), with a focus on using hydrogen as an energy carrier for transportation. Hydrogen production techniques (including reforms and electrolysis), hydrogen storage and transport methods for pure hydrogen and hydrogen carriers, point-based and flow-based HRS planning models, and all major types of fuel cell technologies are covered in this chapter. The limitations and technical challenges faced by each of these techniques,methods,models and technologies are detailed, such that future researchers can focus on addressing these issues. Since it is not possible to cover all the details of every topic, additional references are provided for readers that may have a particular interest.

In Chapter 3 (**published**), a market-based planning model for EVCSs is developed, in which different service providers compete with each other in the same region. A data-driven framework of EVCS planning is proposed. In this frame work, a matrix factorisation-based spatial-temporal analysis is used to impute the missing data in the traffic flows. To predict the EV charging demand, a deep learning approach is developed with a multi-relation GCN encoder-decoder architecture. The optimal budget allocations for each competing company are derived from a Cournot competition model. A parallel algorithm is deployed to find the equilibrium. To make the planning framework more practical, DN constraints are considered in the final step of sizing each of the EVCSs. A real world case study of Sydney, Australia, is used to validate the proposed framework.

In Chapter 4 (**published**), a multi-objective optimisation model that can simultaneously plan the sizing and sitting of EVCSs as well as the local DN expansion is developed while adopting a novel scenario generation to speed up computation and improve accuracy. Wind power is included in this planning model. EV charging demand is calculated with a probabilistic model using the SG method. Finally, the optimal planning results are obtained with MONAA. Comparison experiments show that the SG method outperforms commonly used FFS and BR approaches in terms of both computation time and approximation accuracy. The inclusion of renewable generation lowered the overall cost. Moreover, simulation studies show that MONAA can achieve better results in less time compared to widely used multi objective optimisation tools, namely NSGA-II and MOEA/D.

A planning model that optimise the location and capacity of HRSs and their components (electrolysers, solar panels and storage tanks) while maximizing the captured traffic flow and profit is developed in Chapter 5 (**accepted for publication**). The formulation of the planning model is modified from CFRLM with HRS specific constrains and DN constraints. A sensitivity study is conducted to examine the profitability of the HRSs under varying component costs. To address the issue of hydrogen imbalance during HRS operation, a hydrogen redistribution method under mild assumption is adopted based on the 1-PDTSP.

A case study of western Sydney is carried out with real-life TN and DN data. Two different experiment with current and projected component costs are conducted. The case study shows that, as expected, the profitability of HRSs will increase as the component costs decrease. Additionally, it is observed that the lowered component cost resulted in different operating modes in some of the HRSs. It is also noted that even with current cost levels, PV modules will reduce the overall cost of HRSs thereby increasing profitability, while BESs are not feasible-even at the projected (reduced) cost level.

6.2 Future works

The research covered in this thesis still has many areas for improvement. Specifically, in terms of coordinated planning of EVCSs and DN expansion (Chapter 4), here are some working directions

- Currently, capacity and the placement of renewable generation (if any) are chosen in advance. The Pareto frontier can be further improved if the optimization of the renewable generation can also included in the planning step. Further studies can also include other forms of renewable generations,such as Solar and hydro.
- Battery Energy Storage System (BESS) is often considered as a potential solution to alleviate the uncertainty problem of EV charging demand and renewable generation. Another advantage of BESS is its ability to improve distribution network stability. Hence, BESSs should be included in the next iteration of the planning model.
- More parochially relevant planning results can be obtained by using real WORLD DATA FOR transportation network and distribution network
- Several issues may arise during the operations of the EVCSs, for example, sensor failure, latency problems and packet loss. One can leverage data processing approaches like deep learning to address these issues.

Here are some directions for future research regarding the whole thesis.

- In this thesis the planning models only considers HRSs or EVCSs. In reality both BEVs and FCEVs are going to be mass adopted in order to reduce GHG emissions. HRSs and EVCSs will likely coexist in the same area. Thus, there is an imperative for a coordinated planning model that optimally locates and sizes both EVCSs and HRSs in the same region while considering other practical problems such as DN expansions.

- EVCSs and BEVs have long been viewed as useful tools for peak shaving [289]. With the advance of reversible fuel cell systems [290], there exists the potential for using HRSs as peak shaving and load levelling devices by producing and storing hydrogen from grid power during off-peak hours, then releasing electricity from said hydrogen to the grid in peak hours.

- The BEVs or FCEVs in each study are assumed to be homogeneous; in other words, all BEVs have the same battery capacity and all FCEVs have the same fuel tank size. But, as the market shares of BEVs and FCEVs grow, the homogeneous assumption will no longer be valid due to the increased number of models and makes of BEVs and FCEVs. Consequently, future planning models should consider heterogeneous traffic flows or even use the detailed traffic flow breakdown.

References

[1] IEA, "World energy balances 2020." [Online]. Available: https://www.iea.org/subscribe-to-data-services/world-energy-balances-and-statistics

[2] Deloitte, "Fueling the future of mobility hydrogen and fuel cell solutions for transportation."

[3] J. M. Andújar and F. Segura, "Fuel cells: History and updating. a walk along two centuries," *Renewable and sustainable energy reviews*, vol. 13, no. 9, pp. 2309–2322, 2009.

[4] B. Salvi and K. Subramanian, "Sustainable development of road transportation sector using hydrogen energy system," *Renewable and Sustainable Energy Reviews*, vol. 51, pp. 1132–1155, 2015.

[5] U.S. Department of Energy, "H2@scale," 2021. [Online]. Available: https://www.energy.gov/eere/fuelcells/h2scale

[6] "Time of use pricing," 2021. [Online]. Available: https://www.ausgrid.com.au/Your-energy-use/Meters/Time-of-use-pricing

[7] I. Dincer and C. Acar, "Review and evaluation of hydrogen production methods for better sustainability," *International journal of hydrogen energy*, vol. 40, no. 34, pp. 11 094–11 111, 2015.

[8] J. Chi and H. Yu, "Water electrolysis based on renewable energy for hydrogen production," *Chinese Journal of Catalysis*, vol. 39, no. 3, pp. 390–394, 2018.

[9] A. Buttler and H. Spliethoff, "Current status of water electrolysis for energy storage, grid balancing and sector coupling via power-to-gas and power-to-liquids: A review," *Renewable and Sustainable Energy Reviews*, vol. 82, pp. 2440–2454, 2018.

[10] S. Grigoriev, V. Fateev, D. Bessarabov, and P. Millet, "Current status, research trends, and challenges in water electrolysis science and technology," *International Journal of Hydrogen Energy*, vol. 45, no. 49, pp. 26 036–26 058, 2020.

[11] R. Moradi and K. M. Groth, "Hydrogen storage and delivery: Review of the state of the art technologies and risk and reliability analysis," *International Journal of Hydrogen Energy*, vol. 44, no. 23, pp. 12 254–12 269, 2019.

[12] A. Kirubakaran, S. Jain, and R. Nema, "A review on fuel cell technologies and power electronic interface," *Renewable and Sustainable Energy Reviews*, vol. 13, no. 9, pp. 2430–2440, 2009.

[13] O. Z. Sharaf and M. F. Orhan, "An overview of fuel cell technology: Fundamentals and applications," *Renewable and sustainable energy reviews*, vol. 32, pp. 810–853, 2014.

[14] S. Badwal, S. Giddey, A. Kulkarni, J. Goel, and S. Basu, "Direct ethanol fuel cells for transport and stationary applications–a comprehensive review," *Applied Energy*, vol. 145, pp. 80–103, 2015.

[15] R. G. Akay and A. B. Yurtcan, *Direct Liquid Fuel Cells: Fundamentals, Advances and Future.* Academic Press, 2020.

[16] A. Motieshirazi and M. R. Rahimpour, "Chapter 2 - application of membranes in district energy systems," in *Current Trends and Future Developments on (Bio-) Membranes*, A. Basile and G. Spazzafumo, Eds. Elsevier, 2020, pp. 31–47. [Online]. Available: https://www.sciencedirect.com/science/article/pii/B9780128178072000022

[17] IEA, "Renewable energy market update 2021," Paris, Tech. Rep., 2021. [Online]. Available: https://www.iea.org/reports/renewable-energy-market-update-2021

[18] ——, “CCUS in clean energy transitions,” Paris, Tech. Rep., 2020. [Online]. Available: https://www.iea.org/reports/ccus-in-clean-energy-transitions

[19] ——, “Global ev outlook 2021,” Paris, Tech. Rep., 2021. [Online]. Available: https://www.iea.org/reports/global-ev-outlook-2021

[20] ——, “Hydrogen,” Paris, Tech. Rep., 2020. [Online]. Available: https://www.iea.org/reports/hydrogen

[21] “Electric vessels are making waves,” Jun 2018. [Online]. Available: https://safety4sea.com/cm-electric-vessels-are-making-waves/?__cf_chl_jschl_tk__=pmd_YIOM8bTBzWHlnKzhaatoPxx_Cin2mlTLTQpTLvDvCuA-1634686722-0-gqNtZGzNAiWjcnBszQiR

[22] E. Pickrell, “Time to clean the skies, electric planes have arrived,” Jul 2021. [Online]. Available: https://www.forbes.com/sites/uhenergy/2021/07/12/time-to-clean-the-skies-electric-planes-have-arrived/?sh=2571c937734a

[23] IEA, “The future of rail,” Paris, Tech. Rep., 2019. [Online]. Available: https://www.iea.org/reports/the-future-of-rail

[24] J. Tollefson, “Hydrogen vehicles: fuel of the future?” *Nature News*, vol. 464, no. 7293, pp. 1262–1264, 2010.

[25] R. Lin, Z. Ye, Z. Guo, and B. Wu, “Hydrogen station location optimization based on multiple data sources,” *International Journal of Hydrogen Energy*, vol. 45, no. 17, pp. 10 270–10 279, 2020.

[26] M. F. Shaaban, S. Mohamed, M. Ismail, K. A. Qaraqe, and E. Serpedin, “Joint planning of smart ev charging stations and dgs in eco-friendly remote hybrid microgrids,” *IEEE Transactions on Smart Grid*, vol. 10, no. 5, pp. 5819–5830, 2019.

[27] S. Shojaabadi, S. Abapour, M. Abapour, and A. Nahavandi, “Simultaneous planning of plug-in hybrid electric vehicle charging stations and wind power generation in distribution networks considering uncertainties,” *Renewable energy*, vol. 99, pp. 237–252, 2016.

[28] W. Yao, J. Zhao, F. Wen, Z. Dong, Y. Xue, Y. Xu, and K. Meng, "A multi-objective collaborative planning strategy for integrated power distribution and electric vehicle charging systems," *IEEE Transactions on Power Systems*, vol. 29, no. 4, pp. 1811–1821, 2014.

[29] S. Wang, Z. Y. Dong, F. Luo, K. Meng, and Y. Zhang, "Stochastic collaborative planning of electric vehicle charging stations and power distribution system," *IEEE Transactions on Industrial Informatics*, vol. 14, no. 1, pp. 321–331, 2017.

[30] H. Yang, H. Pan, F. Luo, J. Qiu, Y. Deng, M. Lai, and Z. Y. Dong, "Operational planning of electric vehicles for balancing wind power and load fluctuations in a microgrid," *IEEE Transactions on Sustainable Energy*, vol. 8, no. 2, pp. 592–604, 2016.

[31] M. Mozaffari, H. A. Abyaneh, M. Jooshaki, and M. Moeini-Aghtaie, "Joint expansion planning studies of ev parking lots placement and distribution network," *IEEE Transactions on Industrial Informatics*, vol. 16, no. 10, pp. 6455–6465, 2020.

[32] P. M. de Quevedo, G. Muñoz-Delgado, and J. Contreras, "Joint expansion planning of distribution networks, ev charging stations and wind power generation under uncertainty," in *2017 IEEE Power & Energy Society General Meeting.* IEEE, 2017, pp. 1–5.

[33] ——, "Impact of electric vehicles on the expansion planning of distribution systems considering renewable energy, storage, and charging stations," *IEEE Transactions on Smart Grid*, vol. 10, no. 1, pp. 794–804, 2017.

[34] N. B. Arias, A. Tabares, J. F. Franco, M. Lavorato, and R. Romero, "Robust joint expansion planning of electrical distribution systems and ev charging stations," *IEEE Transactions on Sustainable Energy*, vol. 9, no. 2, pp. 884–894, 2017.

[35] S. Karimi-Arpanahi, M. Jooshaki, M. Fotuhi-Firuzabad, and M. Lehtonen, "Flexibility-oriented collaborative planning model for distribution network and ev parking lots considering uncertain behaviour of evs," in *2020 International Confer-*

ence on Probabilistic Methods Applied to Power Systems (PMAPS). IEEE, 2020, pp. 1–6.

[36] C. Shao, T. Qian, Y. Wang, and X. Wang, "Coordinated planning of extreme fast charging stations and power distribution networks considering on-site storage," *IEEE Transactions on Intelligent Transportation Systems*, vol. 22, no. 1, pp. 493–504, 2020.

[37] X. Wang, M. Shahidehpour, C. Jiang, and Z. Li, "Coordinated planning strategy for electric vehicle charging stations and coupled traffic-electric networks," *IEEE Transactions on Power Systems*, vol. 34, no. 1, pp. 268–279, 2018.

[38] H. Kim, M. Eom, and B.-I. Kim, "Development of strategic hydrogen refueling station deployment plan for korea," *International Journal of Hydrogen Energy*, vol. 45, no. 38, pp. 19 900–19 911, 2020.

[39] W. Tian, J. He, J. Jiang, L. Niu, and X. Wang, "Multi-objective optimization of charging dispatching for electric vehicle battery swapping station based on adaptive mutation particle swarm optimization," *Power System Technology*, vol. 36, no. 11, pp. 25–29, 2012.

[40] A. R. Bhatti, Z. Salam, B. Sultana, N. Rasheed, A. B. Awan, U. Sultana, and M. Younas, "Optimized sizing of photovoltaic grid-connected electric vehicle charging system using particle swarm optimization," *International Journal of Energy Research*, vol. 43, no. 1, pp. 500–522, 2019.

[41] Q. Dai, J. Liu, and Q. Wei, "Optimal photovoltaic/battery energy storage/electric vehicle charging station design based on multi-agent particle swarm optimization algorithm," *Sustainability*, vol. 11, no. 7, p. 1973, 2019.

[42] Z. Bao, S. You, Z. Hu, and Y. Wen, "Coordinated operation of hydrogen refuelling and fast charging combo station under normal and contingent conditions," *Energy Conversion and Economics*, vol. 1, no. 3, pp. 171–183, 2020. [Online]. Available: https://ietresearch.onlinelibrary.wiley.com/doi/abs/10.1049/enc2.12012

[43] J. Zhang, C. Li, G. Chen, Z. Y. Dong, and Q.-L. Han, "Review on hydrogen technology in the e-mobility transformation: Challenges and opportunities," Submitted for publication.

[44] C. Li, Z. Dong, G. Chen, B. Zhou, J. Zhang, and X. Yu, "Data-driven planning of electric vehicle charging infrastructure: A case study of sydney, australia," *IEEE Transactions on Smart Grid*, pp. 1–1, 2021.

[45] J. Zhang, S. Wang, C. Zhang, F. Luo, Z. Y. Dong, and Y. Li, "Planning of electric vehicle charging stations and distribution system with highly renewable penetrations," *IET Electrical Systems in Transportation*, 2021.

[46] J. Zhang, C. Li, G. Chen, and Z. Dong, "Planning of hydrogen refueling stations in urban setting while considering hydrogen redistribution," *IEEE Transactions on Industry Applications*, vol. 58, no. 2, pp. 2898–2908, 2022.

[47] K. T. Møller, T. R. Jensen, E. Akiba, and H.-w. Li, "Hydrogen-a sustainable energy carrier," *Progress in Natural Science: Materials International*, vol. 27, no. 1, pp. 34–40, 2017.

[48] World Nuclear Association, "Hydrogen production and uses," May 2021. [Online]. Available: https://www.world-nuclear.org/information-library/energy-and-the-environment/hydrogen-production-and-uses.aspx

[49] IEA, "The future of hydrogen," Paris, Tech. Rep., 2019. [Online]. Available: https://www.iea.org/reports/the-future-of-hydrogen

[50] G. Buffo, P. Marocco, D. Ferrero, A. Lanzini, and M. Santarelli, "Power-to-x and power-to-power routes," in *Solar Hydrogen Production.* Elsevier, 2019, pp. 529–557.

[51] IEA, "Energy technology perspectives 2020," Paris, Tech. Rep., 2020. [Online]. Available: https://www.iea.org/reports/energy-technology-perspectives-2020

[52] ETC, “Making the hydrogen economy possible: Accelerating clean hydrogen in an electrified economy,” London, Tech. Rep., 2020. [Online]. Available: https://www.energy-transitions.org/publications/making-clean-hydrogen-possible/

[53] K. Reddi, A. Elgowainy, N. Rustagi, and E. Gupta, “Impact of hydrogen refueling configurations and market parameters on the refueling cost of hydrogen,” *International Journal of Hydrogen Energy*, vol. 42, no. 34, pp. 21 855–21 865, 2017.

[54] J. M. Ogden, “Developing an infrastructure for hydrogen vehicles: a southern california case study,” *International Journal of Hydrogen Energy*, vol. 24, no. 8, pp. 709–730, 1999.

[55] J. M. Ogden, M. M. Steinbugler, and T. G. Kreutz, “A comparison of hydrogen, methanol and gasoline as fuels for fuel cell vehicles: implications for vehicle design and infrastructure development,” *Journal of power sources*, vol. 79, no. 2, pp. 143–168, 1999.

[56] F. Wu and R. Sioshansi, “A stochastic flow-capturing model to optimize the location of fast-charging stations with uncertain electric vehicle flows,” *Transportation Research Part D: Transport and Environment*, vol. 53, pp. 354–376, 2017.

[57] C. M. Kalamaras and A. M. Efstathiou, “Hydrogen production technologies: current state and future developments,” in *Conference papers in science*, vol. 2013. Hindawi, 2013.

[58] J. O. Abe, A. Popoola, E. Ajenifuja, and O. Popoola, “Hydrogen energy, economy and storage: review and recommendation,” *International Journal of Hydrogen Energy*, vol. 44, no. 29, pp. 15 072–15 086, 2019.

[59] R.-H. Lin, Z.-Z. Ye, and B.-D. Wu, “A review of hydrogen station location models,” *International Journal of Hydrogen Energy*, 2020.

[60] A. Molino, S. Chianese, and D. Musmarra, “Biomass gasification technology: The state of the art overview,” *Journal of Energy Chemistry*, vol. 25, no. 1, pp. 10–25, 2016.

[61] M. Puig-Arnavat, J. C. Bruno, and A. Coronas, "Review and analysis of biomass gasification models," *Renewable and sustainable energy reviews*, vol. 14, no. 9, pp. 2841–2851, 2010.

[62] C. Acar and I. Dincer, "Review and evaluation of hydrogen production options for better environment," *Journal of cleaner production*, vol. 218, pp. 835–849, 2019.

[63] R. Pinsky, P. Sabharwall, J. Hartvigsen, and J. O'Brien, "Comparative review of hydrogen production technologies for nuclear hybrid energy systems," *Progress in Nuclear Energy*, vol. 123, p. 103317, 2020.

[64] V. S. Sikarwar, M. Zhao, P. Clough, J. Yao, X. Zhong, M. Z. Memon, N. Shah, E. J. Anthony, and P. S. Fennell, "An overview of advances in biomass gasification," *Energy & Environmental Science*, vol. 9, no. 10, pp. 2939–2977, 2016.

[65] J. D. Holladay, J. Hu, D. L. King, and Y. Wang, "An overview of hydrogen production technologies," *Catalysis today*, vol. 139, no. 4, pp. 244–260, 2009.

[66] M. Voldsund, K. Jordal, and R. Anantharaman, "Hydrogen production with co2 capture," *International Journal of Hydrogen Energy*, vol. 41, no. 9, pp. 4969–4992, 2016.

[67] J. C. Molburg and R. D. Doctor, "Hydrogen from steam-methane reforming with co2 capture," in *20th annual international Pittsburgh coal conference*, 2003, pp. 1–21.

[68] J. Hinkley, J. Hayward, R. McNaughton, R. Gillespie, A. Matsumoto, M. Watt, and K. Lovegrove, "Cost assessment of hydrogen production from pv and electrolysis," *Report to ARENA as part of Solar Fuels Roadmap, Project A-3018*, pp. 1–4, 2016.

[69] M. David, C. Ocampo-Martínez, and R. Sánchez-Peña, "Advances in alkaline water electrolyzers: A review," *Journal of Energy Storage*, vol. 23, pp. 392–403, 2019.

[70] V. Utgikar and T. Thiesen, "Life cycle assessment of high temperature electrolysis for hydrogen production via nuclear energy," *International Journal of Hydrogen Energy*, vol. 31, no. 7, pp. 939–944, 2006.

[71] S. D. Ebbesen and M. Mogensen, "Electrolysis of carbon dioxide in solid oxide electrolysis cells," *Journal of Power Sources*, vol. 193, no. 1, pp. 349–358, 2009.

[72] Y. Zheng, J. Wang, B. Yu, W. Zhang, J. Chen, J. Qiao, and J. Zhang, "A review of high temperature co-electrolysis of h 2 o and co 2 to produce sustainable fuels using solid oxide electrolysis cells (soecs): advanced materials and technology," *Chemical Society Reviews*, vol. 46, no. 5, pp. 1427–1463, 2017.

[73] S. Pfenninger and J. Keirstead, "Renewables, nuclear, or fossil fuels? scenarios for great britain's power system considering costs, emissions and energy security," *Applied Energy*, vol. 152, pp. 83–93, 2015.

[74] Z. Wang, M. Mori, and T. Araki, "Steam electrolysis performance of intermediate-temperature solid oxide electrolysis cell and efficiency of hydrogen production system at 300 nm3 h- 1," *International journal of hydrogen energy*, vol. 35, no. 10, pp. 4451–4458, 2010.

[75] C. M. Stoots, J. E. O'Brien, K. G. Condie, and J. J. Hartvigsen, "High-temperature electrolysis for large-scale hydrogen production from nuclear energy–experimental investigations," *International Journal of Hydrogen Energy*, vol. 35, no. 10, pp. 4861–4870, 2010.

[76] X. Tao, M. Bai, X. Li, H. Long, S. Shang, Y. Yin, and X. Dai, "Ch4–co2 reforming by plasma–challenges and opportunities," *Progress in Energy and Combustion Science*, vol. 37, no. 2, pp. 113–124, 2011.

[77] D. L. King, L. Zhang, G. Xia, A. M. Karim, D. J. Heldebrant, X. Wang, T. Peterson, and Y. Wang, "Aqueous phase reforming of glycerol for hydrogen production over pt–re supported on carbon," *Applied Catalysis B: Environmental*, vol. 99, no. 1-2, pp. 206–213, 2010.

[78] J. Kim, D. Um, and O. Kwon, "Hydrogen production from burning and reforming of ammonia in a microreforming system," *Energy conversion and management*, vol. 56, pp. 184–191, 2012.

[79] F. Safari and I. Dincer, "A review and comparative evaluation of thermochemical water splitting cycles for hydrogen production," *Energy Conversion and Management*, vol. 205, p. 112182, 2020.

[80] J. Luo, J.-H. Im, M. T. Mayer, M. Schreier, M. K. Nazeeruddin, N.-G. Park, S. D. Tilley, H. J. Fan, and M. Grätzel, "Water photolysis at 12.3% efficiency via perovskite photovoltaics and earth-abundant catalysts," *Science*, vol. 345, no. 6204, pp. 1593–1596, 2014.

[81] X. M. Guo, E. Trably, E. Latrille, H. Carrere, and J.-P. Steyer, "Hydrogen production from agricultural waste by dark fermentation: a review," *International journal of hydrogen energy*, vol. 35, no. 19, pp. 10 660–10 673, 2010.

[82] T. Zhang, D. Jiang, H. Zhang, Y. Jing, N. Tahir, Y. Zhang, and Q. Zhang, "Comparative study on bio-hydrogen production from corn stover: Photo-fermentation, dark-fermentation and dark-photo co-fermentation," *International Journal of Hydrogen Energy*, vol. 45, no. 6, pp. 3807–3814, 2020.

[83] A. Kadier, Y. Simayi, P. Abdeshahian, N. F. Azman, K. Chandrasekhar, and M. S. Kalil, "A comprehensive review of microbial electrolysis cells (mec) reactor designs and configurations for sustainable hydrogen gas production," *Alexandria Engineering Journal*, vol. 55, no. 1, pp. 427–443, 2016.

[84] C. White, R. Steeper, and A. Lutz, "The hydrogen-fueled internal combustion engine: a technical review," *International journal of hydrogen energy*, vol. 31, no. 10, pp. 1292–1305, 2006.

[85] H. Barthélémy, M. Weber, and F. Barbier, "Hydrogen storage: recent improvements and industrial perspectives," *International Journal of Hydrogen Energy*, vol. 42, no. 11, pp. 7254–7262, 2017.

[86] Ube Industries, "Ube industries supplying nylon 6 resin for high-pressure hydrogen tanks in latest toyota mirai fuel cell vehicle," Mar 2021. [Online]. Available: https://www.ube-ind.co.jp/ube/en/news/2020/20210303_01.html

[87] U. Eberle, B. Müller, and R. Von Helmolt, “Fuel cell electric vehicles and hydrogen infrastructure: status 2012,” *Energy & Environmental Science*, vol. 5, no. 10, pp. 8780–8798, 2012.

[88] M. Penev, J. Zuboy, and C. Hunter, “Economic analysis of a high-pressure urban pipeline concept (hyline) for delivering hydrogen to retail fueling stations,” *Transportation Research Part D: Transport and Environment*, vol. 77, pp. 92–105, 2019.

[89] K. Reddi, A. Elgowainy, and E. Sutherland, “Hydrogen refueling station compression and storage optimization with tube-trailer deliveries,” *International journal of hydrogen energy*, vol. 39, no. 33, pp. 19 169–19 181, 2014.

[90] J. Gillette and R. Kolpa, “Overview of interstate hydrogen pipeline systems.” Argonne National Lab.(ANL), Argonne, IL (United States), Tech. Rep., 2008.

[91] U.S. Department of Energy, “Hydrogen pipelines.” [Online]. Available: https://www.energy.gov/eere/fuelcells/hydrogen-pipelines

[92] Hydrogen Tools, “Hydrogen pipelines,” Sep 2016. [Online]. Available: https://h2tools.org/hyarc/hydrogen-data/hydrogen-pipelines

[93] Offshore Technology, “North america has the highest oil and gas pipeline length globally,” 2019. [Online]. Available: https://www.offshore-technology.com/comment/north-america-has-the-highest-oil-and-gas-pipeline-length-globally/

[94] D. Haeseldonckx and W. D’haeseleer, “The use of the natural-gas pipeline infrastructure for hydrogen transport in a changing market structure,” *International Journal of Hydrogen Energy*, vol. 32, no. 10-11, pp. 1381–1386, 2007.

[95] S. Niaz, T. Manzoor, and A. H. Pandith, “Hydrogen storage: Materials, methods and perspectives,” *Renewable and Sustainable Energy Reviews*, vol. 50, pp. 457–469, 2015.

[96] Y.-h. Zhang, Z.-c. Jia, Z.-m. Yuan, T. Yang, Y. Qi, and D.-l. Zhao, “Development and application of hydrogen storage,” *Journal of Iron and Steel Research International*, vol. 22, no. 9, pp. 757–770, 2015.

[97] A. Züttel, "Materials for hydrogen storage," *Materials today*, vol. 6, no. 9, pp. 24–33, 2003.

[98] R. Ahluwalia, J.-K. Peng, and T. Hua, "5 - cryo-compressed hydrogen storage," in *Compendium of Hydrogen Energy*, ser. Woodhead Publishing Series in Energy, R. B. Gupta, A. Basile, and T. N. Veziroglu, Eds. Woodhead Publishing, 2016, pp. 119–145.

[99] Y. Kojima, "Hydrogen storage materials for hydrogen and energy carriers," *International Journal of Hydrogen Energy*, vol. 44, no. 33, pp. 18 179–18 192, 2019.

[100] J.-F. Petit, P. Miele, and U. B. Demirci, "Ammonia borane h3nbh3 for solid-state chemical hydrogen storage: Different samples with different thermal behaviors," *international journal of hydrogen energy*, vol. 41, no. 34, pp. 15 462–15 470, 2016.

[101] R. Lan, J. T. Irvine, and S. Tao, "Ammonia and related chemicals as potential indirect hydrogen storage materials," *International Journal of Hydrogen Energy*, vol. 37, no. 2, pp. 1482–1494, 2012.

[102] N. Rusman and M. Dahari, "A review on the current progress of metal hydrides material for solid-state hydrogen storage applications," *International Journal of Hydrogen Energy*, vol. 41, no. 28, pp. 12 108–12 126, 2016.

[103] B. Sakintuna, F. Lamari-Darkrim, and M. Hirscher, "Metal hydride materials for solid hydrogen storage: a review," *International journal of hydrogen energy*, vol. 32, no. 9, pp. 1121–1140, 2007.

[104] J. M. B. von Colbe, G. Lozano, O. Metz, T. Bücherl, R. Bormann, T. Klassen, and M. Dornheim, "Design, sorption behaviour and energy management in a sodium alanate-based lightweight hydrogen storage tank," *International Journal of Hydrogen Energy*, vol. 40, no. 7, pp. 2984–2988, 2015.

[105] A. Zaluska, L. Zaluski, and J. Ström-Olsen, "Sodium alanates for reversible hydrogen storage," *Journal of Alloys and Compounds*, vol. 298, no. 1-2, pp. 125–134, 2000.

[106] C. Fellay, P. J. Dyson, and G. Laurenczy, "A viable hydrogen-storage system based on selective formic acid decomposition with a ruthenium catalyst," *Angewandte Chemie International Edition*, vol. 47, no. 21, pp. 3966–3968, 2008.

[107] F. Joó, "Breakthroughs in hydrogen storage-formic acid as a sustainable storage material for hydrogen," *ChemSusChem: Chemistry & Sustainability Energy & Materials*, vol. 1, no. 10, pp. 805–808, 2008.

[108] Y.-H. P. Zhang, "Renewable carbohydrates are a potential high-density hydrogen carrier," *international journal of hydrogen energy*, vol. 35, no. 19, pp. 10 334–10 342, 2010.

[109] P. Preuster, C. Papp, and P. Wasserscheid, "Liquid organic hydrogen carriers (lohcs): toward a hydrogen-free hydrogen economy," *Accounts of chemical research*, vol. 50, no. 1, pp. 74–85, 2017.

[110] D. Teichmann, W. Arlt, and P. Wasserscheid, "Liquid organic hydrogen carriers as an efficient vector for the transport and storage of renewable energy," *International Journal of Hydrogen Energy*, vol. 37, no. 23, pp. 18 118–18 132, 2012.

[111] Y. Xia, Z. Yang, and Y. Zhu, "Porous carbon-based materials for hydrogen storage: advancement and challenges," *Journal of Materials Chemistry A*, vol. 1, no. 33, pp. 9365–9381, 2013.

[112] R. Ströbel, J. Garche, P. Moseley, L. Jörissen, and G. Wolf, "Hydrogen storage by carbon materials," *Journal of power sources*, vol. 159, no. 2, pp. 781–801, 2006.

[113] H. Langmi, D. Book, A. Walton, S. Johnson, M. Al-Mamouri, J. Speight, P. Edwards, I. Harris, and P. Anderson, "Hydrogen storage in ion-exchanged zeolites," *Journal of alloys and compounds*, vol. 404, pp. 637–642, 2005.

[114] J. Weitkamp, M. Fritz, and S. Ernst, "Zeolites as media for hydrogen storage," in *Proceedings from the ninth international zeolite conference.* Elsevier, 1993, pp. 11–19.

[115] N. Zhevago, E. Denisov, and V. Glebov, "Experimental investigation of hydrogen storage in capillary arrays," *international journal of hydrogen energy*, vol. 35, no. 1, pp. 169–175, 2010.

[116] N. Zhevago, A. Chabak, E. Denisov, V. Glebov, and S. Korobtsev, "Storage of cryo-compressed hydrogen in flexible glass capillaries," *International journal of hydrogen energy*, vol. 38, no. 16, pp. 6694–6703, 2013.

[117] G. D. Rambach, "Hydrogen transport and storage in engineered glass microspheres," Lawrence Livermore National Lab., CA (United States), Tech. Rep., 1994.

[118] S. H. Owen and M. S. Daskin, "Strategic facility location: A review," *European journal of operational research*, vol. 111, no. 3, pp. 423–447, 1998.

[119] Z. Drezner and H. W. Hamacher, *Facility location: applications and theory.* Springer Science & Business Media, 2001.

[120] M. T. Melo, S. Nickel, and F. Saldanha-Da-Gama, "Facility location and supply chain management–a review," *European journal of operational research*, vol. 196, no. 2, pp. 401–412, 2009.

[121] R. M. Hekmatfar, "Facility location," *Physica-Verlag*, 2009.

[122] W. Tu, Q. Li, Z. Fang, S.-l. Shaw, B. Zhou, and X. Chang, "Optimizing the locations of electric taxi charging stations: A spatial–temporal demand coverage approach," *Transportation Research Part C: Emerging Technologies*, vol. 65, pp. 172–189, 2016.

[123] C. Toregas, R. Swain, C. ReVelle, and L. Bergman, "The location of emergency service facilities," *Operations research*, vol. 19, no. 6, pp. 1363–1373, 1971.

[124] A. Caprara, P. Toth, and M. Fischetti, "Algorithms for the set covering problem," *Annals of Operations Research*, vol. 98, no. 1, pp. 353–371, 2000.

[125] J. E. Kang and W. Recker, "Strategic hydrogen refueling station locations with scheduling and routing considerations of individual vehicles," *Transportation Science*, vol. 49, no. 4, pp. 767–783, 2015.

[126] R. Church and C. ReVelle, “The maximal covering location problem,” in *Papers of the regional science association*, vol. 32, no. 1. Springer-Verlag, 1974, pp. 101–118.

[127] K. M. Curtin, K. Hayslett-McCall, and F. Qiu, “Determining optimal police patrol areas with maximal covering and backup covering location models,” *Networks and spatial economics*, vol. 10, no. 1, pp. 125–145, 2010.

[128] R. Z. Farahani, N. Asgari, N. Heidari, M. Hosseininia, and M. Goh, “Covering problems in facility location: A review,” *Computers & Industrial Engineering*, vol. 62, no. 1, pp. 368–407, 2012.

[129] S. L. Hakimi, “Optimum locations of switching centers and the absolute centers and medians of a graph,” *Operations research*, vol. 12, no. 3, pp. 450–459, 1964.

[130] M. S. Daskin and K. L. Maass, “The p-median problem,” in *Location science*. Springer, 2015, pp. 21–45.

[131] H. Calik and H. Çalık, “Exact solution methodologies for the p-center problem under single and multiple allocation strategies,” Ph.D. dissertation, bilkent university, 2013.

[132] C.-C. Lin and C.-C. Lin, “The p-center flow-refueling facility location problem,” *Transportation Research Part B: Methodological*, vol. 118, pp. 124–142, 2018.

[133] B. Du, H. Zhou, and R. Leus, “A two-stage robust model for a reliable p-center facility location problem,” *Applied Mathematical Modelling*, vol. 77, pp. 99–114, 2020.

[134] C. S. ReVelle and H. A. Eiselt, “Location analysis: A synthesis and survey,” *European journal of operational research*, vol. 165, no. 1, pp. 1–19, 2005.

[135] M. Boccia, A. Sforza, and C. Sterle, “Flow intercepting facility location: Problems, models and heuristics,” *Journal of Mathematical Modelling and Algorithms*, vol. 8, no. 1, pp. 35–79, 2009.

[136] M. J. Hodgson, “A flow capturing location allocation model,” *Geographical Analysis*, vol. 22, no. 3, pp. 270–279, 1990.

[137] M. Kuby and S. Lim, "The flow-refueling location problem for alternative-fuel vehicles," *Socio-Economic Planning Sciences*, vol. 39, no. 2, pp. 125–145, 2005.

[138] O. Berman, R. C. Larson, and N. Fouska, "Optimal location of discretionary service facilities," *Transportation Science*, vol. 26, no. 3, pp. 201–211, 1992.

[139] M. J. Hodgson, K. Rosing, A. Leontien, and G. Storrier, "Applying the flow-capturing location-allocation model to an authentic network: Edmonton, canada," *European journal of operational research*, vol. 90, no. 3, pp. 427–443, 1996.

[140] Y. Li, F. Cui, and L. Li, "An integrated optimization model for the location of hydrogen refueling stations," *International Journal of Hydrogen Energy*, vol. 43, no. 42, pp. 19 636–19 649, 2018.

[141] K.-i. Tanaka and T. Furuta, "A hierarchical flow capturing location problem with demand attraction based on facility size, and its lagrangian relaxation solution method," *Geographical Analysis*, vol. 44, no. 1, pp. 15–28, 2012.

[142] S. Melkote and M. S. Daskin, "Capacitated facility location/network design problems," *European journal of operational research*, vol. 129, no. 3, pp. 481–495, 2001.

[143] O. Berman, D. Bertsimas, and R. C. Larson, "Locating discretionary service facilities, ii: maximizing market size, minimizing inconvenience," *Operations Research*, vol. 43, no. 4, pp. 623–632, 1995.

[144] F. Hooshmand and S. MirHassani, "An effective bilevel programming approach for the evasive flow capturing location problem," *Networks and Spatial Economics*, vol. 18, no. 4, pp. 909–935, 2018.

[145] W. Zeng, M. J. Hodgson, and I. Castillo, "The pickup problem: consumers' locational preferences in flow interception," *Geographical Analysis*, vol. 41, no. 1, pp. 107–126, 2009.

[146] W. Zeng, I. Castillo, and M. J. Hodgson, "A generalized model for locating facilities on a network with flow-based demand," *Networks and Spatial Economics*, vol. 10, no. 4, pp. 579–611, 2010.

[147] I. Capar and M. Kuby, "An efficient formulation of the flow refueling location model for alternative-fuel stations," *Iie Transactions*, vol. 44, no. 8, pp. 622–636, 2012.

[148] I. Capar, M. Kuby, V. J. Leon, and Y.-J. Tsai, "An arc cover–path-cover formulation and strategic analysis of alternative-fuel station locations," *European Journal of Operational Research*, vol. 227, no. 1, pp. 142–151, 2013.

[149] S. MirHassani and R. Ebrazi, "A flexible reformulation of the refueling station location problem," *Transportation Science*, vol. 47, no. 4, pp. 617–628, 2013.

[150] R. Riemann, D. Z. Wang, and F. Busch, "Optimal location of wireless charging facilities for electric vehicles: flow-capturing location model with stochastic user equilibrium," *Transportation Research Part C: Emerging Technologies*, vol. 58, pp. 1–12, 2015.

[151] M. Hosseini, S. A. MirHassani, and F. Hooshmand, "Deviation-flow refueling location problem with capacitated facilities: Model and algorithm," *Transportation Research Part D: Transport and Environment*, vol. 54, pp. 269–281, 2017.

[152] J. Ko, T.-H. T. Gim, and R. Guensler, "Locating refuelling stations for alternative fuel vehicles: a review on models and applications," *Transport Reviews*, vol. 37, no. 5, pp. 551–570, 2017.

[153] M. J. Hodgson and K. E. Rosing, "A network location-allocation model trading off flow capturing and p-median objectives," *Annals of Operations Research*, vol. 40, no. 1, pp. 247–260, 1992.

[154] M. Karatas and E. Yakıcı, "An iterative solution approach to a multi-objective facility location problem," *Applied Soft Computing*, vol. 62, pp. 272–287, 2018.

[155] Q. Liu, X. Li, H. Liu, and Z. Guo, "Multi-objective metaheuristics for discrete optimization problems: A review of the state-of-the-art," *Applied Soft Computing*, p. 106382, 2020.

[156] H. Abdi, R. Rasouli Nezhad, and M. Salehimaleh, "Chapter 5 - fuel cells," in *Distributed Generation Systems*, G. Gharehpetian and S. M. Mousavi Agah, Eds. Butterworth-Heinemann, 2017, pp. 221–300.

[157] H. Nagamoto, "Fuel cells: Electrochemical reactions," in *Encyclopedia of Materials: Science and Technology*, K. J. Buschow, R. W. Cahn, M. C. Flemings, B. Ilschner, E. J. Kramer, S. Mahajan, and P. Veyssière, Eds. Oxford: Elsevier, 2001, pp. 3359–3367.

[158] A. Buis, "The Atmosphere: Getting a Handle on Carbon Dioxide - Climate Change: Vital Signs of the Planet," Oct 2019. [Online]. Available: https://climate.nasa.gov/news/2915/the-atmosphere-getting-a-handle-on-carbon-dioxide/

[159] D. R. Dekel, "Review of cell performance in anion exchange membrane fuel cells," *Journal of Power Sources*, vol. 375, pp. 158–169, 2018.

[160] F. Markus, "1966 gm electrovan fuel cell prototype turns 50," Nov 2016. [Online]. Available: https://www.motortrend.com/news/1966-gm-electrovan-fuel-cell-prototype-turns-50/

[161] "Phosphoric acid fuel cell," Dec 2018. [Online]. Available: https://fuelcellsworks.com/knowledge/technologies/pafc/

[162] U.S. Department of Energy, "Types of fuel cells." [Online]. Available: https://www.energy.gov/eere/fuelcells/types-fuel-cells

[163] Planning & Facilities Management, Georgetown University, "Past projects," Nov 2019. [Online]. Available: https://facilities.georgetown.edu/energy-utilities/past-projects/

[164] A. C. Bhosale, S. Suseendiran, R. Ramya, S. R. Choudhury, and R. Rengaswamy, "Phosphoric acid fuel cells," in *Reference Module in Earth Systems and Environmental Sciences*. Elsevier, 2020.

[165] A. M. Taylor, "Science review of internal combustion engines," *Energy Policy*, vol. 36, no. 12, pp. 4657–4667, 2008.

[166] M. Åhman, "Primary energy efficiency of alternative powertrains in vehicles," *Energy*, vol. 26, no. 11, pp. 973–989, 2001.

[167] Y. Sudhakar, M. Selvakumar, and D. K. Bhat, *Biopolymer electrolytes: Fundamentals and applications in energy storage*. Elsevier, 2018.

[168] N. Sammes, R. Bove, and K. Stahl, "Phosphoric acid fuel cells: Fundamentals and applications," *Current opinion in solid state and materials science*, vol. 8, no. 5, pp. 372–378, 2004.

[169] Office of Energy Efficiency Renewable Energy, U.S. Department of Energy, "3.4 fuel cells, 2016," in *Hydrogen and Fuel Cell Technologies Office Multi-Year Research, Development, and Demonstration Plan*, May 2017.

[170] J. Baschuk and X. Li, "Carbon monoxide poisoning of proton exchange membrane fuel cells," *International Journal of Energy Research*, vol. 25, no. 8, pp. 695–713, 2001.

[171] V. F. Valdés-López, T. Mason, P. R. Shearing, and D. J. Brett, "Carbon monoxide poisoning and mitigation strategies for polymer electrolyte membrane fuel cells–a review," *Progress in Energy and Combustion Science*, vol. 79, p. 100842, 2020.

[172] A. M. Henstra and A. J. Stams, "Deep conversion of carbon monoxide to hydrogen and formation of acetate by the anaerobic thermophile carboxydothermus hydrogenoformans," *International journal of microbiology*, vol. 2011, 2011.

[173] O. Ijaodola, Z. El-Hassan, E. Ogungbemi, F. Khatib, T. Wilberforce, J. Thompson, and A. Olabi, "Energy efficiency improvements by investigating the water flooding management on proton exchange membrane fuel cell (pemfc)," *Energy*, vol. 179, pp. 246–267, 2019.

[174] Gore, "Gore's membrane technology enables toyota's second-generation fuel cell vehicle," Dec 2020. [Online]. Available: https://www.gore.com/news-events/press-release/gore-membrane-enables-toyota-second-generation-fuel-cell-vehicle

[175] L. An and R. Chen, "Recent progress in alkaline direct ethylene glycol fuel cells for sustainable energy production," *Journal of Power Sources*, vol. 329, pp. 484–501, 2016.

[176] "Annual u.s. & world fuel ethanol production," Mar 2021. [Online]. Available: https://ethanolrfa.org/statistics/annual-ethanol-production/

[177] The Methanol Institute, "Methanol price and supply/demand," Apr 2021. [Online]. Available: https://www.methanol.org/methanol-price-supply-demand/

[178] "Mono-ethylene glycol production, price and market," Oct 2020. [Online]. Available: https://www.plasticsinsight.com/resin-intelligence/resin-prices/mono-ethylene-glycol-meg/

[179] J. Garche, C. K. Dyer, P. T. Moseley, Z. Ogumi, D. A. Rand, and B. Scrosati, *Encyclopedia of electrochemical power sources.* Newnes, 2013.

[180] R. Crisafulli, A. O. Neto, M. Linardi, and E. V. Spinacé, "Preparation of ptsn/c skeletal-type electrocatalyst for ethanol oxidation," in *Studies in Surface Science and Catalysis.* Elsevier, 2010, vol. 175, pp. 559–562.

[181] C. J. Shearer, A. Cherevan, and D. Eder, "Application of functional hybrids incorporating carbon nanotubes or graphene," in *Carbon Nanotubes and Graphene.* Elsevier, 2014, pp. 387–433.

[182] P. P. Kundu and K. Dutta, *Progress and recent trends in microbial fuel cells.* Elsevier, 2018.

[183] S. Campanari and G. Guandalini, "Chapter 18 - fuel cells: opportunities and challenges," in *Catalysis, Green Chemistry and Sustainable Energy*, ser. Studies in Surface Science and Catalysis, A. Basile, G. Centi, M. D. Falco, and G. Iaquaniello, Eds. Elsevier, 2020, vol. 179, pp. 335–358.

[184] S. K. Kamarudin, F. Achmad, and W. R. W. Daud, "Overview on the application of direct methanol fuel cell (dmfc) for portable electronic devices," *International Journal of hydrogen energy*, vol. 34, no. 16, pp. 6902–6916, 2009.

[185] M. Kamarudin, S. Kamarudin, M. Masdar, and W. Daud, "Direct ethanol fuel cells," *International Journal of Hydrogen Energy*, vol. 38, no. 22, pp. 9438–9453, 2013.

[186] V. P. McConnell, "Fuel cells in forklifts extend commercial reach," *Fuel Cells Bulletin*, vol. 2010, no. 9, pp. 12–19, 2010.

[187] "Gumpert supercar with methanol fuel cell ready for production," *Fuel Cells Bulletin*, vol. 2020, no. 6, p. 2, 2020.

[188] X. Yu and P. G. Pickup, "Recent advances in direct formic acid fuel cells (dfafc)," *Journal of Power Sources*, vol. 182, no. 1, pp. 124–132, 2008.

[189] A. Serov and C. Kwak, "Progress in development of direct dimethyl ether fuel cells," *Applied Catalysis B: Environmental*, vol. 91, no. 1-2, pp. 1–10, 2009.

[190] C. P. De Leon, F. Walsh, D. Pletcher, D. Browning, and J. Lakeman, "Direct borohydride fuel cells," *Journal of Power Sources*, vol. 155, no. 2, pp. 172–181, 2006.

[191] A. Serov and C. Kwak, "Direct hydrazine fuel cells: A review," *Applied Catalysis B: Environmental*, vol. 98, no. 1-2, pp. 1–9, 2010.

[192] F. S. Da Silva and T. M. de Souza, "Novel materials for solid oxide fuel cell technologies: A literature review," *international journal of hydrogen energy*, vol. 42, no. 41, pp. 26 020–26 036, 2017.

[193] S. Park, J. M. Vohs, and R. J. Gorte, "Direct oxidation of hydrocarbons in a solid-oxide fuel cell," *Nature*, vol. 404, no. 6775, pp. 265–267, 2000.

[194] N. Q. Minh, "Solid oxide fuel cell technology-features and applications," *Solid State Ionics*, vol. 174, no. 1-4, pp. 271–277, 2004.

[195] S. C. Singhal, "Solid oxide fuel cells for stationary, mobile, and military applications," *Solid State Ionics*, vol. 152, pp. 405–410, 2002.

[196] R. T. Leah, A. Bone, E. Hammer, A. Selcuk, M. Rahman, A. Clare, L. Rees, N. Lawrence, A. Ballard, T. Domanski *et al.*, "Development of high efficiency steel

cell technology for multiple applications," *ECS Transactions*, vol. 78, no. 1, p. 2005, 2017.

[197] M. C. Williams, J. P. Strakey, and W. A. Surdoval, "The us department of energy, office of fossil energy stationary fuel cell program," *Journal of power sources*, vol. 143, no. 1-2, pp. 191–196, 2005.

[198] K. Huang and J. B. Goodenough, "Solid oxide fuel cell technology: principles, performance and operations," 2009.

[199] S. C. Singhal, "Solid oxide fuel cells," *The Electrochemical Society Interface*, vol. 16, no. 4, p. 41, 2007.

[200] A. Selimovic, M. Kemm, T. Torisson, and M. Assadi, "Steady state and transient thermal stress analysis in planar solid oxide fuel cells," *Journal of Power Sources*, vol. 145, no. 2, pp. 463–469, 2005.

[201] Z. Yang, M. Guo, N. Wang, C. Ma, J. Wang, and M. Han, "A short review of cathode poisoning and corrosion in solid oxide fuel cell," *International Journal of Hydrogen Energy*, vol. 42, no. 39, pp. 24 948–24 959, 2017.

[202] H. Yokokawa, H. Tu, B. Iwanschitz, and A. Mai, "Fundamental mechanisms limiting solid oxide fuel cell durability," *Journal of Power Sources*, vol. 182, no. 2, pp. 400–412, 2008, selected papers from the International Workshop on Degradation Issues in Fuel Cells.

[203] M. Brahmayya, S. A. Dai, and S.-Y. Suen, "Sulfonated reduced graphene oxide catalyzed cyclization of hydrazides and carbon dioxide to 1, 3, 4-oxadiazoles under sonication," *Scientific reports*, vol. 7, no. 1, pp. 1–13, 2017.

[204] A. Nakajo, F. Mueller, J. Brouwer, D. Favrat *et al.*, "Mechanical reliability and durability of sofc stacks. part ii: Modelling of mechanical failures during ageing and cycling," *International Journal of Hydrogen Energy*, vol. 37, no. 11, pp. 9269–9286, 2012.

[205] A. M. Abdalla, S. Hossain, A. T. Azad, P. M. I. Petra, F. Begum, S. G. Eriksson, and A. K. Azad, "Nanomaterials for solid oxide fuel cells: a review," *Renewable and Sustainable Energy Reviews*, vol. 82, pp. 353–368, 2018.

[206] A. Lanzini, H. Madi, V. Chiodo, D. Papurello, S. Maisano, M. Santarelli *et al.*, "Dealing with fuel contaminants in biogas-fed solid oxide fuel cell (sofc) and molten carbonate fuel cell (mcfc) plants: Degradation of catalytic and electro-catalytic active surfaces and related gas purification methods," *Progress in Energy and Combustion Science*, vol. 61, pp. 150–188, 2017.

[207] M. A. Azizi and J. Brouwer, "Progress in solid oxide fuel cell-gas turbine hybrid power systems: System design and analysis, transient operation, controls and optimization," *Applied energy*, vol. 215, pp. 237–289, 2018.

[208] A. S. Martinez, J. Brouwer, and G. S. Samuelsen, "Feasibility study for sofc-gt hybrid locomotive power: Part i. development of a dynamic 3.5 mw sofc-gt fortran model," *Journal of Power Sources*, vol. 213, pp. 203–217, 2012.

[209] Nissan, "Nissan unveils world's first solid-oxide fuel cell vehicle," *Official Global Newsroom*, Aug 2016. [Online]. Available: https://global.nissannews.com/en/releases/nissan-unveils-worlds-first-solid-oxide-fuel-cell-vehicle?source=nng&lang=en-US

[210] M. Bischoff, "Molten carbonate fuel cells: A high temperature fuel cell on the edge to commercialization," *Journal of Power Sources*, vol. 160, no. 2, pp. 842–845, 2006.

[211] N. J. Cherepy, R. Krueger, K. J. Fiet, A. F. Jankowski, and J. F. Cooper, "Direct conversion of carbon fuels in a molten carbonate fuel cell," *Journal of the Electrochemical Society*, vol. 152, no. 1, p. A80, 2004.

[212] S. Cavallaro, N. Mondello, and S. Freni, "Hydrogen produced from ethanol for internal reforming molten carbonate fuel cell," *Journal of Power Sources*, vol. 102, no. 1-2, pp. 198–204, 2001.

[213] E. Antolini, "The stability of molten carbonate fuel cell electrodes: A review of recent improvements," *Applied energy*, vol. 88, no. 12, pp. 4274–4293, 2011.

[214] C. O. Colpan, Y. Nalbant, and M. Ercelik, "4.28 fundamentals of fuel cell technologies," in *Comprehensive Energy Systems*, I. Dincer, Ed. Oxford: Elsevier, 2018, pp. 1107–1130.

[215] M. Kim, J. Youn, J. Lim, K. Eom, E. Cho, and H. Kwon, "Corrosion-resistant coating for cathode current collector and wet-seal area of molten carbonate fuel cells," *International Journal of Hydrogen Energy*, vol. 43, no. 24, pp. 11 363–11 371, 2018.

[216] A. L. Dicks, "Molten carbonate fuel cells," *Current Opinion in Solid State and Materials Science*, vol. 8, no. 5, pp. 379–383, 2004.

[217] S. Campanari, P. Chiesa, and G. Manzolini, "Co2 capture from combined cycles integrated with molten carbonate fuel cells," *International Journal of Greenhouse Gas Control*, vol. 4, no. 3, pp. 441–451, 2010.

[218] M. Spinelli, D. Di Bona, M. Gatti, E. Martelli, F. Viganò, and S. Consonni, "Assessing the potential of molten carbonate fuel cell-based schemes for carbon capture in natural gas-fired combined cycle power plants," *Journal of Power Sources*, vol. 448, p. 227223, 2020.

[219] C. Gonzalez-Solino and M. D. Lorenzo, "Enzymatic fuel cells: Towards self-powered implantable and wearable diagnostics," *Biosensors*, vol. 8, no. 1, p. 11, 2018.

[220] G. Palanisamy, H.-Y. Jung, T. Sadhasivam, M. D. Kurkuri, S. C. Kim, and S.-H. Roh, "A comprehensive review on microbial fuel cell technologies: Processes, utilization, and advanced developments in electrodes and membranes," *Journal of Cleaner Production*, vol. 221, pp. 598–621, 2019.

[221] C. Koch, F. Aulenta, U. Schröder, and F. Harnisch, "6.43 - microbial electrochemical technologies: Industrial and environmental biotechnologies based on interactions of

microorganisms with electrodes," in *Comprehensive Biotechnology (Third Edition)*, third edition ed., M. Moo-Young, Ed. Oxford: Pergamon, 2016, pp. 545–563.

[222] X. Xiao, H.-q. Xia, R. Wu, L. Bai, L. Yan, E. Magner, S. Cosnier, E. Lojou, Z. Zhu, and A. Liu, "Tackling the challenges of enzymatic (bio) fuel cells," *Chemical reviews*, vol. 119, no. 16, pp. 9509–9558, 2019.

[223] D. P. Clark and N. J. Pazdernik, "Chapter 12 - environmental biotechnology," in *Biotechnology (Second Edition)*, second edition ed., D. P. Clark and N. J. Pazdernik, Eds. Boston: Academic Cell, 2016, pp. 393–418.

[224] G. Ramanjaneyulu and B. R. Reddy, "Chapter 21 - emerging trends of microorganism in the production of alternative energy," in *Recent Developments in Applied Microbiology and Biochemistry*, V. Buddolla, Ed. Academic Press, 2019, pp. 275–305.

[225] I. Gajda, J. Greenman, and I. A. Ieropoulos, "Recent advancements in real-world microbial fuel cell applications," *Current opinion in electrochemistry*, vol. 11, pp. 78–83, 2018.

[226] C. Santoro, C. Arbizzani, B. Erable, and I. Ieropoulos, "Microbial fuel cells: From fundamentals to applications. a review," *Journal of power sources*, vol. 356, pp. 225–244, 2017.

[227] Australian Electric Vehicle Council, "Reports," 2019. [Online]. Available: https://electricvehiclecouncil.com.au/resources/$#$Resources$_$Report

[228] H. Zhang, S. J. Moura, Z. Hu, and Y. Song, "Pev fast-charging station siting and sizing on coupled transportation and power networks," *IEEE Transactions on Smart Grid*, vol. 9, no. 4, pp. 2595–2605, 2018.

[229] M. Gentili and P. B. Mirchandani, "Locating sensors on traffic networks: Models, challenges and research opportunities," *Transportation research part C: emerging technologies*, vol. 24, pp. 227–255, 2012.

[230] B. Zhou, G. Chen, T. Huang, Q. Song, and Y. Yuan, "Planning pev fast-charging stations using data-driven distributionally robust optimization approach based on ϕ-divergence," *IEEE Transactions on Transportation Electrification*, vol. 6, no. 1, pp. 170–180, 2020.

[231] D. Tong, "Regional coverage maximization: a new model to account implicitly for complementary coverage," *Geographical Analysis*, vol. 44, no. 1, pp. 1–14, 2012.

[232] G. Alexandris and I. Giannikos, "A new model for maximal coverage exploiting gis capabilities," *European Journal of Operational Research*, vol. 202, no. 2, pp. 328–338, 2010.

[233] A. Zhang, J. E. Kang, and C. Kwon, "Incorporating demand dynamics in multi-period capacitated fast-charging location planning for electric vehicles," *Transportation Research Part B: Methodological*, vol. 103, pp. 5–29, 2017.

[234] "Scaling up electric vehicle charging infrastructure." [Online]. Available: https://www.nrdc.org/sites/default/files/charging-infrastructure-best-parctices-202007.pdf

[235] C. Luo, Y.-F. Huang, and V. Gupta, "Placement of ev charging stations—balancing benefits among multiple entities," *IEEE Transactions on Smart Grid*, vol. 8, no. 2, pp. 759–768, 2015.

[236] Y. Zhao, Y. Guo, Q. Guo, H. Zhang, and H. Sun, "Deployment of the electric vehicle charging station considering existing competitors," *IEEE Transactions on Smart Grid*, vol. 11, no. 5, pp. 4236–4248, 2020.

[237] E. Zavvos, "Planning and analysing competing en-route charging stations for electric vehicles: A game-theoretic approach," Ph.D. dissertation, University of Southampton, 2019.

[238] Y. Xiong, J. Gan, B. An, C. Miao, and A. L. Bazzan, "Optimal electric vehicle fast charging station placement based on game theoretical framework," *IEEE Transactions on Intelligent Transportation Systems*, vol. 19, no. 8, pp. 2493–2504, 2017.

[239] X. Kong, F. Xia, J. Li, M. Hou, M. Li, and Y. Xiang, "A shared bus profiling scheme for smart cities based on heterogeneous mobile crowdsourced data," *IEEE Transactions on Industrial Informatics*, vol. 16, no. 2, pp. 1436–1444, 2019.

[240] M. Li, M. Lenzen, F. Keck, B. McBain, O. Rey-Lescure, B. Li, and C. Jiang, "Gis-based probabilistic modeling of bev charging load for australia," *IEEE Transactions on Smart Grid*, vol. 10, no. 4, pp. 3525–3534, 2018.

[241] H. Zhang, Z. Hu, Y. Song, Z. Xu, and L. Jia, "A prediction method for electric vehicle charging load considering spatial and temporal distribution," *Automation of electric power systems*, vol. 38, no. 1, pp. 13–20, 2014.

[242] M. Sun, I. Konstantelos, and G. Strbac, "A deep learning-based feature extraction framework for system security assessment," *IEEE Transactions on Smart Grid*, vol. 10, no. 5, pp. 5007–5020, 2018.

[243] M. Luo, H. Wen, Y. Luo, B. Du, K. Klemmer, and H. Zhu, "Dynamic demand prediction for expanding electric vehicle sharing systems: A graph sequence learning approach," *arXiv preprint arXiv:1903.04051*, 2019.

[244] C. Liu, K. Deng, C. Li, J. Li, Y. Li, and J. Luo, "The optimal distribution of electric-vehicle chargers across a city," in *2016 IEEE 16th International Conference on Data Mining (ICDM)*. IEEE, 2016, pp. 261–270.

[245] N. Li, L. Chen, and S. H. Low, "Optimal demand response based on utility maximization in power networks," in *2011 IEEE power and energy society general meeting*. IEEE, 2011, pp. 1–8.

[246] L. Gan, N. Li, U. Topcu, and S. H. Low, "Exact convex relaxation of optimal power flow in radial networks," *IEEE Transactions on Automatic Control*, vol. 60, no. 1, pp. 72–87, 2015.

[247] H. Zhang, S. J. Moura, Z. Hu, W. Qi, and Y. Song, "A second-order cone programming model for planning pev fast-charging stations," *IEEE Transactions on power Systems*, vol. 33, no. 3, pp. 2763–2777, 2017.

[248] R. J. Hyndman and G. Athanasopoulos, *Forecasting: principles and practice*. OTexts, 2018.

[249] L. Breiman, "Random forests," *Machine learning*, vol. 45, no. 1, pp. 5–32, 2001.

[250] T. Chen and C. Guestrin, "Xgboost: A scalable tree boosting system," in *Proceedings of the 22nd acm sigkdd international conference on knowledge discovery and data mining*, 2016, pp. 785–794.

[251] Z. Zhao, W. Chen, X. Wu, P. C. Chen, and J. Liu, "Lstm network: a deep learning approach for short-term traffic forecast," *IET Intelligent Transport Systems*, vol. 11, no. 2, pp. 68–75, 2017.

[252] D. Salinas, V. Flunkert, J. Gasthaus, and T. Januschowski, "Deepar: Probabilistic forecasting with autoregressive recurrent networks," *International Journal of Forecasting*, vol. 36, no. 3, pp. 1181–1191, 2020.

[253] L. Zhao, Y. Song, C. Zhang, Y. Liu, P. Wang, T. Lin, M. Deng, and H. Li, "T-gcn: A temporal graph convolutional network for traffic prediction," *IEEE Transactions on Intelligent Transportation Systems*, vol. 21, no. 9, pp. 3848–3858, 2019.

[254] P. C. Chu and J. E. Beasley, "A genetic algorithm for the multidimensional knapsack problem," *Journal of heuristics*, vol. 4, no. 1, pp. 63–86, 1998.

[255] K. Jankauskas, L. G. Papageorgiou, and S. S. Farid, "Fast genetic algorithm approaches to solving discrete-time mixed integer linear programming problems of capacity planning and scheduling of biopharmaceutical manufacture," *Computers & Chemical Engineering*, vol. 121, pp. 212–223, 2019.

[256] S. Mehar and S. M. Senouci, "An optimization location scheme for electric charging stations," in *2013 international conference on smart communications in network technologies (SACONET)*, vol. 1. IEEE, 2013, pp. 1–5.

[257] Y. Xiang, J. Liu, F. Li, Y. Liu, Y. Liu, R. Xu, Y. Su, and L. Ding, "Optimal active distribution network planning: a review," *Electric Power Components and Systems*, vol. 44, no. 10, pp. 1075–1094, 2016.

[258] C. Zhang and Y. Xu, "Hierarchically-coordinated voltage/var control of distribution networks using pv inverters," *IEEE Transactions on Smart Grid*, vol. 11, no. 4, pp. 2942–2953, 2020.

[259] F. Luo, K. Meng, Z. Y. Dong, Y. Zheng, Y. Chen, and K. P. Wong, "Coordinated operational planning for wind farm with battery energy storage system," *IEEE Transactions on Sustainable Energy*, vol. 6, no. 1, pp. 253–262, 2015.

[260] G. Papaefthymiou and B. Klockl, "Mcmc for wind power simulation," *IEEE transactions on energy conversion*, vol. 23, no. 1, pp. 234–240, 2008.

[261] F. Rassaei, W.-S. Soh, and K.-C. Chua, "A statistical modelling and analysis of residential electric vehicles' charging demand in smart grids," in *2015 IEEE Power & Energy Society Innovative Smart Grid Technologies Conference (ISGT)*. IEEE, 2015, pp. 1–5.

[262] A. Vyas and D. Santini, "Use of national surveys for estimating 'full' phev potential for oil use reduction [eb/ol]," 2015. [Online]. Available: https://www.yumpu.com/en/document/view/5049345/use-of-national-surveys-for-estimating-full-phev-potential-for-oil-"

[263] Y. Sheffi, "Urban transportation networks: Equilibrium analysis with mathematical programming methods," 1984.

[264] F. Luo, Z. Y. Dong, Y. Chen, and J. Zhao, "Natural aggregation algorithm: A new efficient metaheuristic tool for power system optimizations," in *2016 IEEE International Conference on Smart Grid Communications (SmartGridComm)*. IEEE, 2016, pp. 186–192.

[265] V. Miranda, J. Ranito, and L. M. Proenca, "Genetic algorithms in optimal multistage distribution network planning," *IEEE Transactions on power systems*, vol. 9, no. 4, pp. 1927–1933, 1994.

[266] NREL, "Wind integration data sets." [Online]. Available: https://www.nrel.gov/grid/wind-integration-data.html

[267] K. Deb, A. Pratap, S. Agarwal, and T. Meyarivan, “A fast and elitist multiobjective genetic algorithm: Nsga-ii,” *IEEE transactions on evolutionary computation*, vol. 6, no. 2, pp. 182–197, 2002.

[268] Q. Zhang and H. Li, “Moea/d: A multiobjective evolutionary algorithm based on decomposition,” *IEEE Transactions on evolutionary computation*, vol. 11, no. 6, pp. 712–731, 2007.

[269] “Population and energy consumption,” 2018. [Online]. Available: https://www.worldpopulationbalance.org/population_energy

[270] B. Bilgin, P. Magne, P. Malysz, Y. Yang, V. Pantelic, M. Preindl, A. Korobkine, W. Jiang, M. Lawford, and A. Emadi, “Making the case for electrified transportation,” *IEEE Transactions on Transportation Electrification*, vol. 1, no. 1, pp. 4–17, 2015.

[271] G. Wang, Z. Xu, F. Wen, and K. P. Wong, “Traffic-constrained multiobjective planning of electric-vehicle charging stations,” *IEEE Transactions on Power Delivery*, vol. 28, no. 4, pp. 2363–2372, 2013.

[272] Y. Zheng, Z. Y. Dong, Y. Xu, K. Meng, J. H. Zhao, and J. Qiu, “Electric vehicle battery charging/swap stations in distribution systems: Comparison study and optimal planning,” *IEEE Transactions on Power Systems*, vol. 29, no. 1, pp. 221–229, 2014.

[273] N. Liu, Q. Chen, X. Lu, J. Liu, and J. Zhang, “A charging strategy for pv-based battery switch stations considering service availability and self-consumption of pv energy,” *IEEE Transactions on Industrial Electronics*, vol. 62, no. 8, pp. 4878–4889, 2015.

[274] “New hydrogen fuel cell-powered fast chargers,” 2021. [Online]. Available: https://fuelcellsworks.com/news/new-hydrogen-fuel-cell-powered-fast-chargers/

[275] Z. Ding, Y. Lu, L. Zhang, W. Lee, and D. Chen, “A stochastic resource-planning scheme for phev charging station considering energy portfolio optimization and price-

responsive demand," *IEEE Transactions on Industry Applications*, vol. 54, no. 6, pp. 5590–5598, 2018.

[276] L. Li, H. Manier, and M.-A. Manier, "Integrated optimization model for hydrogen supply chain network design and hydrogen fueling station planning," *Computers & Chemical Engineering*, vol. 134, p. 106683, 2020.

[277] S. Deb, K. Tammi, K. Kalita, and P. Mahanta, "Impact of electric vehicle charging station load on distribution network," *Energies*, vol. 11, no. 1, p. 178, 2018.

[278] W. Xiao, Y. Cheng, W. Lee, V. Chen, and S. Charoensri, "Hydrogen filling station design for fuel cell vehicles," in *2010 IEEE Industrial and Commercial Power Systems Technical Conference - Conference Record*, 2010, pp. 1–6.

[279] B. Kocuk, S. S. Dey, and X. A. Sun, "Strong socp relaxations for the optimal power flow problem," *Operations Research*, vol. 64, no. 6, pp. 1177–1196, 2016.

[280] J. D. Palacio and J. C. Rivera, "Mixed-integer linear programming models for one-commodity pickup and delivery traveling salesman problems," in *Workshop on engineering applications*. Springer, 2019, pp. 735–751.

[281] S. N. Parragh, K. F. Doerner, and R. F. Hartl, "A survey on pickup and delivery problems," *Journal für Betriebswirtschaft*, vol. 58, no. 2, pp. 81–117, 2008.

[282] "Energy made easy." [Online]. Available: https://www.energymadeeasy.gov.au/

[283] "Solar pv maps and tools." [Online]. Available: https://pv-map.apvi.org.au/

[284] Toyota, "Toyota mirai product information," 2017. [Online]. Available: https://pressroom.toyota.com/2017-toyota-mirai-product/

[285] Commercial solar prices: Current averages by capital city. Solar Choice. [Online]. Available: https://www.solarchoice.net.au/commercial-solar-power-system-prices

[286] B. D. James, C. Houchins, J. M. Huya-Kouadio, and D. A. DeSantis, "hydrogen storage system cost analysis," Strategic Analysis Inc., Arlington, VA (United States), Tech. Rep., 2016.

[287] G. Newsom, "Joint agency staff report on assembly bill 8: 2019 annual assessment of time and cost needed to attain 100 hydrogen refueling stations in california," California Energy Commission, Tech. Rep., 2019.

[288] C. Yang and J. Ogden, "Determining the lowest-cost hydrogen delivery mode," *International Journal of Hydrogen Energy*, vol. 32, no. 2, pp. 268–286, 2007.

[289] N. Leemput, F. Geth, B. Claessens, J. Van Roy, R. Ponnette, and J. Driesen, "A case study of coordinated electric vehicle charging for peak shaving on a low voltage grid," in *2012 3rd IEEE PES Innovative Smart Grid Technologies Europe (ISGT Europe)*. IEEE, 2012, pp. 1–7.

[290] H. Ito, N. Miyazaki, M. Ishida, and A. Nakano, "Efficiency of unitized reversible fuel cell systems," *International Journal of Hydrogen Energy*, vol. 41, no. 13, pp. 5803–5815, 2016.